

Rockslide-debris avalanche of May 18, 1980, Mount St. Helens Volcano, Washington

Harry GLICKEN*

Harry GLICKEN (1998) Rockslide-debris avalanche of May 18, 1980, Mount St. Helens Volcano, Washington. *Bull. Geol. Surv. Japan*, vol. 48(2/3), p. 55-106, 32 figs., 5 tables., 2 plates.

Abstract: The Mount St. Helens rockslide-debris avalanche moved as three slide blocks. Slide block I occurred in association with a magnitude 5.1 earthquake at 8:32 a.m. Pacific Daylight Time (PDT) on May 18, 1980. An exploding cryptodome burst through slide block II to produce the "blast surge." Slide block III consisted of many discrete failures carried along by continuing pyroclastic currents generated from the exploding cryptodome. The hummocky 2.5-km³ debris-avalanche deposit consists of block facies (pieces of the pre-eruption mountain transported relatively intact) and matrix facies (a mixture of rocks from the old mountain and cryptodome dacite). Block facies is divided into five lithologic units. Matrix facies was derived from the explosively generated current of slide block III as well as from disaggregation and mixing of debris-avalanche blocks.

The debris avalanche dilated at the mountain rather than during transport. The debris-avalanche flow can be considered a grain flow, where particles - either debris-avalanche blocks or the clasts within the blocks - collided and created dispersive stress normal to the movement of material. The dispersive stress preserved the dilation of the material and allowed it to flow.

Note: The publication "Rockslide-debris avalanche of May 18, 1980, Mount St. Helens Volcano, Washington," was nearly ready for publication as a Professional Paper by the U.S. Geological Survey when Harry Glicken was killed at Mount Unzen, Japan on June 3, 1991. The death of Dr. Glicken slowed down the progress of publication, although it was eventually released as Open File Report 96-677 on the web page of the Cascades Volcano Observatory, U.S. Geological Survey. It can be accessed at <http://vulcan.wr.usgs.gov/Projects/Glicken/framework.html>.

The Geological Survey of Japan held a symposium on reduction of natural disasters in Asia in January, 1997. The GSJ decided to publish a special volume from this symposium in the Bulletin of the Geological Survey of Japan. Part of this special volume focuses on volcanic disaster, with an emphasis on debris avalanches. The 1980 Mount St. Helens debris avalanche is the most recent example of this hazardous phenomenon. The GSJ found the electronic publication of USGS Open File Report 96-677 by Harry Glicken to be the best description of the 1980 Mount St. Helens debris avalanche deposit. The GSJ asked the USGS for permission to include Glicken's publication in this special volume to distribute his excellent work to Japan and other Asian countries.

Unfortunately, length restrictions precluded full publication of the original document. To reduce the original contribution, we deleted many entire paragraphs that contributed peripherally to the description and interpretation of the debris avalanche. Physically, we reduced the font size, ran many paragraphs together and reduced the size of the figures, drawings and tables. Many photographs that did not provide data or visual confirmation of data were deleted. Figure and plate numbers differ from the original text; see the table for explanation appended to this text. We also delete references that do not appear in the abridged version.

We feel that the final reduced version retains the most useful descriptive material and interpretive discussion presented by Harry Glicken and preserves the important points of his classic contribution to the understanding of avalanche phenomenon. [Richard V. Fisher and Jon J. Major]

1. Introduction

The May 18, 1980 eruption of Mount St. Helens produced the largest mass movement in recorded history. The explosion that resulted from depressur-

ization of the volcano devastated the surrounding landscape, and the subsequent Plinian eruption produced tephra that spread around the world. Large volcanic debris avalanches are not uncommon around

Keywords: Mount St. Helens, 1980 eruption, volcano, debris avalanche, Cascade Mountain, Washington, debris avalanche hummocks, grain flow, blast surge, pyroclastic current, pyroclastic flow

*Geological Sciences, University of California, Santa Barbara (Deceased June 3, 1991)

volcanoes (Siebert, 1984) but they are not well understood. The 1980 debris avalanche at Mount St. Helens is the best exposed of these deposits. This detailed study of the geology of the 1980 Mount St. Helens deposit should provide information that will help interpret old, poorly-exposed deposits at volcanoes around the world.

2. Geology of the source area

2.1 General statement

The source of the rockslide-debris avalanche is the cone of Mount St. Helens. The 2.8-km³ crater (Fig. 1) was formed during the May 18 eruption as a result of the failure of the edifice because of the rockslide and the associated lateral blast. The geology of the volcano was mapped by C.A. Hopson (written commun., 1980) before 1980, and the walls of the crater were mapped by Hopson after the eruption (Hopson and Melson, 1982; written commun., 1984). Smith (1984) and Smith and Leeman (1987) studied the petrography and geochemistry of some of the pre-1980 rocks. Cross-sections of the mountain as it was just before the eruption (Fig. 2) were constructed using Hopson's work and pre-May 18 deformation data (Lipman and others, 1981; Moore and Albee, 1981; Jordan and Kieffer, 1981).

Three units are differentiated in the part of the pre-1980 mountain that became the debris-avalanche

deposit (Fig. 3). The older dacite unit makes up the core of the old mountain, forming the light-colored exposures in the crater below an altitude of about 7,000 to 7,500 ft (2,100 to 2,300 m), and it is overlain by the dark-colored andesite and basalt unit. The Goat Rocks and Summit domes, removed during the rockslide-debris avalanche, make up the modern dacite unit. The three pre-1980 units were intruded by a dacite magma body (called the cryptodome) in the weeks prior to the May 18 eruption.

2.2 Description of rock units

2.2.1 Older dacite unit

Hornblende-hypersthene dacite makes up the light-colored exposures in the crater below an altitude of about 7,000-7,500 ft (2,100 to 2,300 m). The rock consists of a complex assemblage of fresh and hydrothermally altered dome lavas and dome flank breccias (C.A. Hopson, written commun., 1984) that make up the core of Mount St. Helens (Figs. 2 and 4). This older foundation of Mount St. Helens was first recognized by Verhoogen (1937), who referred to the older dacite as "the old Mount St. Helens lavas."

The older dacite rocks in the crater are not dated. By correlation with exposures on the outside of the crater and stratigraphic position under andesites and basalts dated by paleomagnetic and radiocarbon methods, the older dacite unit is assigned an age of pre-Castle Creek (Fig. 3), older than 2,500 years (Hopson and Melson, 1982). Most of the older dacite in the crater is likely of Pine Creek age, 2,500 to 3,000 years old (C.A. Hopson, written commun., 1986).

2.2.2 Andesite and basalt unit

Dark-colored andesite and basalt in the crater, termed the "andesite and basalt unit," rest on the older dacite unit. These rocks are lava flows as well as lithic and scoriaceous tephra of andesitic and basaltic composition. They are correlated with the eruptive products of the Castle Creek and Kalama eruptive periods (Fig. 3) that were mapped on and around the flanks of the pre-1980 mountain (C.A. Hopson, written commun., 1980) and dated at about 2,200 to 350 yr B. P. (Mullineaux and Crandell, 1981). However, some of these rocks in the crater are magnetized in a direction characteristic of rocks dated at 2,500-3,000 yrs (R.T. Holcomb, oral commun., 1981).

2.2.3 Modern dacite unit

Dacite named here the "modern dacite unit" was present on the pre-eruption cone of Mount St. Helens. It consists of the Goat Rocks dome of the Goat Rocks eruptive period and the Summit dome of the Kalama eruptive period (Fig. 3) as well as deposits of hot avalanches from these domes. The domes themselves were carried away in the rockslide-debris avalanche of May 18, but the hot avalanche deposits remain on

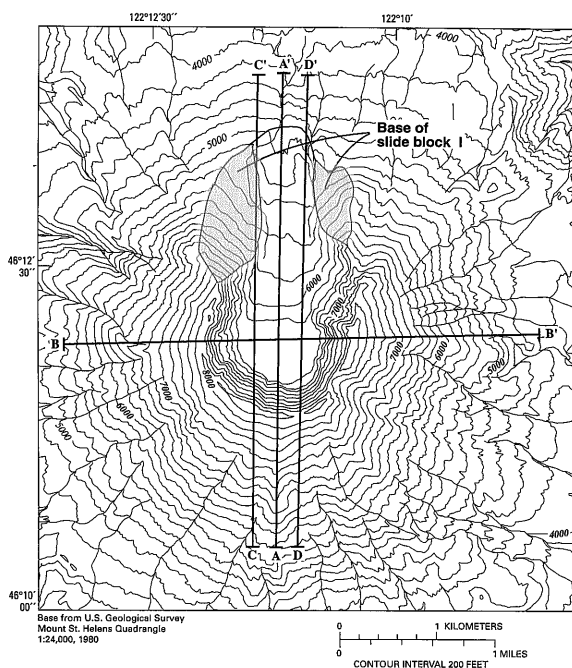


Fig. 1 Topographic map of volcanic edifice and crater formed on May 18, 1980. Map shows inferred base of slide block I, and locations of cross sections A-A', B-B', C-C', D-D' of Fig. 2. Base from Mount St. Helens quadrangle map (1:24,000 scale; map date 1983), which shows summer 1980 topography. Contour interval 200 feet.

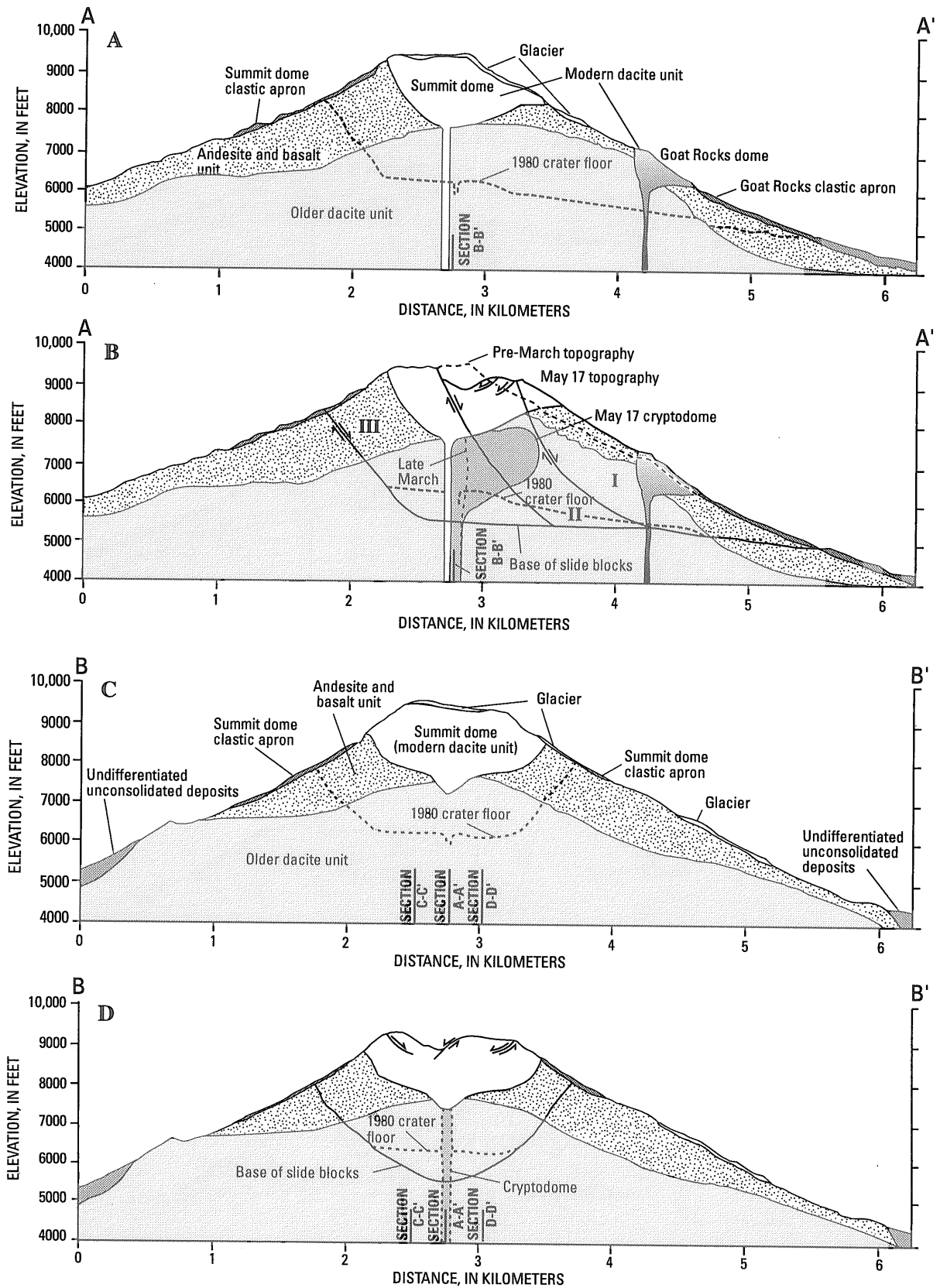


Fig. 2 Cross sections of Mount St. Helens. I,II,III are slide blocks. Locations on Fig. 1. A, A-A' pre-March 1980. B, A-A' at time of failure, 8:32 AM, May 18, 1980. C, B-B' pre-March 1980. D, B-B' at time of failure. E, C-C' pre-March 1980. F, C-C' at time of failure. G, D-D' pre-March 1980. H, D-D' at time of failure.

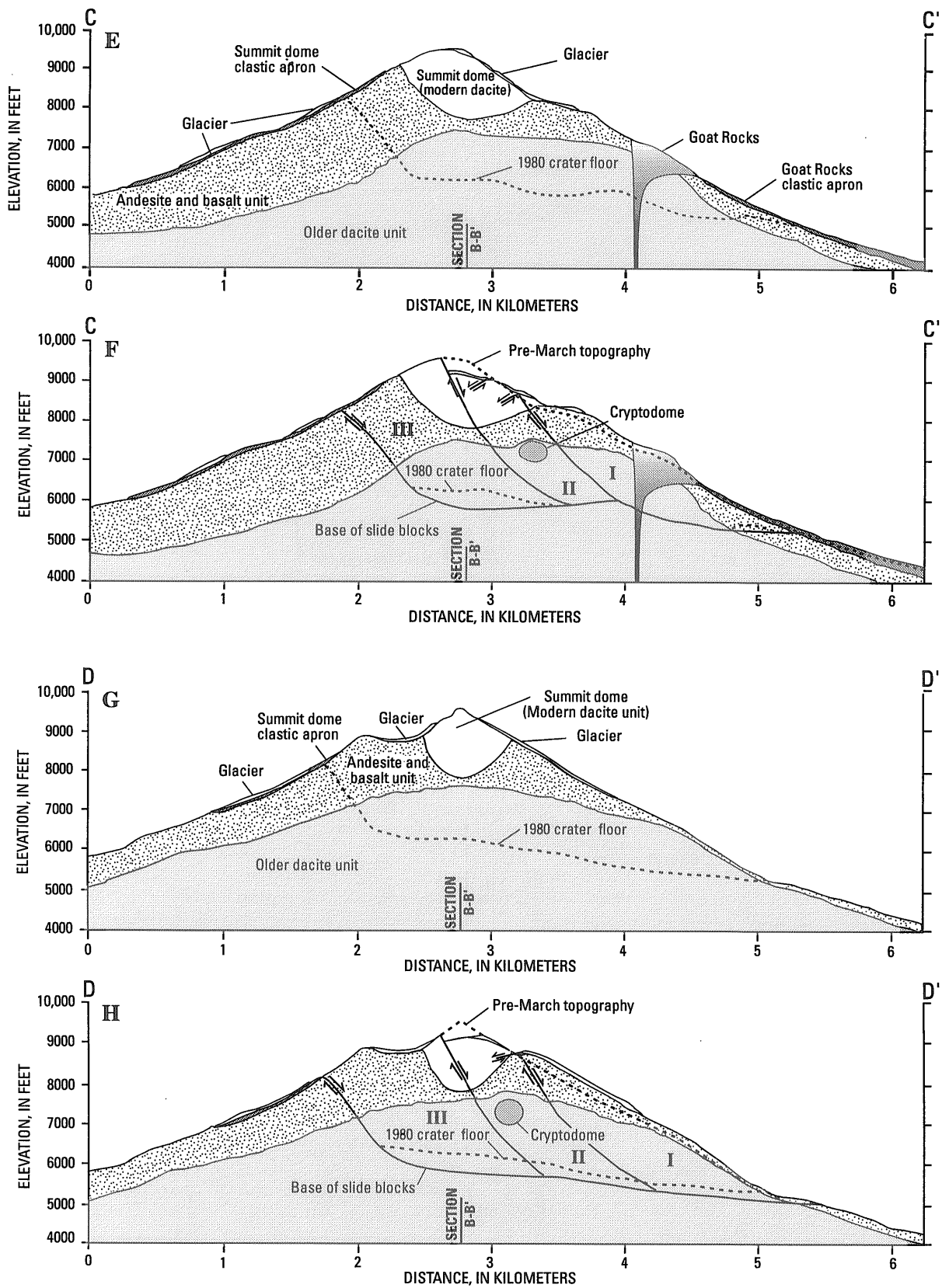


Fig. 2 (Continued.)

the flanks. Summit dome was dated by Hoblitt and others (1980) to be approximately 350 yr old. More recent tree-ring analyses suggest that dome emplacement began in A.D. 1647 and that the dome was intermittently active for about 100 years (Yamaguchi and Hoblitt, 1995). Goat Rocks was dated at approximately 123 to 180 yr before 1980 (Hoblitt and others, 1980). Tree-ring evidence indicates the dome was active in A.D. 1842-1843 (Yamaguchi and Lawrence, 1993). The rocks are called "modern" dacite to distinguish them from the older dacite, which is older than 2,500 yr. The rocks from the Goat Rocks and Summit domes are indistinguishable from each other in hand specimen and thin section (Table 1; Fig. 4). Moreover, available chemical analyses (Hoblitt and others, 1980; Smith and Leeman, 1987; C.A. Hopson, written commun., 1984) show considerable overlap in the chemical compositions (Fig. 5).

2.2.4 Cryptodome

The dacite magma body that rose up inside the mountain prior to May 18 is known as the cryptodome. The cryptodome was almost all molten material; on the exposed 1980-86 dome at Mount St. Helens, the outer margin cooled at a rate of <5 cm/day (Dzurisin and others, 1990). Because the cryptodome was not exposed, its rate of cooling was probably much less, and the cryptodome was <2 months old on May 18.

The rock that formed from this cryptodome was found throughout the blast deposit and parts of the debris-avalanche deposit. It is a distinctive gray, microvesicular to subpumiceous hypersthene-hornblende dacite (Hoblitt and others, 1981; Hoblitt and Harmon, 1993) called the juvenile "blast" dacite. Clasts of the dacite are characterized by prismatic jointing when struck with a hammer, indicating that the rock was hot when the deposits were emplaced. Clasts commonly have one or more breadcrusted surfaces.

2.3 Pre-eruption structure

Cross sections of the volcano as it existed prior to the 1980 eruptions were constructed from geologic maps of the old volcano (C.A. Hopson, written commun., 1980) and measured sections of the 1980 crater (C.A. Hopson, written commun., 1984). Three cross sections trend approximately north-south through the axis of the crater, and one trends approximately east-west perpendicular to the axis (Fig. 2). Preliminary cross sections were constructed by Voight and others (1981, 1983) and Moore and Albee (1981).

The structure of the part of the pre-1980 volcano that was removed in the rockslide was relatively simple (Figs. 2A,C,E,G). The older, pre-Castle Creek dacite made up the bulk of the mountain and was topped by the andesite and basalt lavas of the Castle

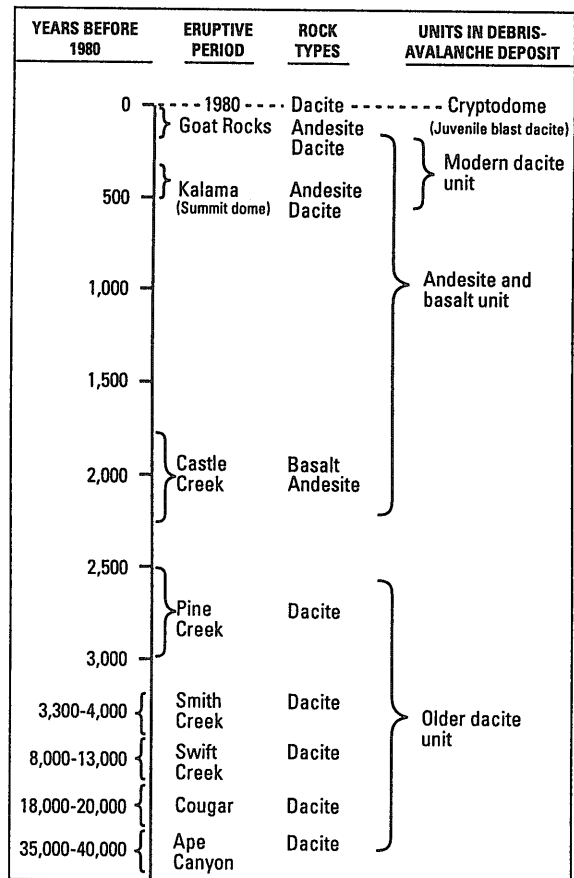


Fig. 3 Eruptive periods of Mount St. Helens that produced rocks in debris avalanche, showing generalized units designated for this work. After Mullineaux and Crandell (1981).

Creek and Kalama eruptive periods. Feeders for the modern dacite domes (Goat Rocks dome and Summit dome) intruded through the older dacite and the andesite and basalt units. According to C.A. Hopson (Hopson and Melson, 1985), the Summit dome erupted into a summit crater at the beginning of the Kalama eruptive period. The volcano rests on well-lithified Tertiary bedrock (Evarts and others, 1987).

The intrusion that was unroofed in the May 18 lateral blast (the cryptodome) deformed the north side of the mountain (Fig. 2B). Displacements of various points within a 1.5- by 2.0-km area (called "the bulge"), which were measured by geodetic techniques, showed subhorizontal northerly movements of 1.5-2.5 m/day (Lipman and others, 1981). Comparison of topographic maps made from aerial photographs taken in 1979 and at various times during March-May 1980 (Voight and others, 1981; Jordan and Kieffer, 1981; Moore and Albee, 1981) shows dominantly northerly movements with local uplift of as much as 5.6 m/day. Moore and Albee (1981) modeled the geometry of the cryptodome as a bulbous mass slightly displaced to the north of the summit crater. Voight and others (1981, 1983) inferred a thick, sheetlike body

Table 1 Modal analyses of modern dacite rocks from Mount St. Helens. [All samples from C.A. Hopson unless noted. plag, plagioclase; hbl, hornblende; opx, orthopyroxene; cpx, clinopyroxene; opaque, opaque minerals; xeno, xenolith; grdms, groundmass; vesicle, vesicles]

Rock	plag	hbl	opx	cpx	opaque	xeno	grdms	vesicle	Total
Goat Rocks									
259-1	416	3	87	5	26	36	413	19	1003
442-1	399	7	65	5	16	8	446	53	1000
28-1	435	9	52	6	22	64	430	23	1040
1318-6	373	5	76	4	17	52	387	87	1001
8117#1 ¹	311	4	72	7	34	15	471	47	1001
8171#2 ¹	333	13	67	5	24	27	465	57	1000
Summit dome									
394-1#1	387	11	48	2	29	4	466	63	1010
394-1#2	416	11	33	1	17	3	482	59	1020
355-2	414	6	70	5	37	1	415	53	1001
151-1#1	423	18	46	2	33	2	472	25	1017
151-1#2	351	15	67	1	27	50	536	21	1022
1337-3	470	14	37	8	24	25	410	16	1004
Modern dacite from debris avalanche (unkown dome)									
913G#1 ¹	385	5	24	2	27	26	549	1	1000
913G#2 ¹	400	3	50	3	27	25	503	3	1011

¹Collected by author in 1981.

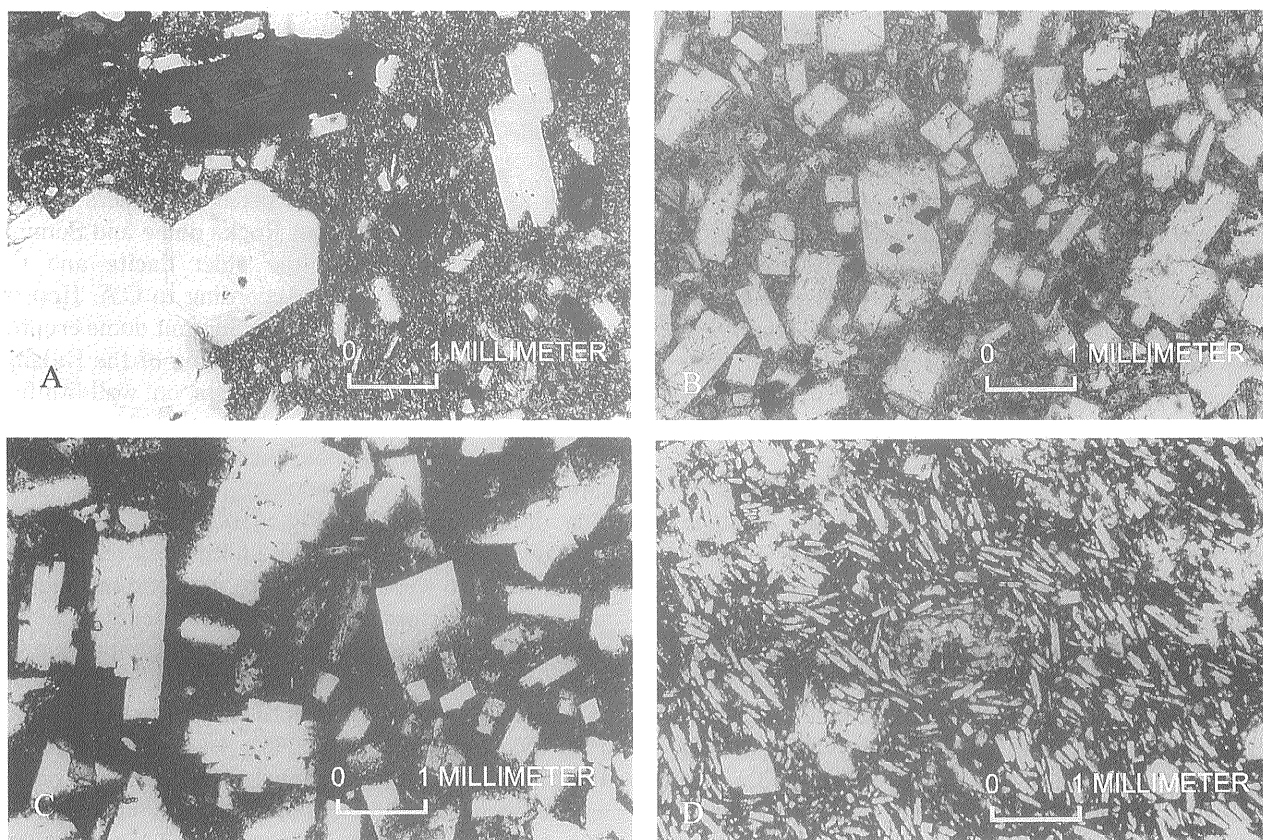


Fig. 4 Thin sections of rock from the old mountain. A, Older dacite. B, Modern dacite. C, Andesite. D, Basalt.

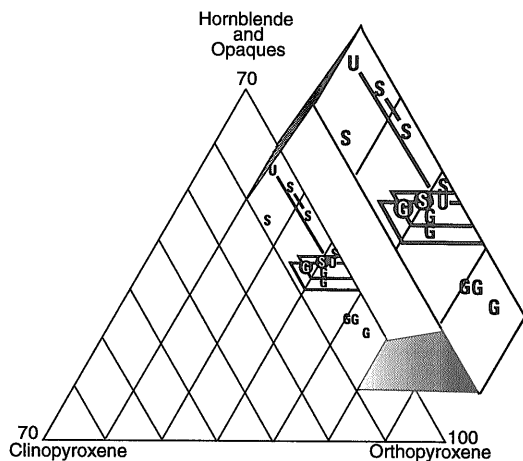


Fig. 5 Ternary diagram of orthopyroxene, clinopyroxene, and hornblende+opaques for modern dacite dome rocks. S, summit dome; G, Goat Rocks dome; U, modern dacite of unknown origin from debris-avalanche deposit. Lines between points indicate duplicate thin sections of same rock. Boxes represent error at 95.4 percent confidence level (Kelley, 1971) for samples contained in circles.

bending in a northward direction within the andesite and basalt lavas.

The volume increase of the volcano from March to May 17, 1980, is calculated to have been 0.11-0.12 km³ (Moore and Albee, 1981; Jordan and Kieffer, 1981). This is more than the 0.08 km³ volume of the cryptodome found within the deposits; about 0.05 km³ was found in the blast surge deposit (Moore and Sisson, 1981) and about 0.03 km³ in the debris-avalanche deposit. The difference may be due in part to inaccuracies in the methods used to compute volumes, it may reflect volume increase owing to dilation of the material that made up the mountain or injection of fluids released from the magma (Voight and others, 1981), or the difference may result from cryptodome material exploding into ash too fine to be recognized as juvenile in the deposits.

2.4 Geology of the slide blocks

The initial movement of the rockslide-debris avalanche is modeled as three slide blocks (Fig. 2; Table 2). The slide blocks represent a series of retrogressive

A. Slide blocks in each cross section						
Slide block	Cross section				Mean	Volume using means and assuming 3.0 km ³ total volume (km ³)
	A-A'	C-C'	D-D'	(percent)		
I	32	33	32	32		0.96
II	24	23	27	25		0.75
III	43	44	41	43		1.29

B. Geologic units in each slide block without cryptodome and Goat Rocks												
Unit	Slide block											
	I				II				III			
	A-A'	C-C'	D-D'	Mean	A-A'	C-C'	D-D'	Mean	A-A'	C-C'	D-D'	Mean
Older dacite unit	50	46	67	54	69	51	64	61	51	46	55	51
Andesite and basalt unit	45	52	33	43	2	19	17	12	27	36	37	33
Modern dacite unit	5	2	0	2	30	31	20	27	21	18	7	15

Using means computed above including Goat Rocks and cryptodome												
Older dacite unit	52				56				49			
Andesite and basalt unit	42				11				31			
Modern dacite unit	5				25				14			
Cryptodome	0				8				5			

Table 2 Slide blocks in each cross section and geologic units in each slide block. [Based on analysis of Fig. 2; methodology discussed in text. Total volume of slide blocks includes source area for debris avalanche (including proximal units), blast, and lithic airfall deposits]

slope failures. Slide blocks I and II were individual discrete failures, but the area outlined as slide block III probably generated many discrete, successive failures that mixed with juvenile (cryptodome) and non-juvenile material generated from the continuing blast explosions (Voight and others, 1983).

3. Geometry of the deposit

The debris-avalanche deposit covers about 64 km², including the material within Spirit Lake. Nearly all the deposit is contained in a contiguous mass measuring about 26 km from the east to west ends along its axis, and from 0.5 to 5 km wide measured perpendicular to the axis. The longest travel path of the debris avalanche was 29 km, measured from the source of the material (taken as the site of the 1980-85 lava dome) to the distal (west) end.

3.1 Volume and thickness

An isopach map of the material in the North Fork Toutle River valley and in the valley of South Coldwater Creek was constructed by K.A. Cameron (written commun., 1982) using 1:24,000-scale topographic maps based on summer 1980 aerial photographs as well as 1954 1:62,500-scale maps. The volume of the material on the isopach map was computed to be 2.3 km³ (K.A. Cameron, written commun., 1984). Adding the 0.43 km³ of material in Spirit Lake (Meyer and Carpenter, 1982) and subtracting the 0.25 km³ volume of the 1980 pyroclastic-flow deposit (C.W. Criswell, written commun., 1985) gives a net volume of 2.5 km³ for the debris-avalanche deposit. This value is based on more accurate data than the preliminary estimate of 2.8 km³ (Voight and others, 1981, 1983). Neither calculation includes the approximately 0.2 km³ of the crater-filling proximal unit.

The thickness of the debris-avalanche deposit is in part a function of the underlying topography and the configuration of the valley walls. The deposit is thickest and the surface has the greatest relief and the largest hummocks in the channel of the pre-eruption North Fork Toutle River.

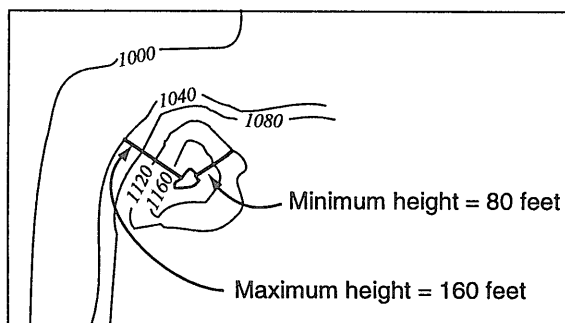


Fig. 6 Example of a hummock on a topographic map, showing maximum and minimum measured heights.

3.2 Morphology of hummocks

Hummocks are the most characteristic morphologic feature of the debris avalanche deposit. Various parameters of hummocks were measured on 1:24,000-scale USGS topographic maps (with a 40-ft [12.2 m] contour interval) made from summer 1980 aerial photographs. The measurements quantify the characterization of the morphology and provide clues regarding the emplacement of the deposit.

For the purpose of the topographic map analysis, a hummock is considered to be represented by one or more closed contours (Fig. 6). The minimum height of a hummock is measured as: (number of closed contours - 1) x 40 ft [12.2 m]. The maximum height of a hummock is measured as: (number of contours to base of slope - 1) x 40 ft [12.2 m].

The volume of each hummock is calculated by multiplying the area of each closed contour by the contour interval (40 ft) and adding the volume increments together. The 40-ft contour interval limits the accuracy of the measurements. The contour interval results in a total error of ± 20 ft [6.1 m] for the measurements of hummock heights. The error for the hummock volume is: ± 20 ft [6.1 m] x area of the largest closed contour. Six hundred seventy-five hummocks were identified on the 1:24,000-scale topographic maps. The hummocks of the proximal unit on the north flank of the mountain and in the crater were not used in this analysis. The maximum and minimum heights, length, width, and orientation of the long axis for each hummock were measured and the volume of each hummock was calculated. Fig. 7 illustrates hummock size relations versus distance from source.

3.3 Orientation of elongate hummocks

The long axes of elongate hummocks of the debris-avalanche deposit generally are aligned approximately with the direction of flow of the avalanche. However, at the distal end of the debris-avalanche deposit, and at the constrictions in the valley of the North Fork Toutle River where much of the avalanche material stopped, the hummocks have relatively random orientations.

3.4 Hummock types

The hummocks of the debris-avalanche deposit are divided into three different types based on the relation of block facies to matrix facies (Fig. 8). Block facies consist of debris-avalanche blocks, unconsolidated or poorly consolidated pieces of the old mountain transported relatively intact. Matrix facies is an unconsolidated mixture of all rock types from the old mountain and the juvenile dacite; it contains clasts that range in size from microns to meters.

Type A, block facies hummocks with no matrix facies. One or more debris-avalanche blocks extend from hummock to hummock (Figs. 8 and 9A). There

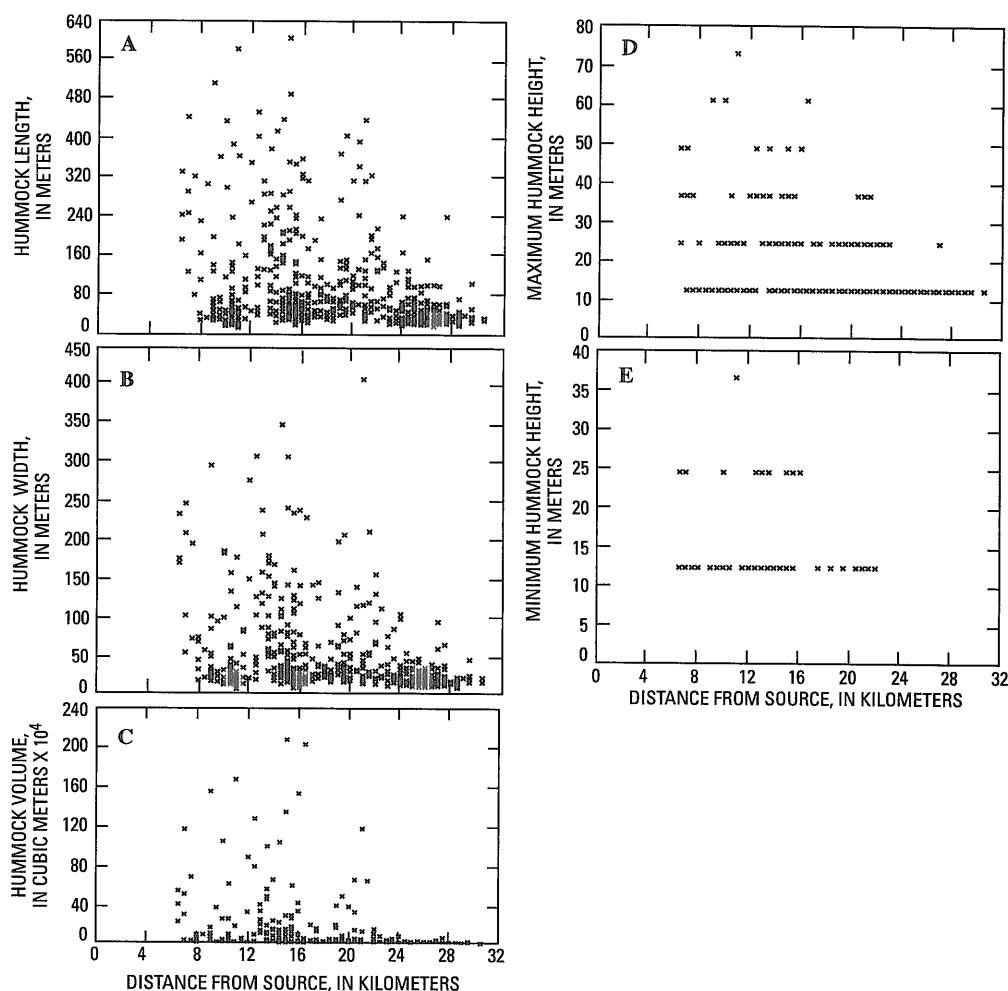


Fig. 7 Hummock parameters versus distance from source. A, Length versus distance from source. B, Width versus distance from source. C, Volume versus distance from source. D, Maximum height versus distance from source. E, Minimum height versus distance from source.

is no matrix facies in the hummocks or in the inter-hummock areas. Most of the hummocks of the eastern part of the debris-avalanche deposit are type A hummocks.

Type B, predominantly matrix facies hummocks. These hummocks are made up almost entirely of matrix facies (Figs. 8 and 9B). Vertical exposures show that there is no debris-avalanche block at the cores of the hummocks, but there may be small debris-avalanche blocks scattered throughout the hummocks (Fig. 8). These hummocks are generally much smaller than type A hummocks.

Type C, hummocks made of debris-avalanche blocks resting in matrix facies. These hummocks are made entirely of large debris-avalanche blocks of the block facies that rest in and likely were carried by the matrix facies (Figs. 8 and 9C). Type C hummocks occur only in the western part of the deposit. At other volcanic debris-avalanche deposits (for example, the deposit north of Mount Shasta, Calif.; Crandell and others, 1984), most of the hummocks are interpreted

to be type C hummocks, but type C hummocks are very rare in the Mount St. Helens debris-avalanche deposit.

3.5 Formation of the hummocks

Three mechanisms caused the formation of the hummocks. Many hummocks probably formed from a combination of two or more of the proposed mechanisms.

Mechanism 1. Some hummocks represent the horsts of a simple horst and graben system (Voight and others, 1981, 1983). This is most evident in type A hummocks, where contacts from the old mountain were preserved intact during transport and the contacts are faulted down between the hummocks.

Mechanism 2. Some hummocks probably represent the surface topography of debris-avalanche blocks (pieces of the old mountain). This is illustrated by hummocks that show strata parallel to the surface of the hummock, not faulted down between hummocks. In the eastern part of the avalanche deposit, these

hummocks are type A hummocks, where debris-avalanche blocks about debris-avalanche blocks. In the eastern part of the deposit the orientations of the long axes of several hummocks are transverse to the direction of flow of the debris avalanche, and the hummocks are anomalously large, suggesting that they were formed by mechanism 2. In the western part of the deposit, these hummocks are type C hummocks, where debris-avalanche blocks are suspended in matrix facies and a hummock is made of only one debris-avalanche block.

Mechanism 3. Some hummocks (both type A and type B) formed as material was decelerated by basal or lateral shear. There are two classes of hummocks formed by this mechanism.

3A. Hummocks with long axes parallel to flow. Many hummocks with long axes parallel to the direction of flow probably formed as material decelerated by basal shear was sculpted by material moving at a higher speed. Hummocks adjacent to valley walls can be considered to be levees. The levees are interpreted to represent "dead regions" (Johnson and Rodine, 1984) at the flow margins of a Coulomb-viscous material.

3B. Hummocks with randomly oriented long axes. Near the terminus of the deposit, as well as just upstream from constrictions in the valley of the North Fork Toutle River, the debris avalanche decelerated as a result of basal shear and piled up. In these areas, the hummocks are either not elongate or are elongate with randomly oriented long axes. Wood-bearing hummocks of the distal 4 km of the debris-avalanche deposit (the distal material) display relations that are suggestive of the mechanism of hummock formation in these areas. In the distal area, tree orientation is random in the hummocks, but between the hummocks, the trees are oriented parallel to the direction of flow.

3.6 Interpretation of size data

Fig. 7 shows that the number of large hummocks decreases with distance from source. This is interpreted to reflect decreasing debris-avalanche block size as well as the increasing amount of matrix-facies material with distance from source. Type A hummocks are generally made up of one or a few debris-avalanche blocks and are generally formed by mechanisms 1 and 3. As the debris-avalanche blocks broke up during transport, smaller hummocks formed from the smaller debris-avalanche blocks. Hummocks consisting primarily of matrix facies material (type B hummocks) are present only in the western part of the avalanche deposit - these hummocks are generally much smaller than the type A hummocks that characterize the eastern part of the deposit. Type C hummocks are rare and have little effect on the plots.

The size parameters (Fig. 7) show evidence of a "background" of small hummocks throughout the

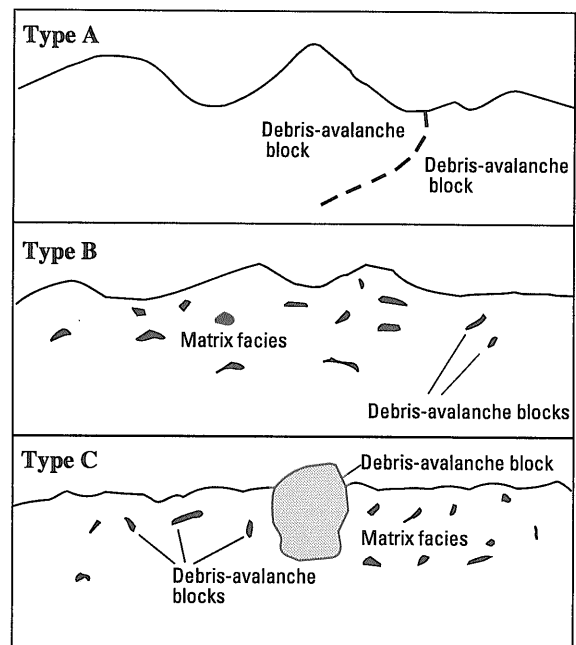


Fig. 8 Hummock types. Type A, block facies with no matrix facies. Type B, predominantly matrix facies, debris-avalanche blocks scattered throughout. Type C, debris-avalanche block suspended in matrix facies; matrix facies probably carried debris-avalanche block.

deposit. The smaller hummocks are far more common than larger hummocks. This suggests that in all parts of the debris avalanche, small volumes of homogeneous material (debris-avalanche blocks or aggregates of blocks with similar properties) are more common than larger debris-avalanche blocks.

4. Geological maps of the deposit

4.1 General statement

Two kinds of geologic maps of the debris avalanche were compiled for this report. Units in the first kind (Pl. 1) are defined primarily on the basis of morphology. The second kind (Pl. 2) is a detailed geologic map of lithologic units in the debris-avalanche deposit.

An important purpose of the geologic maps is to provide a basis for improved understanding of the processes of flow and emplacement of the debris avalanche. Examination of the patterns of units on these two kinds of maps allows interpretation of the various phases of flow of the debris avalanche and leads to interpretations of relative velocities of various parts of the once-moving mass. The lithologic map of the debris-avalanche deposit allows interpretation of the travel paths of parts of the material from their original positions on the cone to their eventual sites of deposition.

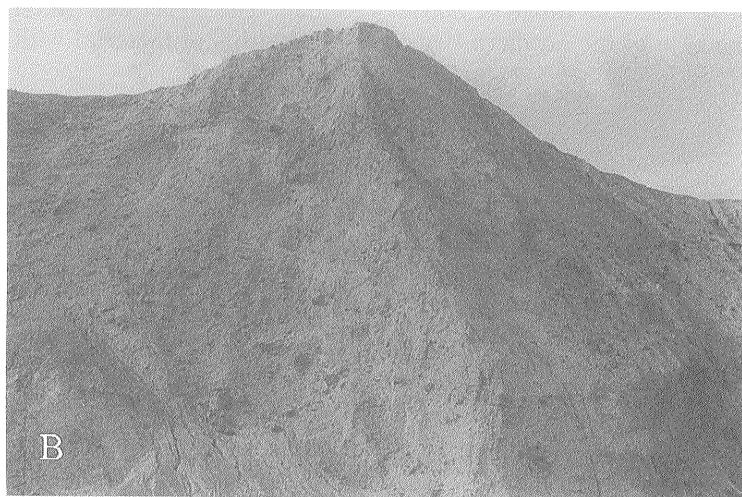


Fig. 9 Photographs of types of hummocks. A, Type A. Oblique aerial photograph looking east toward Spirit Lake. View about 500 m wide. Hummocks are horsts in single debris-avalanche block. Contact of dark andesite and basalt unit overlying light-colored, older dacite unit preserved intact from old mountain. B, Type B. Hummock composed primarily of matrix facies. Small debris-avalanche blocks are scattered throughout the hummock. C, Type C. Debris-avalanche block suspended in matrix facies. Note person for scale (circle).

4.2 Morphologic map of the debris-avalanche deposit

Six morphologic map units are defined within the avalanche deposit (modified slightly from Voight and others, 1981). They are referred to here as the North Fork, Johnston Ridge, Spirit Lake, marginal, proximal, and distal units, named according to representative locations in the deposit (Pl. 1). Other kinds of deposits of the May 18 eruption, including blast deposits, lahar deposits, and pyroclastic-flow deposits (Lipman, 1981), partly cover the avalanche deposit and are mapped where they conceal the hummocky surface.

4.2.1 North Fork unit

The North Fork unit comprises the bulk of the debris-avalanche deposit. It is defined as the part of the debris-avalanche deposit between and including the levees in the valley of the North Fork Toutle River that did not encounter Johnston Ridge or Spirit Lake. It extends from the base of the northern flank

of the mountain to within 1 km of the distal end. The most characteristic morphologic feature of the North Fork unit is hummocks (Fig. 10) that have as much as 75 m of relief. The shape of the hummocks is very irregular, but some are roughly circular in plan and rise to a peak or a dome. Locally, they are elongate in the direction of flow and are difficult to distinguish from levees. Levees as much as 30 m high are also characteristic features of the North Fork unit. Levees are defined as linear ridges near the margins of the avalanche deposit that locally widen into linear zones of irregular positive topography (Fig. 11). The morphology of the levee that blocks Coldwater Lake suggests that it is an imbricate structure made up of discrete masses of debris separated by thrust faults. The chaotic lithologic pattern of the area (Pl. 2) is consistent with a thrust imbricate structure, even though the imbrication is not readily apparent on the map. The structure is interpreted to result from the deposition of material with enough shear strength to

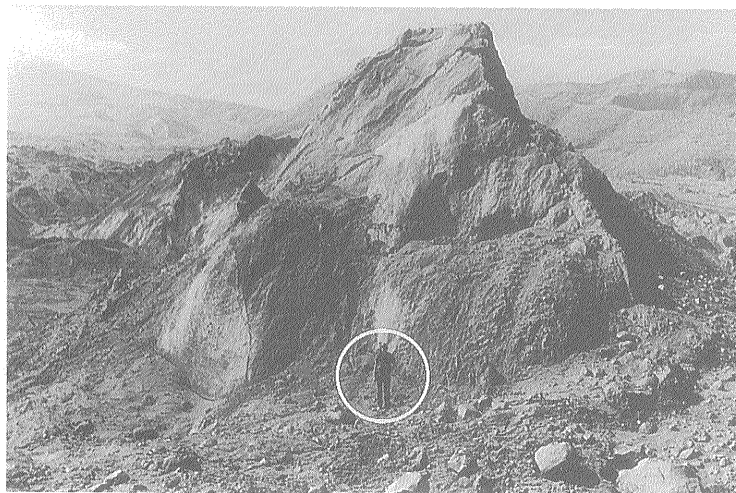


Fig. 10 Typical hummock of North Fork unit. Note person for scale (circle).

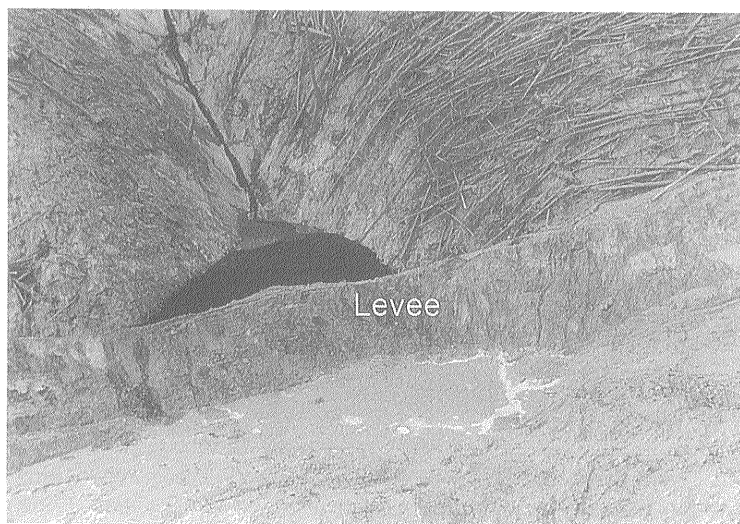


Fig. 11 Levee of North Fork unit blocking mouth of small stream near sample locality DXS-32. Blasted trees rest on Tertiary bedrock.

remain intact except along narrow zones.

Closed depressions are also common features of the North Fork unit. Most of the depressions that are irregular in plan usually represent interhummock areas. A few of the closed depressions are roughly circular, measure as much as 240 m wide and 50 m deep, and have sides considerably steeper than the surrounding local relief (base map of Pl. 2). Nearly all the circular closed depressions visible on the topographic maps probably formed within hours to days after emplacement of the debris-avalanche deposit. The circular closed depressions (craters) are interpreted to have been formed by collapse into void space. The void space may have been between debris-avalanche blocks of the block facies or may have been created by melted glacial ice. Most of the ice must have melted within hours to days after emplacement. However, ice was observed on the surface of the deposit for many weeks after May 18 and ice was uncovered during excavations for an outlet for Spirit Lake in summer 1982 (Glicken and others, 1989). Some authors (for example, Fairchild, 1985, 1987) suggest that most of the collapse craters resulted from collapse into void space created by melted ice. However, when the rockslide expanded by more than 20 percent to become the debris-avalanche deposit (see "Texture of the Deposit"), 0.4 km³ of void space was created. This amount is far more than the total void space that would have been created had the 0.1 km³ of ice incorporated in the debris avalanche (Brugman and Meier, 1981) melted completely. This suggests that most of the collapse craters resulted from collapse into void space in the debris-avalanche deposit created during dilation and breakup of the rockslide material rather than from collapse into void space created by melting ice.

There were numerous channels near the distal end of the debris-avalanche deposit the day after emplacement. On the afternoon of the eruption, I witnessed some of these channels being filled with flowing mud. Multiple terraces of lahar deposits along these channels suggest that repeated lahar flows, or a lahar with varying depth, came down the channel. The channels probably were eroded by the lahars generated on the debris-avalanche deposit (Fairchild, 1985, 1987). The main channel is the path of the major lahar that flowed west down the North Fork Toutle River valley. The tributary channels likely formed from headward retreat of slumps of the main channel walls.

4.2.2 Johnston Ridge unit

The Johnston Ridge unit is defined as those parts of the debris-avalanche deposit that interacted with Johnston Ridge, and it is present only on and adjacent to Johnston Ridge. It is as much as 195 m thick. In tributary basins of the North Fork Toutle River on the south slope of Johnston Ridge, the debris ava-

lanche has formed thick (as much as 195 m) deposits that are perched as high as 150 m above the deposit in the North Fork Toutle Valley. In a tributary channel just west of Harry's Ridge, the Johnston Ridge unit forms a ramp that extends from the Pumice Plain to the top of Johnston Ridge. This feature is called "The Spillover." The debris avalanche crossed Johnston Ridge at The Spillover and at a pass 1 km west of The Spillover. The debris avalanche scoured Johnston Ridge and adjacent Harry's Ridge of all soil and trees before depositing material in South Coldwater Creek, just north of Johnston Ridge (Fisher and others, 1987).

4.2.3 Spirit Lake unit

The Spirit Lake unit is that part of the debris-avalanche deposit that moved to the northeast and displaced Spirit Lake. The Spirit Lake unit occurs only in the region surrounding the lake. It is only a few meters thick on the shores of the lake, but it is as much as 100 m thick beneath the lake (Meyer and Carpenter, 1982). The avalanche and blast caused a seiche to rise up from the lake. The seiche, along with the avalanche itself, scoured the trees, vegetation, and soil from the ridges adjacent to the lake to heights of more than 260 m (Voight and others, 1981). The scoured area is part of the area designated as the "tree removal zone" by Lipman (1981).

4.2.4 Marginal unit

The marginal unit, as much as 75 m thick, backfills tributaries of the North Fork Toutle River. It is defined as the parts of the debris-avalanche deposit on the valley wall side of the levees of the North Fork unit. It generally forms lobate deposits, but hummocks that closely resemble those in the valley of the North Fork Toutle River are also locally present. The lobes of the marginal unit are truncated by levees of the North Fork unit. This distribution suggests that the marginal unit was pushed in front and to the side of the main mass of the moving debris avalanche and came to rest while the North Fork material was still in motion.

4.2.5 Proximal unit

The proximal unit is the part of the debris-avalanche deposit in the crater and on the north slope of Mount St. Helens. Hummocks of this unit in the north part of the crater are some of the largest hummocks in the debris avalanche; they are as much as 100 m high and 1,000 m wide. Proximal hummocks are much smaller on the mountain slope just north of the crater.

There is abundant evidence for interaction of the debris avalanche with older deposits on the flank of Mount St. Helens that underlie the proximal unit. Scratches resembling glacial striations, interpreted to result from abrasion of the underlying material by the

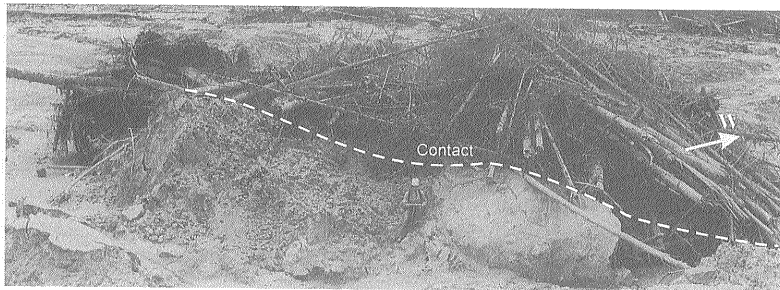


Fig. 12 Dipping contact between distal and North Fork units. Contact dips 5-7° to west.

debris avalanche, are present on most of the surface of the older deposits. On the northeast flank, there are drumlin-shaped remnants of pre-1980 volcanoclastic deposits. All but minor bits of vegetation was stripped from the north flank.

4.2.6 Distal unit

The distal unit, present only at the west end of the debris-avalanche deposit, consists primarily of jumbled mounds of broken trees, wood debris, and organic soil. Mixed with this material are volcanic clasts from Mount St. Helens, in proportions of as much as 30 percent. Also incorporated into the distal unit are pavement fragments and other miscellaneous debris from the North Fork Toutle River valley. The material is generally <10 m thick and probably averages about 5 m thick. Hummocks in the distal unit are very similar in shape and size to those on the west end of the North Fork unit (Pl. 2). They are as much as 9 m high and generally roughly circular in plan. Unlike the hummocks of the North Fork unit, they bristle with trees. The distal unit has a flow front that is as much as 8 m high. Locally, more fluid parts of the unit ramp down from the main mass of material and grade into the lahar deposits of the North Fork Toutle River valley (Fig. 12).

4.3 Lithologic map

Six lithologic units of the debris avalanche are differentiated on the lithologic map (Pl. 2). The older dacite, modern dacite, andesite and basalt, and modern undifferentiated units make up blocks within the block facies (pieces of the old mountain that were transported from their origin relatively intact). The mixed block and matrix facies is composed of blocks of varying lithology as well as the matrix facies, a blended mixture of all rock types from the old mountain, the juvenile blast dacite, and material picked up from the surrounding terrain. Texture and facies are discussed in more detail in "Texture of the deposit." The distal unit is included on the lithologic map; it is described in the preceding section.

4.3.1 Block facies units

(1) Older dacite unit

The older dacite unit consists almost entirely of the hornblende-hypersthene dacite from pre-Castle Creek (older than 2,500 yr) of Mount St. Helens (C.A. Hopson, written commun., 1984; Fig. 13). It is derived from the older dacite unit observed in the 1980 crater. The rock types in the older dacite unit in the debris-avalanche deposit are identical to those in the older dacite unit in the crater. The hornblende-hypersthene dacite is readily recognizable in the field because it has abundant large (>2 mm length) phenocrysts of plagioclase and hornblende. Xenoliths of varying composition are locally present.

(2) Andesite and basalt unit

The andesite and basalt unit is rubble consisting of two-pyroxene andesite and olivine basalt (Fig. 14). The rocks are derived from andesite and basalt lava flows and volcanoclastic rocks from the Castle Creek, Kalama, and Goat Rocks eruptive periods of Mount St. Helens (C.A. Hopson, written commun., 1980), now exposed in the upper part of the 1980 crater. The andesites and basalts are generally black or dark gray but locally are various shades of red and very dark green when hydrothermally altered. The andesites, which are generally plagioclase porphyritic, contain varying amounts of hypersthene and augite. Olivine is rare and usually occurs as phenocrysts <1 mm wide. The basalts generally are olivine phyric. Both andesite and basalt are variably vesicular and locally are extremely scoriaceous. Small amounts of foreign rock types were mixed locally with the andesite and basalt unit. Counts of approximately 100 clasts at selected exposures (Table 3) indicate that locally as much as about 40 percent of the material is composed of rock other than andesite and basalt.

(3) Modern dacite unit

The modern dacite unit is rubble composed of augite-hornblende-hypersthene dacite derived from the Goat Rocks and Summit domes of the modern (<2,500 years old) cone of Mount St. Helens. It is light gray where fresh and various shades of red and pink where altered. The nearly aphyric dacite contains microphenocrysts of hornblende, pyroxene, and plagioclase. The rock is distinguished from the older dacite by the smaller (<2 mm long) size of the hornblende phenocrysts. Inclusions of various compo-

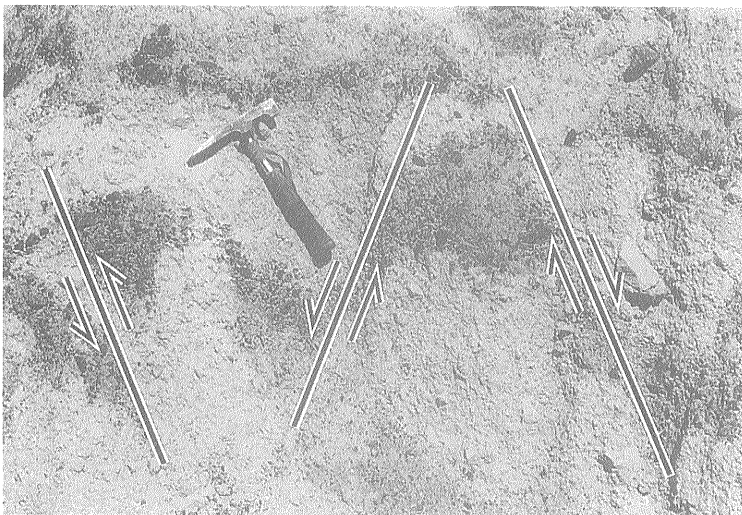


Fig. 13 Narrow and elongate volcanic dikes in older dacite unit of debris-avalanche deposit cross cut by faults.

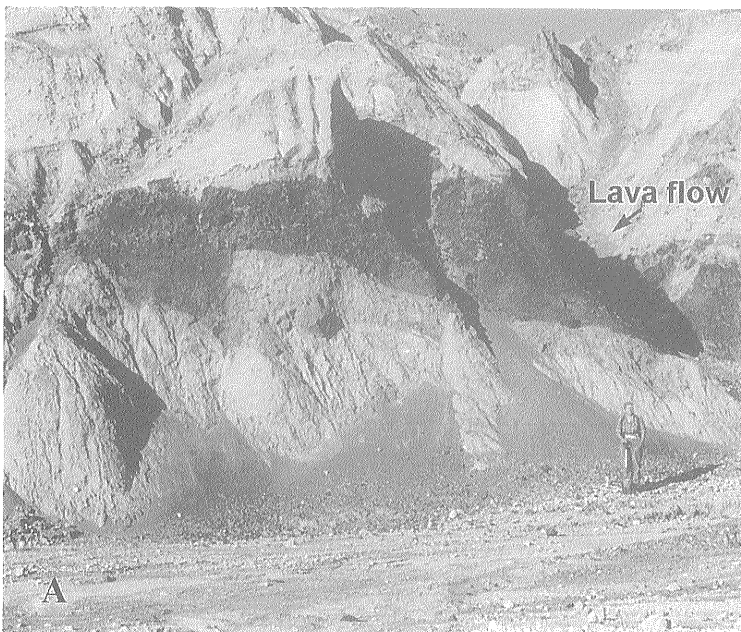


Fig. 14 Lava-flow stratigraphy in debris-avalanche deposit. Clasts in lava flows are shattered. A, Exposure about 950 m west of 825-5 near Spirit Lake, part of "largest block" (see Pl. 2), August 1982. B, Exposure in canyon of North Fork Toutle River, about 300 m north-northwest of DXS-6, October 1984. Canyon is about 25 m high.

Table 3 Lithologic counts of approximately 100 clasts >2cm diameter in 1-m² windows [Sample localities shown on Pl. 2. distsr, distance from source; andbas, andesite and basalt; olddac, older dacite; moddac, modern dacite; Ter, Tertiary bedrock; juvnil, juvenile blast dacite; ?, unidentified; pumice, pre-1980 pumice; wood, incorporated organic matter; Sprt, at Spirit Lake; Cstl, at Castle Lake; Cold, at Coldwater Lake; %, percentage of rock types determined from relative areas of debris-avalanche blocks in windows (Fig. 21); (x), percentage of juvenile clasts]

Sample	distsr (km)	andbas	olddac	moddac	ter	juvnil	?	pumice	wood	Total
Older dacite unit										
DXS-2	25.3	10	81	0	2	0	7	0	0	100
DXS-4	15.1	12	90	0	0	0	3	0	0	105
DXS-6	15.6	0	100	0	0	0	0	0	0	100
DXS-20	12.3	0	100	0	0	0	0	0	0	100
DXS-21	18.4	0	100	0	0	0	0	0	0	100
DXS-22	17.6	0	100	0	0	0	0	0	0	100
DXS-24	13.3	0	100	0	0	0	0	0	0	100
825-3(Sprt)	9.4	12	88	0	0	0	0	0	0	100
827-3(Sprt)	9.7	0	100	0	0	0	0	0	0	100
MS-10(Cold)	16.9	0	100	0	0	0	0	0	0	100
826-3(Cold)	16.4	2	98	2	0	1(1)	1	5	0	109
Andesite and basalt unit										
DXS-11	13.5	100	0	0	0	0	0	0	0	100
DXS-13	2.5	100	0	0	0	0	0	0	0	100
DXS-14	2.7	100	0	0	0	0	0	0	0	100
DXS-16	11.3	100	0	0	0	0	0	0	0	100
DXS-23	13.0	100	0	0	0	0	0	0	0	100
DXS-25	14.6	100	0	0	0	0	0	0	0	100
DXS-27	17.7	75	2	5	0	1(1)	15	0	0	98
DXS-38	29.7	98	2	0	0	0	0	0	0	100
825-5(Sprt)	9.4	100	0	0	0	0	0	0	0	100
827-2(Sprt)	10.6	100	0	0	0	0	0	0	0	100
MS-9(Cold)	16.9	58	0	42	0	0	0	0	0	100
Modern dacite unit										
DXS-3	15.7	0	0	100	0	0	0	0	0	100
DXS-12	13.5	0	0	100	0	0	0	0	0	100
DXS-19	11.7	4	0	96	0	0	0	0	0	100
MS-1(Cold)	17.2	37	17	28	0	13(13)	5	0	0	100
Modern undifferentiated unit										
DXS-17	2.4	65	0	35	0	0	0	0	0	100
826-2(Cstl)	16.2	100	0	0	0	0	0	0	0	100
827-6(Cstl)	15.9	0	0	77	0	15	0	1	7	100
827-7(Cstl)	15.9	22	45	0	0	0	0	0	33	100
Mixed block and matrix facies unit										
DXS-1	29.9	41	35	2	0	7(7)	16	0	0	101
DXS-1 count 2	29.9	23	55	1	0	10(10)	10	1	0	100
DXS-1 count 3	29.9	64	22	1	0	5(5)	6	0	0	98
DXS-8	25.8	38	52	4	0	5(5)	5	0	0	104
DXS-29	21.4	33	39	12	0	2(2)	15	0	0	101
DXS-30	22.2	54	8	7	0	19(19)	12	1	0	101
DXS-31	23.1	33	33	12	0	13(13)	9	0	0	100
DXS-33	24.5	56	13	9	0	17(17)	5	0	0	100
DXS-34	26.8	50	51	5	0	2(2)	1	0	0	109
DXS-35	28.1	19	57	13	0	4(4)	5	0	0	98
DXS-36	31.2	40	47	5	0	9(9)	1	1	0	103
DXS-37	30.7	45	39	5	0	3(3)	2	3	0	97

Table 3 (Continued)

Sample	distr (km)	andbas	olddac	moddac	ter	juvnil	?	pumice	wood	Total
Marginal mixed block and matrix facies unit										
DXS-9	21.7	44	37	7	0	0	11	0	0	99
DXS-26	17.7	42	43	14	3	0	13	1	0	116
DXS-28	21.0	14	5	4	0	0	2	0	0	25
DXS-32	23.6	44	20	30	0	2(2)	9	0	0	105
Blast deposit above the debris avalanche										
DXS-5	13.4	32	6	55	0	8	0	0	0	101
DXS-18	11.5	64	1	10	0	9	15	1	0	100
DXS-21.5	18.0	33	28	2	0	10	26	1	0	100
826-4(Cstl)	16.6	57	18	2	0	12	24	0	0	113

sitions are present locally. The surface of the modern dacite unit of the debris-avalanche deposit has more clasts >10 cm diameter than does the surface of the older dacite unit. This is probably because the ratio of dome rock to volcanoclastic deposits in the modern dacite unit of the old mountain is higher than the same ratio in the older dacite unit of the old mountain.

(4) Modern undifferentiated unit

The modern undifferentiated unit contains a mixture of modern dacite, andesite, and basalt. The rock types are the same as those of the modern dacite and the andesite and basalt units. Minor amounts of older dacite and dacite pumice from the old mountain as well as organic debris are also found in this unit, but proportions are difficult to estimate because of the lack of good exposures. Analysis of four exposures (Table 3) shows abundant organic debris but an insignificant amount of rock material that is not modern dacite, andesite, or basalt.

4.3.2 Mixed block and matrix facies unit

The mixed block and matrix facies unit of the debris-avalanche deposit consists of both matrix facies as well as debris-avalanche blocks of all lithologies from the block facies that are too small to map. Pebble counts of 100 clasts >2 cm diameter were carried out at 10 localities of the mixed block and matrix facies unit (Table 3). The clasts were taken from the 1-m² windows where textures were mapped, samples were taken for grain-size analyses, and field density was measured. Juvenile "blast" dacite from the cryptodome is present in most of the windows. There is as much as 19±8 percent blast dacite (error following the methods of Galehouse, 1971, for 95.4 percent confidence level). The highest quantities of blast dacite are in the exposures that consist entirely of matrix facies; the lowest quantities are in exposures on the margins of the debris avalanche deposit. There is no apparent trend of changing percentages of blast dacite with distance from the volcano (Fig. 15).

The mixed block and matrix facies unit occurs primarily in the western part of the debris-avalanche

deposit, west of a break-in-slope near the junction of Maratta Creek and the North Fork Toutle River (Pl. 2). A few hummocks of the mixed block and matrix facies unit are mapped in South Coldwater Creek. Fisher and others (1987) call this unit "avalanche II" material; they believe the material originated from slide blocks II and III. In South Coldwater Creek, the matrix facies is continuous from the hummocks to flat-surfaced exposures in interhummock areas where it underlies blast deposits. Some of these flat-surfaced exposures are at least 10 m thick (Fisher and others, 1987).

Although matrix facies rests between hummocks, it is not observed to form or to support hummocks within it; instead it overlies material of the block facies. Matrix facies deposits are likely remnants of the final phase of the debris avalanche that traveled over the top of the deposit of avalanche blocks. Exposures of matrix facies resemble exposures of blast deposits that overlie the matrix facies and conceal it on the geologic map.

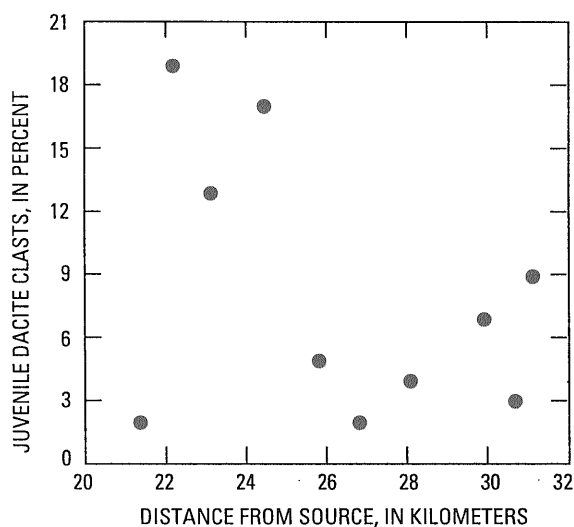


Fig. 15 Percentage of clasts of juvenile blast dacite from matrix facies in windows (from Table 3) versus distance from source (crater). Marginal matrix facies not included.

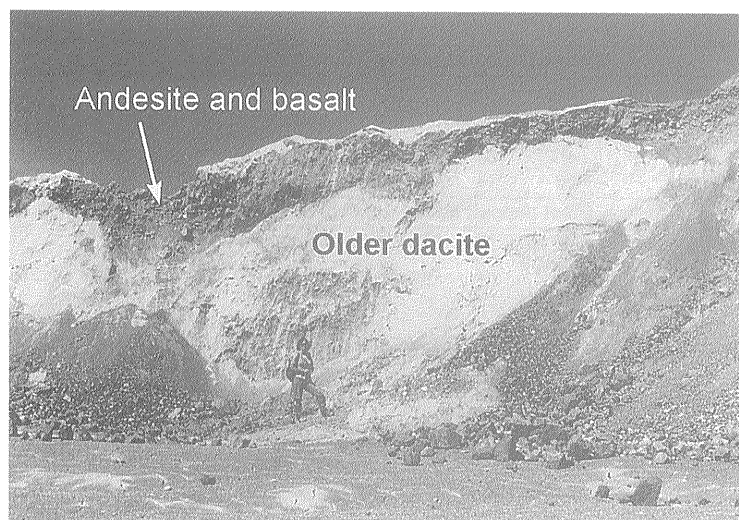


Fig. 16 Andesite and basalt unit overlying older dacite unit in debris-avalanche deposit on Johnston Ridge.

4.3.3 Contacts between lithologic units

Though the contacts between lithologic units of the debris-avalanche deposit are sharp locally, they are generally diffused over as much as 10 m. The contact between the andesite and basalt unit and the older dacite unit, for example, is especially difficult to define locally because the older dacite in the mountain was intruded by many andesite dikes. Where they are sharp, the contacts between lithologic units commonly resemble contacts within the present crater. The sharp contact most frequently observed is the andesite and basalt unit overlying the older dacite unit (Fig. 16). This contact is very similar to the andesite and basalt/older dacite contact in the crater, and it indicates that the material was transported with little deformation.

4.4 Other deposits of the May 18, 1980, eruption

4.4.1 Blast deposits.

On the morphologic map (Pl. 1), blast deposits cover the entire debris avalanche east of the break-in-slope just west of Maratta Creek and are present as a small finger extending west of the break-in-slope. On the lithologic map (Pl. 2), blast deposits are mapped only where they were thick enough (approximately > 1 m) to conceal the lithology of the debris-avalanche deposit in summer 1982. Since 1980, erosion has washed the blast deposits off most of the hummocks so that blast deposits now mantle primarily interhummock areas. The airfall layer (A3 layer) of the blast deposits mantles the entire debris avalanche (Waitt, 1981; Moore and Sisson, 1981; Sisson, 1995), but because it was only a few centimeters thick, its distribution is not shown on either map. Unmapped blast

deposits also blanket the ridges surrounding the debris avalanche.

The first part (slide block I) of the rockslide-debris avalanche released the pressure on the growing cryptodome that resulted in the blast explosions. The initial blast explosions generated a pyroclastic surge (the "blast surge") that quickly overtook slide block I and knocked down the trees over 600 km² (Fisher and others, 1987). The blast surge produced the layered stratigraphy described by Hoblitt and others (1981), Moore and Sisson (1981), and Fisher and others (1987). Although it is difficult to find good exposures of the base of the debris-avalanche deposit, debris-avalanche deposit overlies trees felled by the blast, leaving no doubt that the erosive phase of the blast surge in places preceded deposition of the debris-avalanche deposit. The fact that the debris-avalanche deposit rests on top of some of the blast deposit on the south slope of Johnston Ridge indicates that deposition of the debris avalanche followed some of the blast surge within 10 km of the mountain (Fig. 17). However, the correlation of the layered stratigraphy of the blast that rests on top of the debris avalanche near Spirit Lake with the stratigraphy of the blast surge in South Coldwater Creek (Glicken and others, 1989) indicates that, within 10 km of the mountain, most of the deposition of the blast surge followed the deposition of the debris avalanche (Fig. 18).

Both the blast deposit and the matrix facies of the debris-avalanche deposit are a homogeneous mix of all rock types from the old mountain and the juvenile dacite, and they are commonly difficult to distinguish from one another. However, the blast deposit generally contains a larger percentage of juvenile blast dacite than does the debris avalanche.

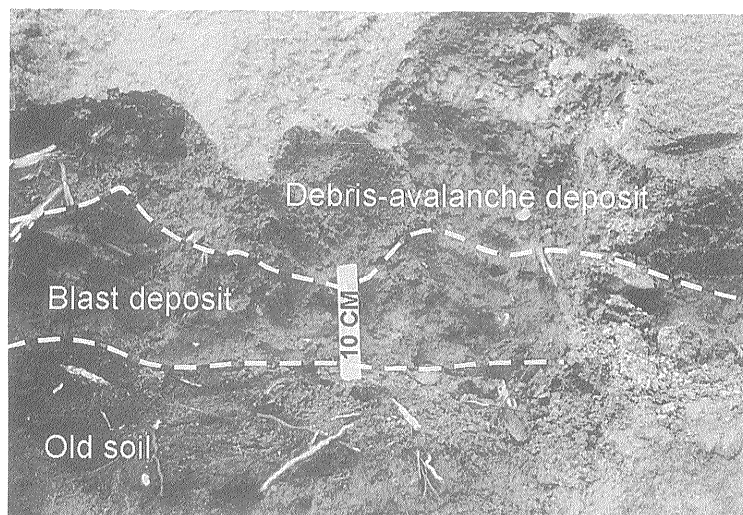


Fig. 17 Blast deposit resting on fir needles and organic material from old forest floor and overlain by debris-avalanche deposit in excavation for spillway draining Coldwater Lake. June 1980 exposure about 100 m east of sample locality DXS-38.

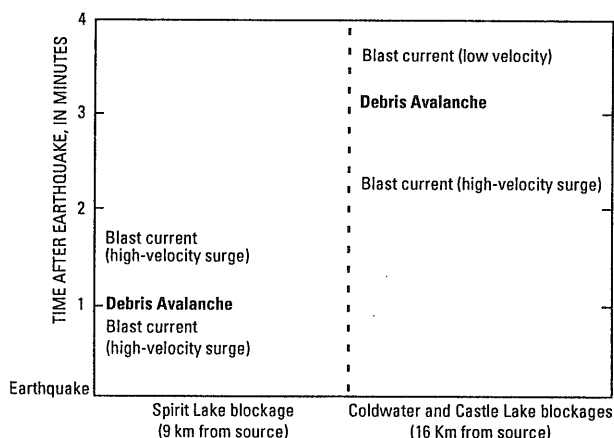


Fig. 18 Timing of deposition of debris avalanche and blast currents in area of Spirit and Coldwater Lakes. Timing of events from Voight (1981), Voight and others (1983), and Moore and Rice (1984).

4.4.2 Lahar deposits

On the morphologic map (Pl. 1), lahar deposits are shown where they cover most of the surface area of the debris-avalanche deposit and also where they flowed off the west end of the avalanche deposit. Within areas mapped as lahar deposits, there are many isolated hummocks not covered with lahars that could not be shown on the scale of the morphologic map.

On the lithologic map, lahar deposits covering the debris-avalanche deposits are mapped only where they are thick enough (approximately >1 m) to prohibit identification of the lithology of the underlying debris-avalanche deposit. Lahar deposits thinly mantle the debris-avalanche deposit in many other areas. Lahars are also mapped on the lithologic map where they

flowed off the west end of the debris-avalanche deposit.

The lahar deposits consist of mudflow, debris flow, and hyperconcentrated lahar-runout deposits (terminology of Pierson and Scott, 1985) that formed from the debris avalanche in the late morning and early afternoon of May 18 (Janda and others, 1981). "Lahar" is the appropriate term here, as it is an inclusive term that describes masses of flowing volcanic debris intimately mixed with water (Fisher and Schmincke, 1984). Voight and others (1981, 1983) and Lipman (1981) referred to the same deposits as "mudflow" units. The lahar deposits have a generally flat but locally ropy surface morphology. They never form hummocks and, where present, cover the debris-avalanche deposit in the areas between hummocks. The texture of the lahar deposits is generally distinct from that of the debris-avalanche deposits. They consist of clasts that are as much as tens of centimeters in diameter dispersed in brown finer grained material; they do not contain debris-avalanche blocks transported intact from the old mountain.

4.4.3 Pyroclastic-flow deposits of the afternoon of May 18

Pumiceous pyroclastic-flow deposits rest on top of the debris-avalanche and blast deposits in the area just north of the crater. They cover the debris-avalanche deposit to depths of more than 40 m and have a volume of about 0.25 km³ (C.W. Criswell, oral commun., 1984). The pumiceous pyroclastic-flow deposits are easy to distinguish from the debris-avalanche and the blast deposits. They consist of highly inflated pumice (mostly white to yellow, with some gray fragments) and subordinate lithic debris in glassy, finer grained material. Nearly all the deposits have

levees and flow fronts consisting of the coarser grained parts of the deposits (Rowley and others, 1981; Criswell, 1984). These deposits formed from the continued emptying of the May 18 magma chamber after the initial avalanche and blast events. For the entire morning, the magma produced only a vertical column, but in the afternoon both a vertical column and pyroclastic-flow deposits were produced (Christiansen and Peterson, 1981; Criswell, 1987).

4.5 Tertiary bedrock

The ridges surrounding the debris-avalanche deposit are composed of well-lithified Tertiary bedrock. These rocks are primarily flows and breccias of basaltic to rhyolitic composition that have been regionally metamorphosed to zeolite or prehnite-pumpellyite facies. Around Spirit Lake, there are some small areas of granitic rocks of the 21- to 22-m. y.-old Spirit Lake pluton (Evarts and others, 1987). The volcanic rocks were correlated with the Oligocene-Miocene Ohanapecosh Formation, which was dated at 31-45 m.y. outside the map area (Fiske and others, 1963; Hammond, 1980). Recent work by Evarts and others (1987) casts doubt upon this correlation.

5. Texture of the deposit

5.1 General statement

The terminology of sedimentology contains many terms that are ambiguous when applied to debris-avalanche deposits. In order to study debris-avalanche deposits, it is necessary to rigorously define and consistently use a single set of definitions. Some of this terminology is drawn from the literature of sedimentology, some is drawn from the literature on volcanoclastic rocks, and some is adapted from previously published studies of large volcanic debris-avalanche deposits.

The texture of volcanoclastic deposits commonly refers to the grain-size distribution of the material (for example, Crandell, 1971, Murai, 1961). Here, it is used in the more general sense (for example, Fisher and Schmincke, 1984) to refer to the size, shape, and fabric (pattern of arrangement) of the particles that form the deposit. A "particle" is usually considered to be a "separable or distinct unit in a rock" (Bates and Jackson, 1980). The word "structure" is applied to features visible on the scale of exposures (for example, Fisher and Heiken, 1982). The distinction between textures and structures is somewhat arbitrary because exposure-scale features also represent the pattern of arrangement of particles. "Texture" is used in this work to refer to these patterns on any scale.

Two different kinds of particles are defined to describe the debris-avalanche deposit. A "clast" is defined as a rock of any size that would not break if

passed through a sieve or immersed in water. Each clast can be considered one particle. A "debris-avalanche block" is defined as a coherent, unconsolidated or poorly consolidated piece of the old mountain that was transported to its place of deposition relatively intact. Each debris-avalanche block may be thought of as one particle that contains many smaller particles (clasts). The usage of the term "debris-avalanche block" is similar to that of "megablock" of Mimura and Kawachi (1981) and Ui (1983). The distinction between consolidated clasts and unconsolidated or poorly consolidated debris-avalanche blocks is essential for the analysis of exposures. Several terms are used to describe the disintegration of material. The breaking of individual clasts is "fracturing." Thorough fracturing of clasts is called "shattering." When material expands from its original density on the mountain (at least in part by shattering of clasts), it is said to "dilate"; when it breaks apart into its constituent clasts which then move apart, it "disaggregates."

Two end-member facies are used to describe the texture of the debris avalanche, the block facies and the matrix facies. This terminology follows the precedent of Crandell and others (1984), and Ui and Glicken (1986). Both facies would be classically described as angular, unstratified, unsorted rubble consisting of material (clasts) that ranges in size from microns to meters in diameter.

The block facies consists entirely of debris-avalanche blocks, coherent unconsolidated or poorly consolidated pieces of the old mountain that were transported relatively intact. Debris-avalanche blocks range in size from a few centimeters to more than a hundred meters wide. Some of the debris-avalanche blocks are smeared out and deformed to varying degrees. The smeared-out debris-avalanche blocks a few centimeters wide that are commonly observed in exposures are called "rubble schlieren." Most of the clasts in the block facies were partially or completely shattered from their origin on the old Mount St. Helens, so that although the original stratigraphy or structure is locally preserved (the "mutual arrangement of separate fragments"; Gorshkov and Dubik, 1970) few clasts meters wide from the old mountain remain. Shreve (1968) observed the same texture in the nonvolcanic Blackhawk slide and named it the "three-dimensional jigsaw puzzle effect." In the Mount St. Helens deposit, the shattering has produced unconsolidated rubble or poorly consolidated rubble that was cohesive enough upon deposition to form hummocks.

The term matrix facies is used here in the sense of Crandell and others (1984) and Ui (1983) to refer to the completely mixed parts of the debris-avalanche deposit. The matrix facies contains all rock types from the old mountain and juvenile "blast" dacite in

an unsorted and unstratified mixture. Locally, fragments of wood and bits of soil and rock from the terrain underlying the deposit are present in the matrix facies. It must be emphasized that "matrix" is not used as a grain-size designation in this study. Other authors, (for example, Horz and others, 1983; Crandell, 1971) in their studies of unsorted or poorly sorted clastic deposits, use "matrix" to refer to finer grained parts of the deposits, but the "matrix facies" of large volcanic debris avalanches can contain clasts that range in size from microns to meters in diameter (Crandell and others, 1984; Ui, 1983).

5.2 Textural interpretation of map relations

The lithologic map of the debris avalanche (Pl. 2) shows two principal divisions of the avalanche deposit. In the eastern part of the North Fork Toutle River valley (east of the prominent break-in-slope at the constriction just west of Maratta Creek), the only units of the debris avalanche that are mapped are units of the block facies. This part of the debris-avalanche deposit is referred to as the "flow of debris-avalanche blocks," and the break-in-slope is the flow front of the flow of debris-avalanche blocks. West of this break-in-slope and in South Coldwater Creek, only isolated areas of the block facies are mapped; the rest are the mixed block and matrix facies unit. Most of the debris avalanche west of the break-in-slope was deposited after deposition of most of the eastern part of the debris-avalanche deposit, and it is part of the deposit from slide block III.

5.2.1 East of the break-in-slope

Each area of one lithologic unit of the debris-avalanche deposit in the eastern part of the North Fork Toutle River valley is composed of one or more blocks. Rarely, block boundaries can be delineated by comparing the stratigraphy or structures in the blocks to those in the old mountain (for example, Figs. 9A and 14). However, because block boundaries do not necessarily coincide with mapped lithologic contacts, map patterns cannot be interpreted as patterns of blocks.

The area near Spirit Lake contains the largest, least deformed debris-avalanche blocks found in the debris-avalanche deposit. A debris-avalanche block was identified that has a minimum exposed area of 1.5×10^5 m² and a volume of 1.7×10^7 m³; the minimum extent of the block is outlined with a dashed line on Pl. 2. A contact between the older dacite unit and the andesite and basalt unit that extends from hummock to hummock across five hummocks defines the debris-avalanche block, because it indicates that one piece of the old mountain was transported relatively intact. The same contact occurs throughout the area west of Spirit Lake and east of the Pumice Pond (called "Spirit Lake Blockage" by Glicken and others, 1989)

so it is possible that this entire area may be one debris-avalanche block. The contact is faulted down between the hummocks.

Areas along the margins of the debris-avalanche deposit (on the north side between Coldwater Lake and Spirit Lake, and on the south side between Castle Lake and Studebaker Ridge) have a chaotic lithologic pattern. The rock types in these areas are primarily modern dacite, andesite, and basalt, with relatively little older dacite. The rock types are jumbled together, and hummocks commonly consist of more than one rock type.

The chaotic distribution of map units probably results from the interaction of the moving avalanche with the underlying terrain. Debris-avalanche blocks were highly deformed when they smashed against the ridges. Debris-avalanche blocks slowed down on the margins of the North Fork Toutle River valley and then broke up and tumbled end-over-end when they came in contact with the irregularities of the underlying topography. This interaction is also reflected in the morphology of the deposit in the marginal areas, where the morphology is much more irregular than the morphology in the central areas.

A few hummocks of the mixed block and matrix facies unit are mapped in South Coldwater Creek. These hummocks are almost entirely matrix facies. Fisher and others (1987) refer to the matrix facies in South Coldwater Creek as "avalanche II" material; they interpreted the material as having originated as slide blocks II and III. This terminology is not used here because it does not apply to the main part of the debris-avalanche deposit.

5.2.2 West of the break-in-slope

The map pattern of the debris-avalanche deposit west of the break-in-slope near Maratta Creek is very different from that of the eastern part of the avalanche. Debris-avalanche blocks as much as a few tens of meters wide occur only locally, because most of the deposit consists of a mixture of matrix facies and debris-avalanche blocks <20 meters wide. Scoured material, which consists primarily of wood, rock debris, and soil from adjacent ridges, is present only on top of the margins of the debris-avalanche deposit. The distal material at the west end of the avalanche deposit consists of jumbled piles of soil and splintered trees felled by the blast and shoved in front of the avalanche.

5.2.3 Lateral variation in debris-avalanche block size

Because each map area does not necessarily represent only one block, the true size of debris-avalanche blocks is uncertain except where original volcanic structures define the blocks. The measurements of Ui (1985), Ui and Glicken (1986), and Siebert

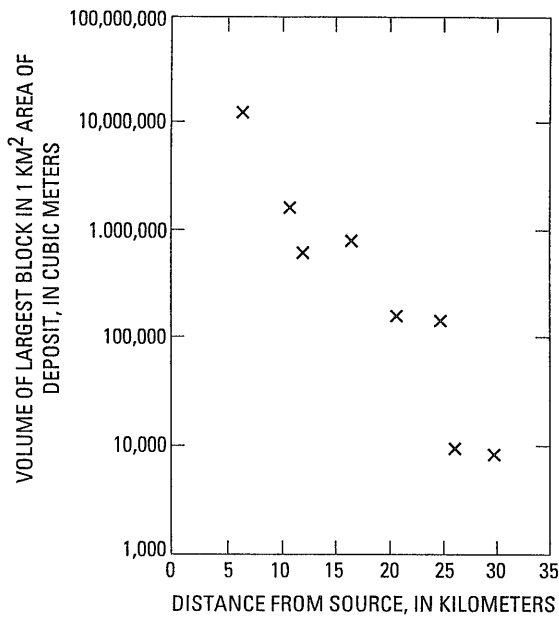


Fig. 19 Volume of identified largest debris-avalanche blocks (log scale) in 1-km² areas versus distance from source (crater). Note general trend of decreasing debris-avalanche block size with distance.

(1984) for volcanoes in Japan and the Cascade Range are very dependent on the size of exposures and generally reflect minimum block size. For this study, where debris-avalanche block boundaries can be identified, volumes were estimated from the topographic map and were plotted on a semi-log scale in Fig. 19. The definite trend of decreasing block size with distance from source indicates disaggregation of blocks during transport.

5.3 Textural interpretation of exposures

5.3.1 General statement

The texture of the avalanche deposit on a scale smaller than the geologic maps was investigated in detail. Flat or inclined surfaces are covered with slope wash and other deposits of May 18, so avalanche textures are rarely visible in natural exposures. Because of the poor natural exposures, 1-m² vertical exposures were cleared with hand tools at 52 locations throughout the avalanche deposit (Pl. 2) in order to study textures. The vertical exposures, here called "windows," were made as flat as possible, sprayed with water to enhance the contrast of colors, and then photographed (Fig. 20).

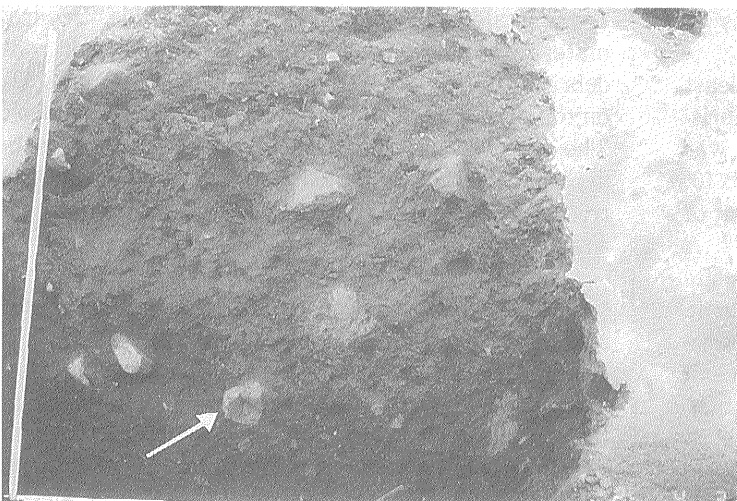
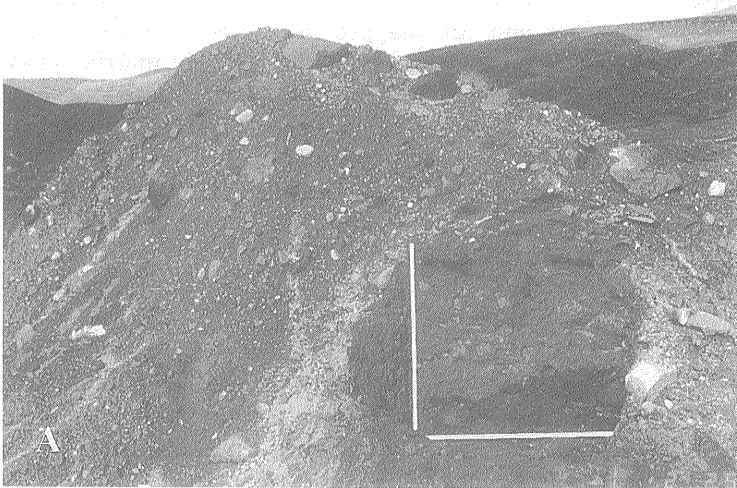


Fig. 20 Photographs of typical 1-m² windows. A, DXS-26, showing both block facies and matrix facies (see line drawing type 6 dmx in Fig. 21). B, DXS-30, showing only matrix facies. Prismatic jointed clast (arrow) is juvenile blast dacite.

Numerous data were gathered from each window. Maps of the distribution of different rock types in the rubble were made by overlaying drafting film on color photographic prints of the windows. The size distribution of clasts coarser than -5ϕ (32 mm) was measured by outlining the areas of the clasts on the prints. A 2- to 3-kg sample was taken and standard sieve and pipette analyses were performed in order to determine the size distribution of clasts finer than -5ϕ . The three dimensions of the 10 largest clasts in each window were measured in order to compare similar measurements from other volcanoclastic deposits. The standard sand-cone test (American Society for Testing of Materials, 1977) was conducted to determine the in-place dry field density of the deposit. If matrix facies material was present in the window, or if block-facies windows were made of more than one rock type, approximately 100 clasts >2 cm wide were classified by rock type (Table 3).

5.3.2 Description of windows

In order to provide a catalog of the different types of exposures in the debris-avalanche deposit, to study the texture of the deposit in a way directly comparable to methods possible in most prehistoric deposits (for example, Shasta Valley debris avalanche; Bandai-san debris avalanche), and to provide data to interpret the processes involved in the transport of the material, line drawings (maps) of the windows (Fig. 21) were constructed. The outlined areas on the windows represent different rock types and/or colors as measured in the field on a Munsell rock-color chart. Each color represents a different rock type or varying degrees of alteration within the old mountain. The textures are classified into seven general types based on examination of the maps in Fig. 21. Four types contain only block facies, two contain both matrix and block facies, and one contains only matrix facies.

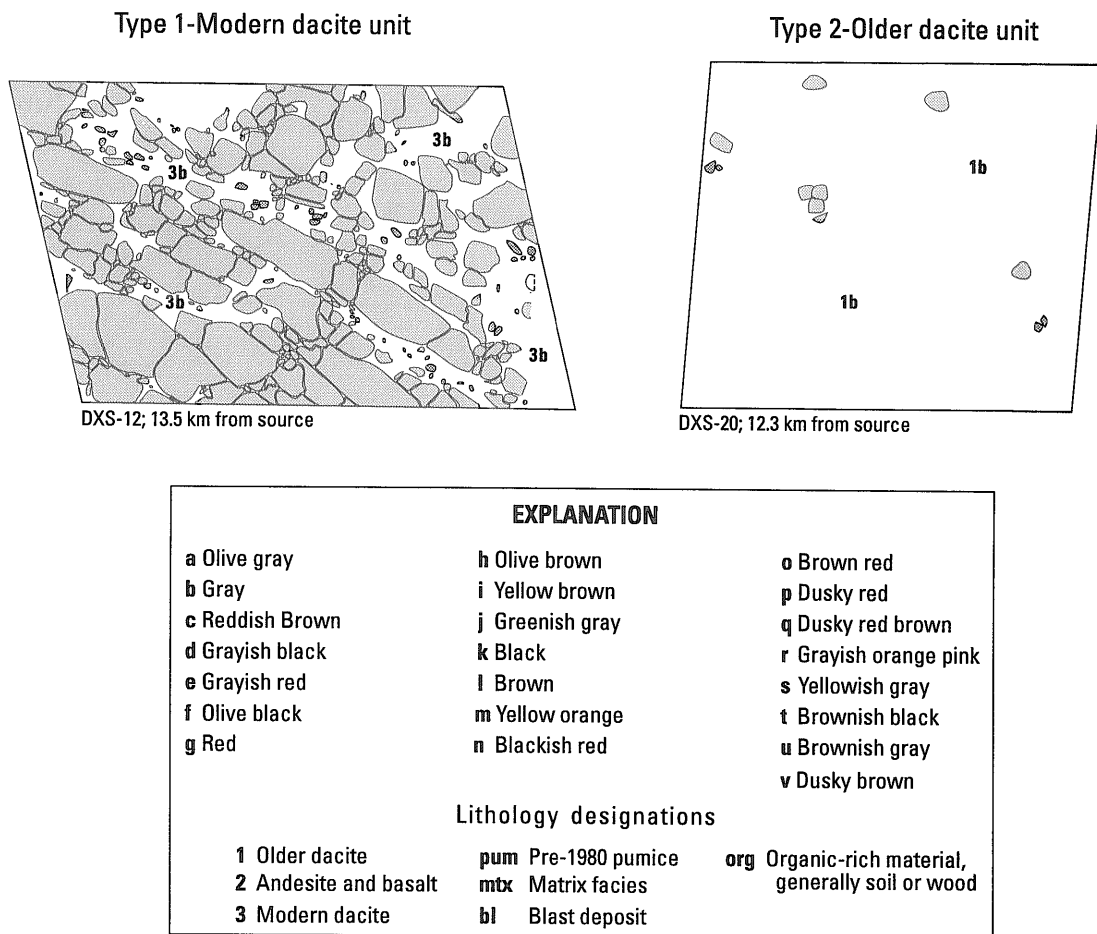
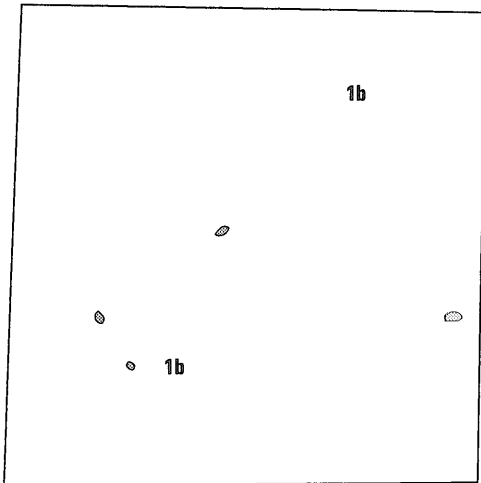


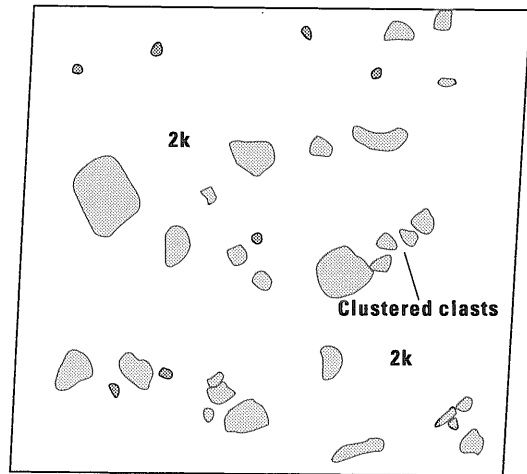
Fig. 21 Line drawings of windows (1-m² exposures cleared of colluvium and slope wash) at various localities throughout avalanche. See plate 2 for localities. Of the seven types of texture, four contain only block facies, two both block and matrix facies, and one only matrix facies. Solid lines bound clasts visible on scale of windows (larger than 1 cm). Long dashes define contacts between colors where sharp to within 2 cm on window. Short dashes indicate diffuse contacts. Color designations from field measurements using Munsell Rock Color Chart. Intensity modifiers (light, dark, etc.) not used.

Type 2-Older dacite unit



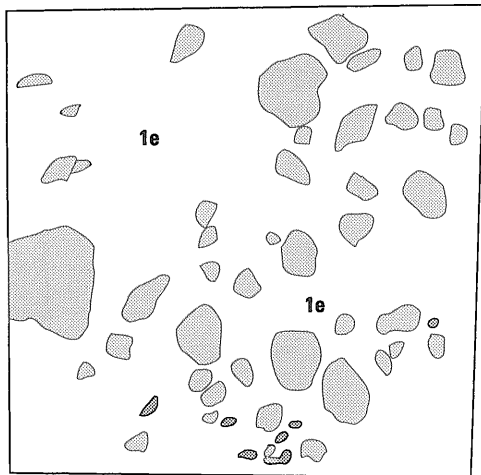
826-3; 16.4 km from source

Type 2-Andesite and basalt unit

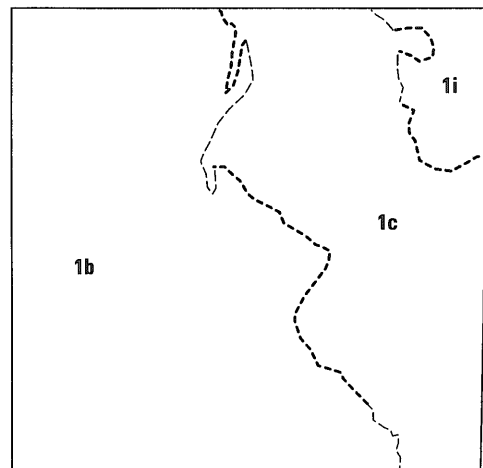


DXS-16; 11.3 km from source

Type 3-Older dacite unit

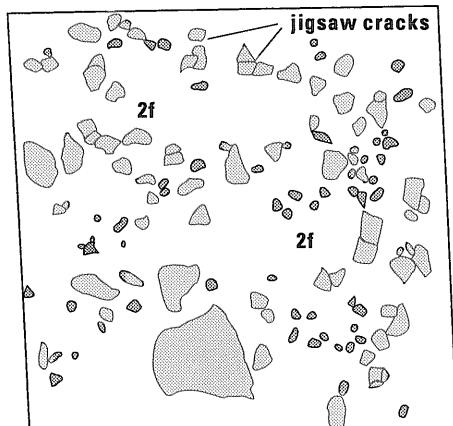


DXS-2; 25.3 km from source

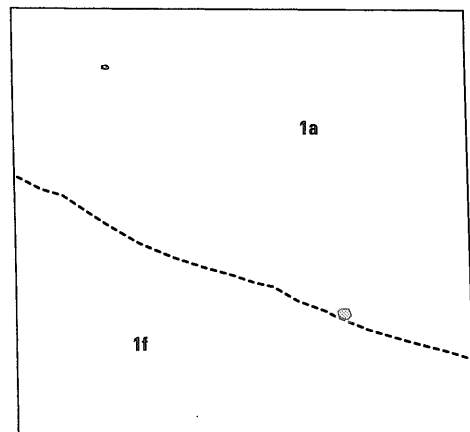


827-3; 9.7 km from source

Type 2-Andesite and basalt unit



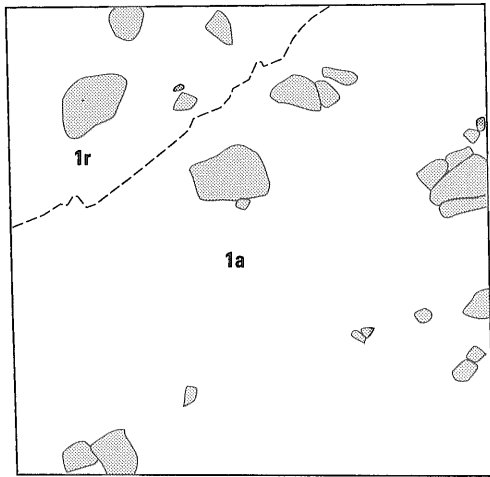
825-5; 9.4 km from source



DXS-24; 13.3 km from source

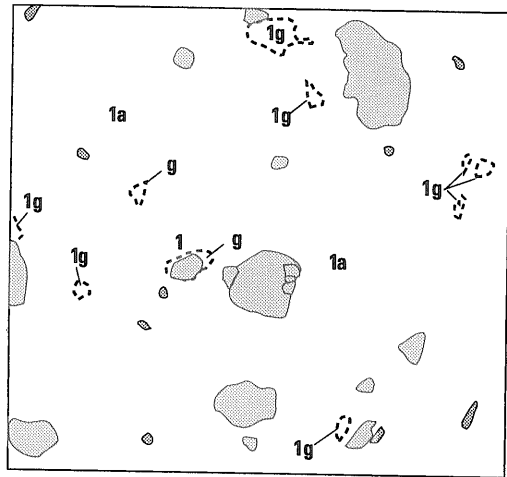
Fig. 21 (Continued.)

Type 3-Older dacite unit

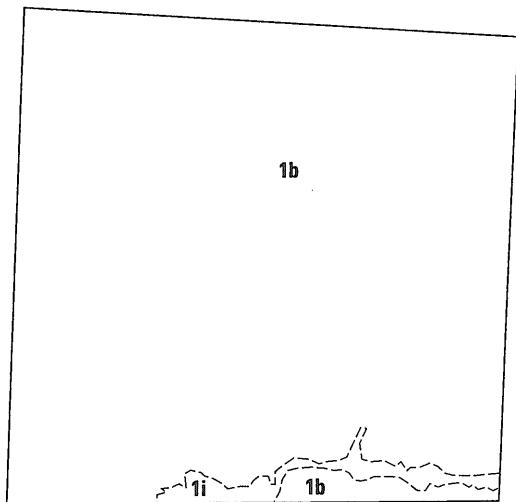


DXS-6; 15.6 km from source

Type 3-Older dacite unit

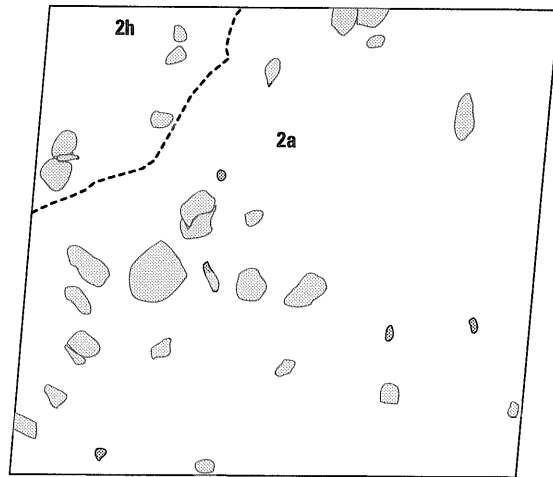


DXS-21; 18.4 km from source

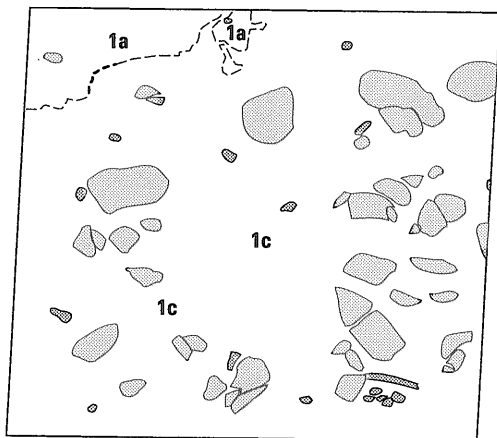


MS-10; 16.9 km from source

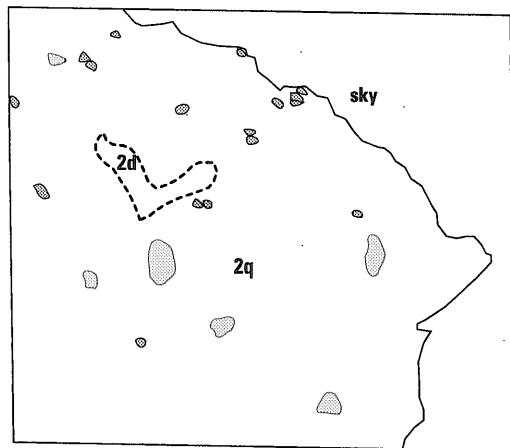
Type 3-Andesite and basalt unit



DXS-13; 2.5 km from source



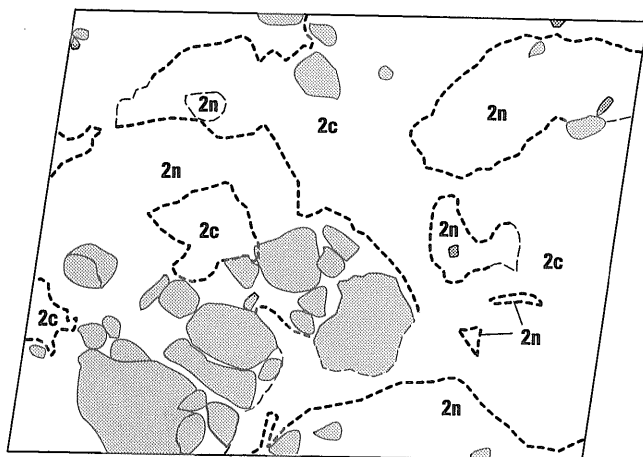
DXS-22; 17.6 km from source



DXS-14; 2.7 km from source

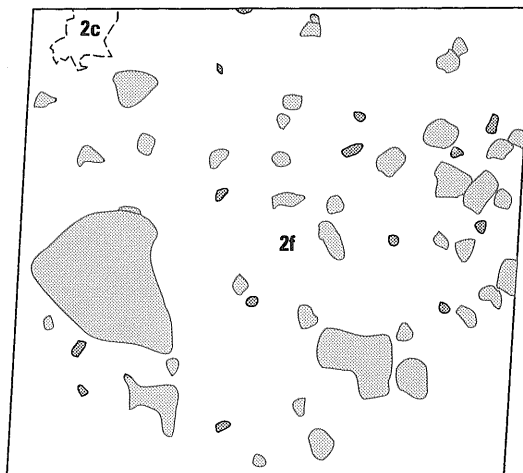
Fig. 21 (Continued.)

Type 3-Andesite and basalt unit

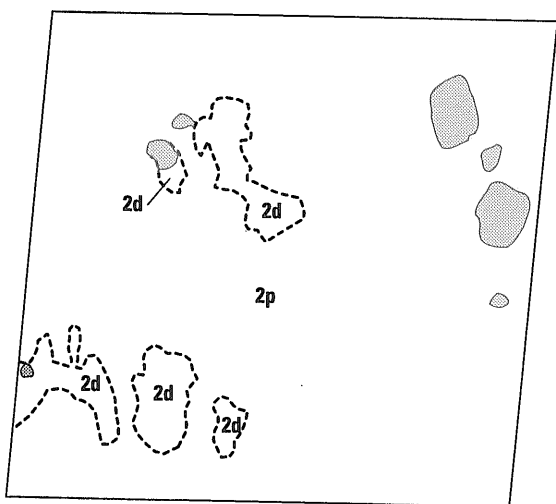


DXS-23; 13 km from source

Type 3-Andesite and basalt unit

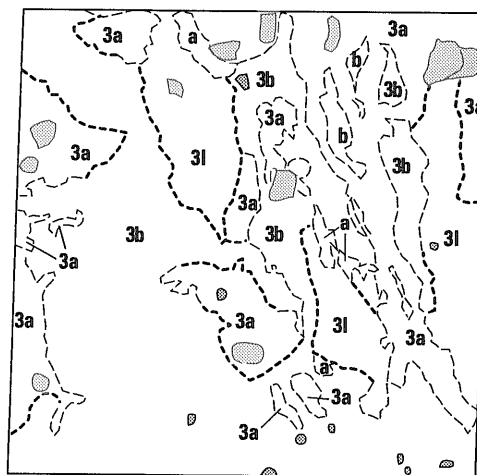


DXS-27; 17.7 km from source

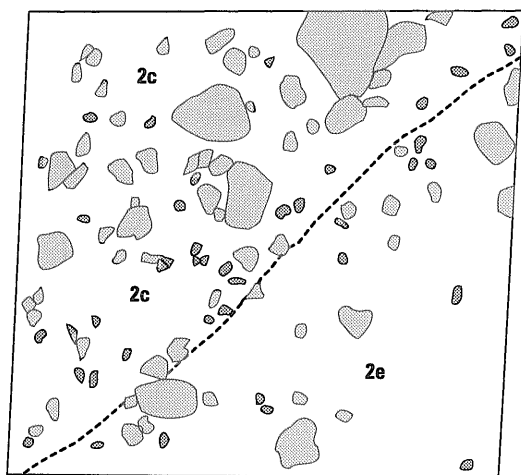


DXS-11; 13.5 km from source

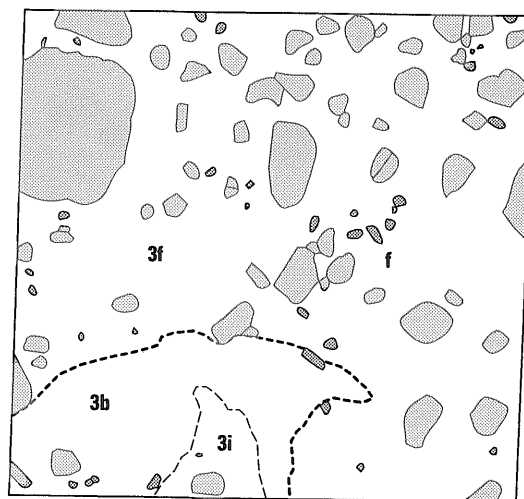
Type 3-Modern dacite unit



DXS-19; 11.7 km from source



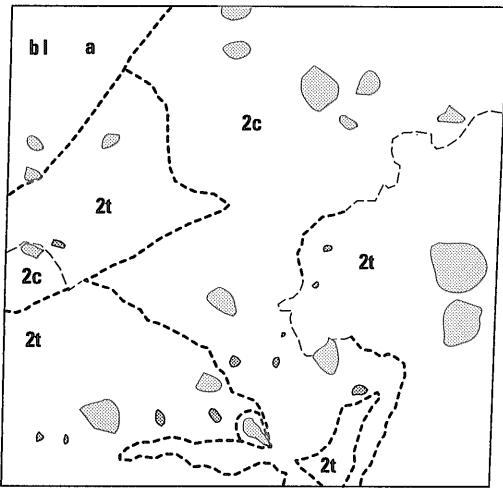
DXS-25; 14.6 km from source



DXS-3; 15.7 km from source

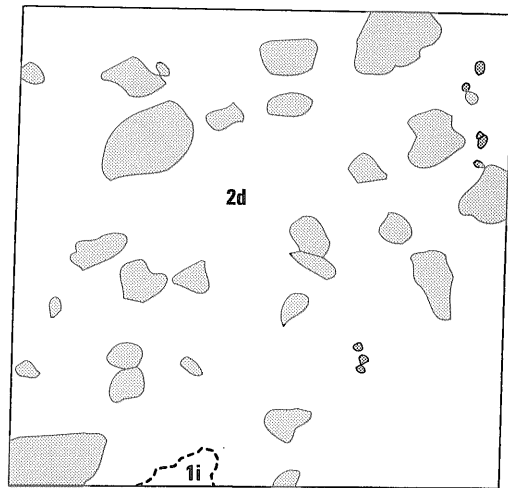
Fig. 21 (Continued.)

Type 3-Modern undifferentiated unit



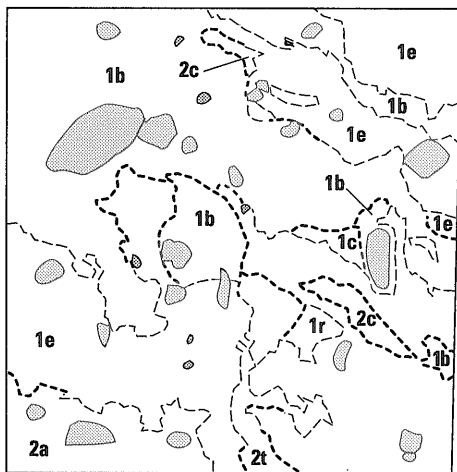
826-2; 16.2 km from source

Type 4-Andesite and basalt unit

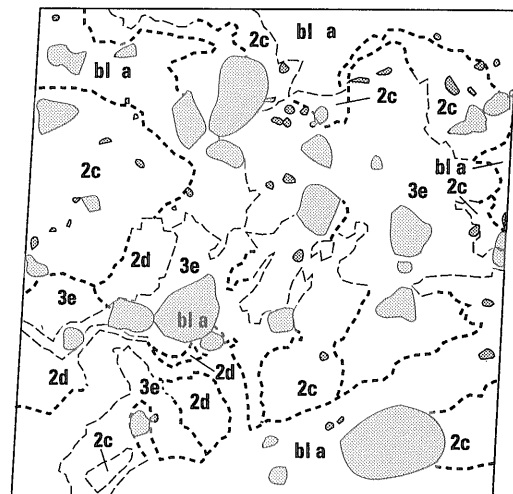


827-2; 10.6 km from source

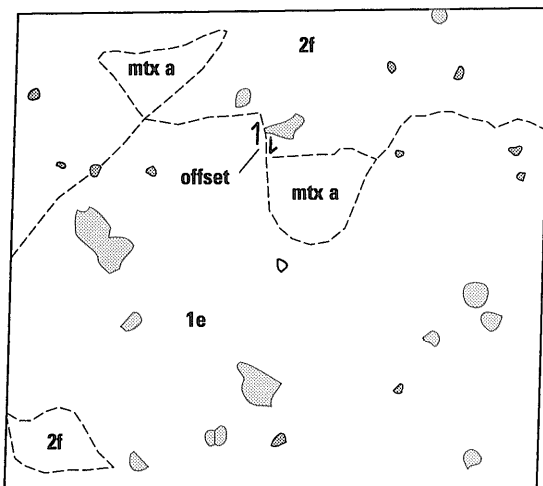
Type 4-Older dacite unit



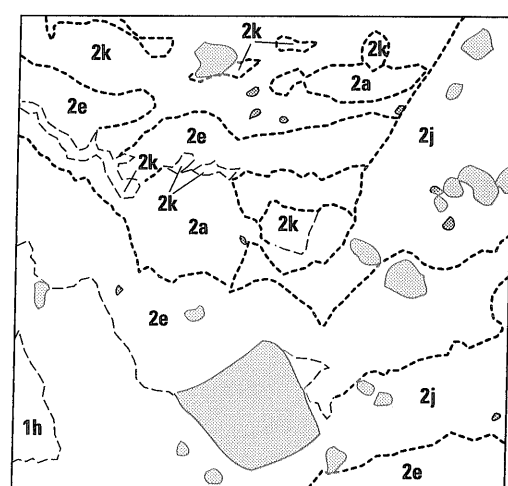
825-3; 9.4 km from source



MS-9; 16.9 km from source



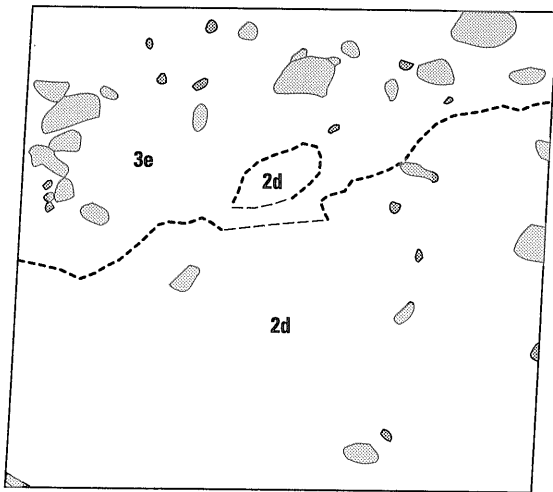
DXS-4; 15.1 km from source



DXS-38; 29.7 km from source

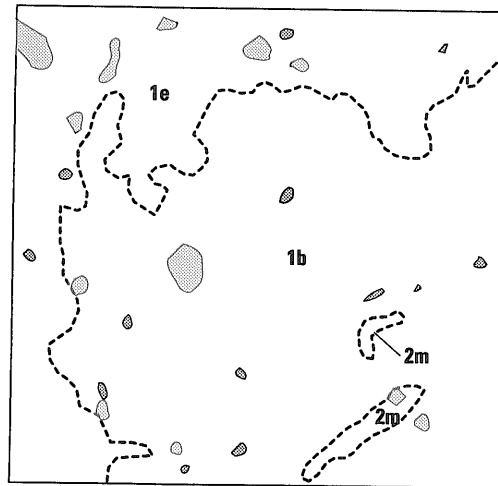
Fig. 21 (Continued.)

Type 4-Modern undifferentiated unit

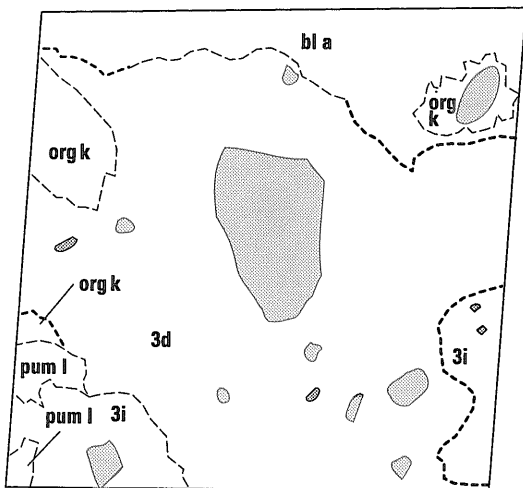


DXS-17; 12.4 km from source

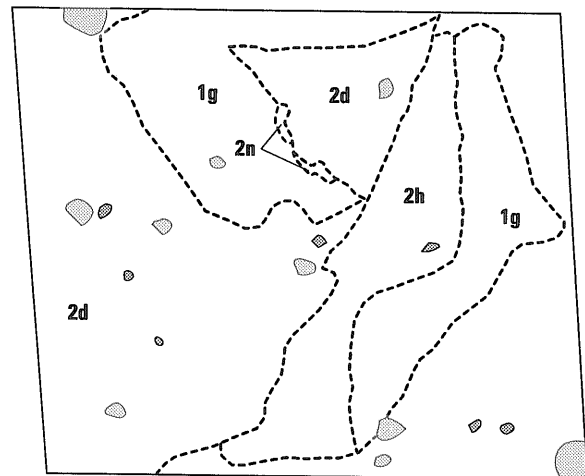
Type 4-Mixed block and matrix facies unit



DXS-8; 25.8 km from source

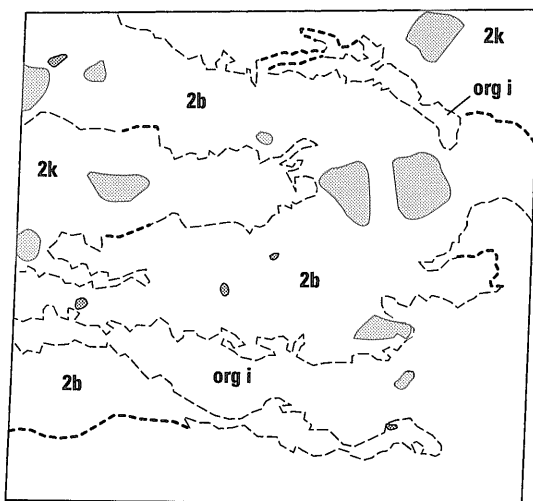


827-6; 15.9 km from source

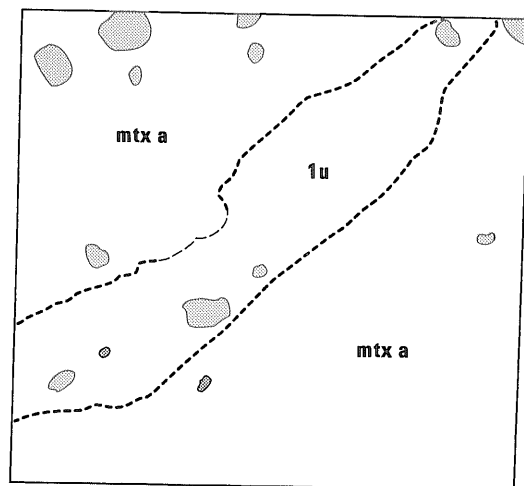


DXS-34; 26.8 km from source

Type 5-Mixed block and matrix facies unit



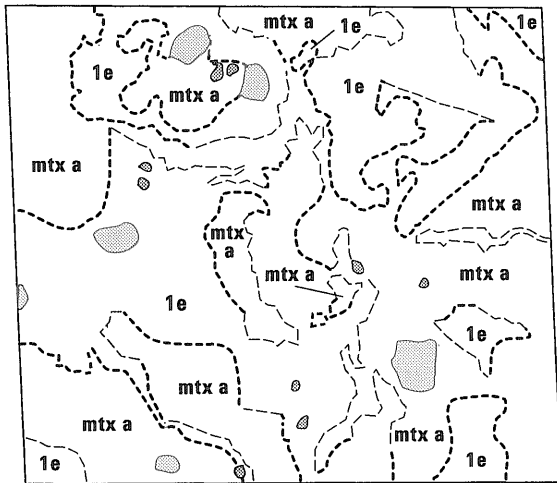
827-7; 15.9 km from source



DXS-29; 21.4 km from source

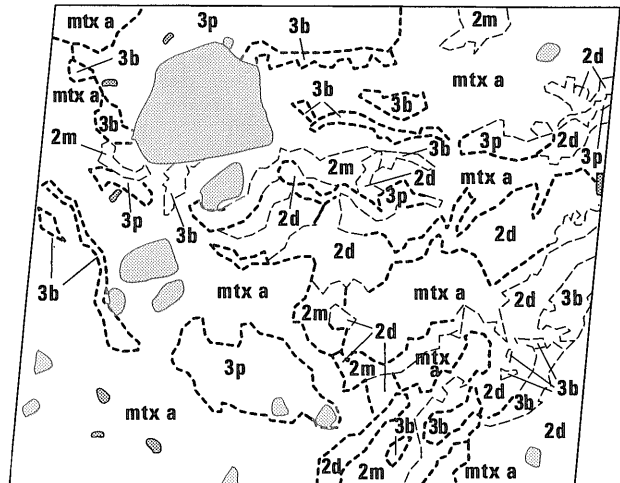
Fig. 21 (Continued.)

Type 5-Mixed block and matrix facies unit

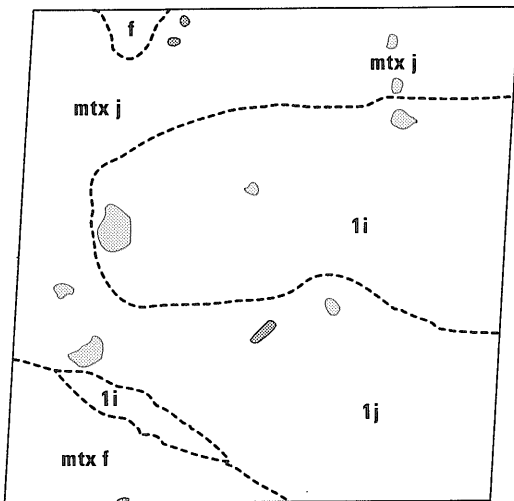


DXS-31; 23.1 km from source

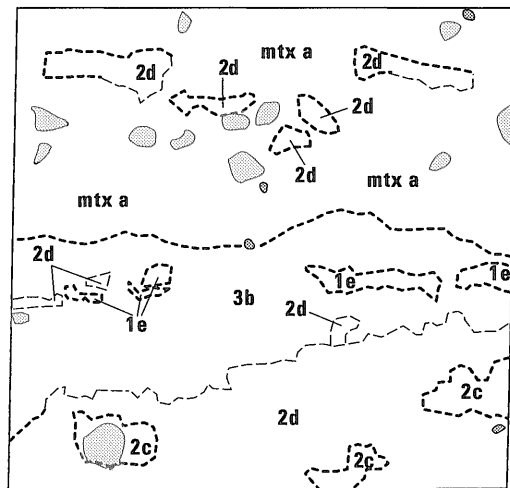
Type 6-Mixed block and matrix facies unit



DXS-32; 3.6 km from source

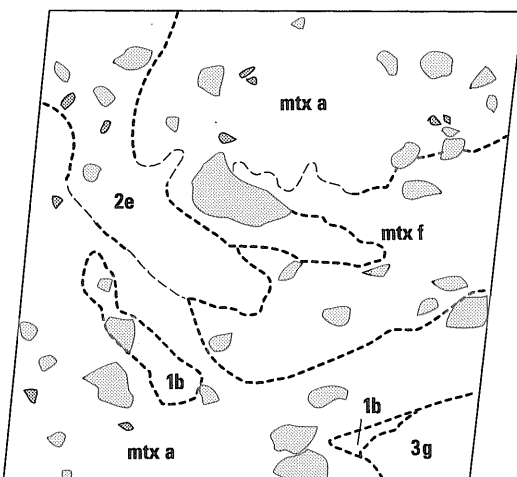


DXS-37; 30.7 km from source

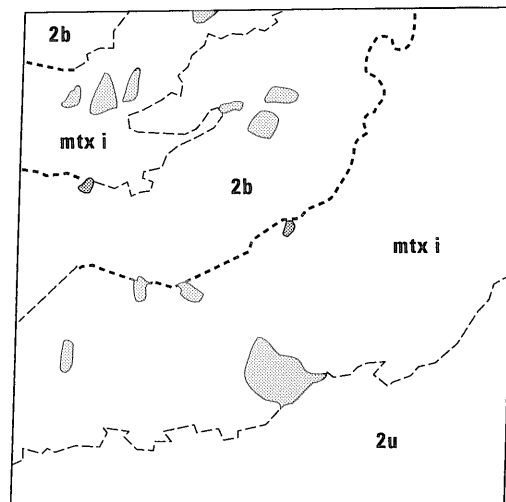


DXS-26; 17.7 km from source

Type 6-Modern dacite unit



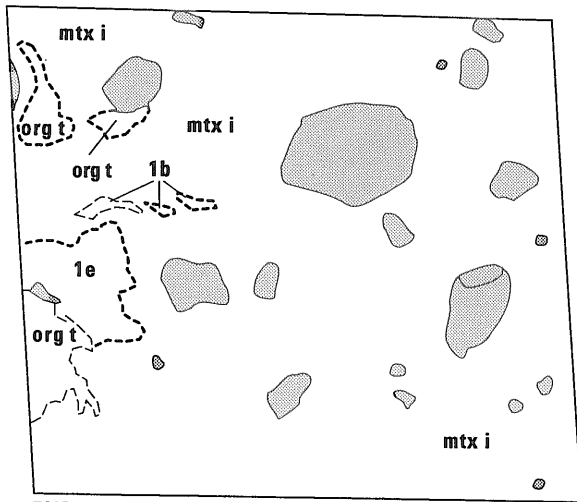
MS-1; 17.2 km from source



DXS-28; 21.0 km from source

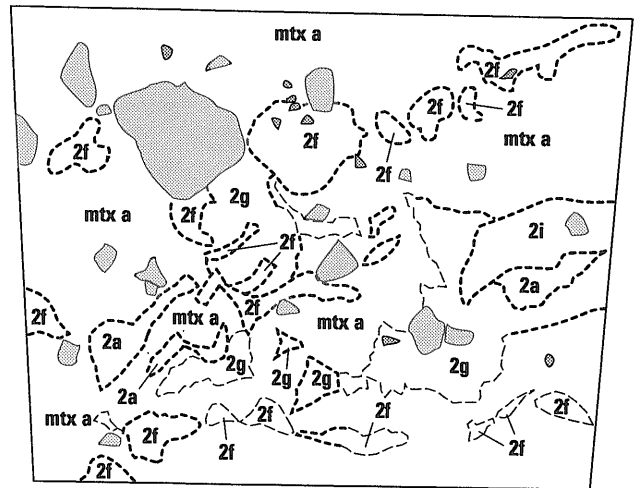
Fig. 21 (Continued.)

Type 6-Mixed block and matrix facies unit

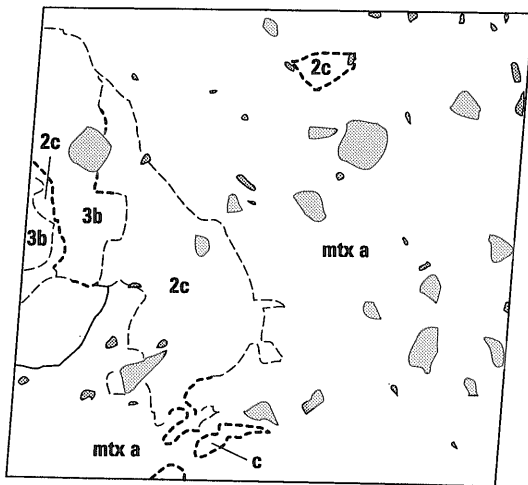


DXS-9; 21.7 km from source

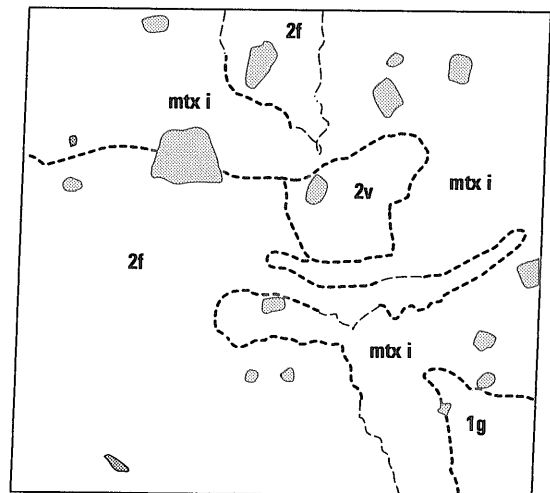
Type 6-Mixed block and matrix facies unit



DXS-1; 29.9 km from source

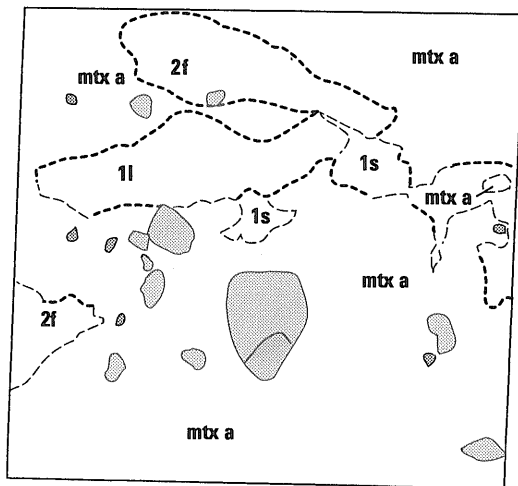


DXS-33; 24.5 km from source

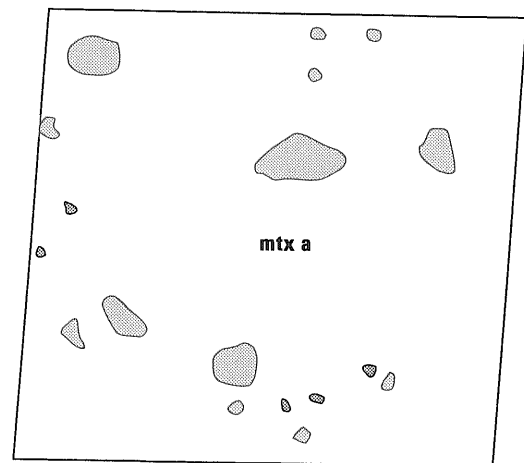


DXS-36; 31.2 km from source

Type 7-Mixed block and matrix facies unit



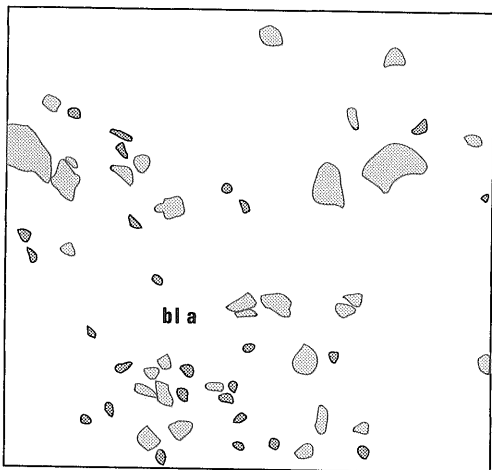
DXS-35; 28.1 km from source



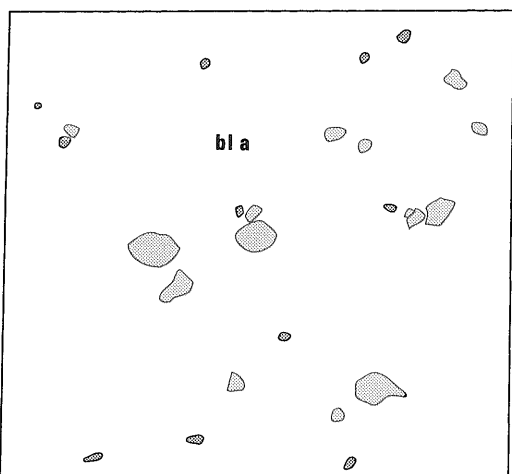
DXS-30; 22.2 km from source

Fig. 21 (Continued.)

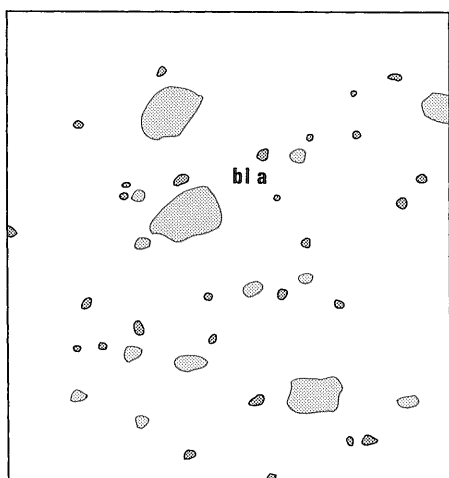
Type 7-Blast Deposit



DXS-18; 11.5 km from source



DXS-5; 13.4 km from source



826-4; 16.6 km from source

Fig. 21 (Continued.)

(1) Block-facies windows

Type 1 exposures contain structures that closely resemble original volcanic structures observed in the crater. The structures are lava flows, platy jointing of domes, dikes, and layered sequences of tephra. Locality DXS-12 is composed entirely of modern dacite rock exhibiting platy dome jointing. The other types of structures were not seen in the windows, but were observed in various localities in the deposit (Figs. 9A, 13 and 14).

Type 2 exposures are composed entirely of one rock type and one color. The homogeneity of the material makes it difficult to determine the amount of deformation and mixing within the material. Locally, the presence of clasts that are fractured but not disaggregated (e.g., 825-5; "jigsaw cracks" of Ui, 1985) and clasts clustered together rather than dispersed throughout the material (probably disaggregated from jigsaw cracks; for example, DXS-16) indicate that parts of the material traveled together as a unit with little deformation.

Type 3 windows show more than one color, but only one rock type. The colors represent different degrees of alteration of the material (Pevear and others, 1982). The boundaries between the colors are either sharp or diffuse. Commonly, the material is deformed into numerous rubble schlieren (for example, DXS-19).

Type 4 windows show more than one rock type and generally more than one color. The boundaries between the rock types and between the colors are either sharp or diffuse and may be deformed into rubble schlieren but show no apparent stratification. The different rock types may represent different debris-avalanche blocks or may represent contacts between different rock types within a block. Commonly, these windows exhibit roughly horizontal stratification of rubble schlieren (for example, 825-3, 827-7).

(2) Block- and matrix-facies windows

Type 5 windows show only one rock type in the block facies and contain some of the blended matrix facies material. The boundaries between the rock types and colors are either sharp or diffuse. Locally, the windows exhibit roughly horizontal stratification of the rubble schlieren (for example, DXS-37).

Type 6 windows show more than one rock type in the block facies and contain some of the blended matrix facies material. The boundaries between the rock types and colors are either sharp or diffuse. Locally, the windows exhibit roughly horizontal stratification of the rubble schlieren (for example, DXS-35).

(3) Matrix-facies windows

Type 7 windows consist entirely of matrix facies material. All the rock types are blended together, so there are no rubble schlieren. These windows are identical in appearance to unsorted and unstratified

exposures of the blast deposit (for example, DXS-18).

5.3.3 Discussion of windows

The windows represent a sampling of the internal texture of the avalanche deposit. They provide evidence for varying degrees of fracturing of clasts and disaggregation and mixing of material during the formation and transport of the rockslide-debris avalanche. In addition, they are close analogs to road-cut or stream-cut exposures in an old deposit, and observations of similar features in an old deposit can help identify it as the deposit of a debris avalanche.

Type 1 exposures show fewer large clasts than similar exposures in the crater indicating that the material was shattered before deposition. This is in contrast with other debris-avalanche deposits (for example, at Mount Shasta; Crandell and others, 1984; Ui and Glicken, 1986) where well-preserved volcanic structures and stratigraphy are common.

Type 2 windows lack well-preserved features, but because they are composed of only one rock type it is difficult to determine the amount of deformation of the material. Jigsaw cracks indicate that the clasts were fractured but not shattered, and that the fragments of the clasts were not dispersed; the paucity of jigsaw cracks at the Mount St. Helens deposit relative to other deposits (Ui and Glicken, 1986; Tadahide Ui, oral commun., 1984) suggests that the clasts in the Mount St. Helens deposit were much more thoroughly shattered than the clasts in most other deposits. However, clustered clasts are apparent in many exposures, which indicates that all clasts were not completely dispersed and at least parts of the material traveled as units from source to place of deposition.

Type 3 windows are composed of only one debris-avalanche block but show colors (representing different degrees of hydrothermal alteration) that enable insight on the amount of internal deformation. Generally, the material is deformed into numerous rubble schlieren. Because the exposures are monolithologic, each exposure probably is from just one debris-avalanche block.

Disaggregation and mixing of debris-avalanche blocks of the block facies were both important processes during the initiation and transport of the debris avalanche. Window types 1 to 3 show little or no mixing, and types 4 to 7 show progressively greater amounts of mixing. The presence of more than one rock type in window types 4 to 6 suggests that there may be more than one debris-avalanche block in each square meter. In these windows, it is apparent that as the avalanche was moving, some of the debris-avalanche blocks disaggregated into their constituent clasts that were mixed together with clasts from other debris-avalanche blocks; this was one of the processes that created the matrix facies present in window types 5, 6, and 7. This process is well illustrated by

windows DXS-9 and DXS-31 (Fig. 21); these exposures consist almost entirely of matrix facies with only a few rubble schlieren of the block facies remaining. The material stopped moving just before mixing was complete.

Breaking up and mixing of the debris-avalanche blocks in the block facies were not the only processes that created the matrix facies. Clasts of juvenile dacite are characteristic of the matrix facies (Table 3), yet no debris-avalanche blocks of juvenile dacite are found in the avalanche deposit. This suggests that masses of juvenile dacite explosively broke apart immediately upon depressurization of the cryptodome. Eyewitness photographs (Voight, 1981) show that explosions burst through slide blocks II and III, mixing pre-1980 rocks with the juvenile dacite. The photographs indicate that the explosions from slide block II created the "blast surge" that spread over the ridges north of the mountain. The explosions that accompanied slide block III were probably less energetic, and the debris from these explosions may have picked up pieces of previously deposited debris avalanche blocks which then disaggregated. The whole mass moved down the North Fork Toutle River valley and was deposited as the matrix facies.

The roughly horizontal stratification of some of the windows may represent original stratigraphy from the mountain or may result from shear within the debris avalanche. If horizontal stratification represents original stratigraphy, it implies that debris-avalanche blocks may have rotated about vertical axes but did not tumble end-over-end during transport. This is consistent with the results of Mimura and Kawachi (1981) and Mimura and others (1982) for the Nirasaki volcanic "dry" avalanche deposit. They found that the inclinations of natural remnant magnetism (NRM) in debris-avalanche blocks of the Nirasaki deposit are similar to one another and generally close to the present magnetic field, but that the declinations are quite different from one another.

Roughly horizontal stratification probably results from shear within the moving avalanche. The stratigraphy within windows generally cannot be recognized as original volcanic stratigraphy. Greater shear takes place at the margins of avalanche flow rather than at the center, and windows at the margins of the deposit commonly exhibit crudely horizontal stratification (e.g., windows 827-7, DXS-26, and DXS-28; Fig. 21). The coherent but deformed debris-avalanche blocks in exposure types 3 to 6 are characteristic of many volcanic debris avalanches around the world (Ui, 1983) and serve as good criteria for recognition of this kind of deposit. Deposits of other poorly-sorted volcanoclastic materials only very rarely show these structures on the scale of the windows. Where they do, it is likely that the blocks were picked up from a pre-existing debris-avalanche deposit and carried

“gently” in a lahar or pyroclastic flow (for example, Scott, 1988, 1989).

As type 7 windows are identical in appearance to many unsorted and unstratified exposures of the blast deposit they cannot provide criteria with which to recognize debris-avalanche deposits. They are only recognized as exposures of the Mount St. Helens debris-avalanche deposit because they are found in hummocks of the deposit.

5.4 Density measurements

To quantify the measure of degree of disaggregation of the debris-avalanche deposit, the density of the deposit and the mountain were determined (Table 4). In-place dry field density of the debris-avalanche deposit was measured by the standard sand-cone test (American Society for Testing of Materials, 1977) on a cleared flat area adjacent to each window. Similar sand-cone density measurements were made at three locations in the older dacite dome complex in the crater walls and at one location in an older dacite pyroclastic-flow deposit in a canyon on the north flank of the mountain. It is not possible to apply the sand-cone technique to the coarse lava flows that make up the bulk of the andesite and basalt unit, so laboratory-determined specific gravity measurements of andesite and basalt clasts >2 cm diameter were assumed to represent the density of the andesite and basalt unit. Laboratory-determined specific gravity measurements of modern dacite clasts >2 cm diameter were assumed to represent the density of the modern dacite unit which is missing from the crater. The density of the least vesiculated juvenile dacite clasts (Hoblitt and others, 1981; Hoblitt and Harmon, 1993) were assumed to approximate the density of the cryptodome.

The mean density of the part of the mountain that became the debris avalanche is calculated to be 2.31 g/cm³.

Sand-cone measurements of the debris-avalanche deposit range from 1.44 to 2.18 g/cm³ and have a mean value of 1.85 g/cm³ (Table 4).

The mean density of the samples from debris avalanche (1.85 g/cm³) is significantly less than the calculated mean density of the old mountain (2.31 g/cm³). In fact, all the density measurements of the debris-avalanche deposit are significantly less than all the measurements of the material making up the old mountain. This suggests that during the events of blast and the rockslide-debris avalanche, the material from the mountain was dilated by about 20 percent before the bulk of it was deposited as the debris-avalanche deposit. There are no trends of increasing or decreasing density with distance from source (Fig. 22). A decreasing trend would be expected if dilation resulted primarily from transport of the material in the debris avalanche or shear within the avalanche.

The lack of this trend suggests that processes that occurred at the mountain were the most important processes that shattered and dilated the material. However, the lower density values for the two units present at the margins of the deposit suggest that shear at the margins of flow contributed to dilation.

5.5 Grain-size analysis

5.5.1 Methods

The wide range in particle size in the debris-avalanche deposit required more than just standard sieve and pipette analyses to properly characterize the deposit. Because the large clasts are rare compared to the smaller sizes, they are not represented in sufficient quantity in the 2- to 4-kg size sample taken for the sieve and pipette analyses. Therefore, the size distribution of coarse clasts was approximated by tracing areas of coarse clasts on photographic prints of the 1-m² windows. The sample for standard sieve and pipette analysis was taken from a cylindrical hole dug in a cleared flat area adjacent to each window.

Sieve and pipette analyses are computed as weight percentages, not volume percentages. In order to integrate the data sets, the volume percentages of the coarse material were converted to weight percentages using the relation

$$W_c = \frac{100\rho_c V_c}{\rho_c V_{ct} + \rho_f (100 - V_{ct})}$$

where

W_c = weight percent of size class coarser than -5ϕ

V_c = volume percent of size class coarser than -5ϕ

V_{ct} = total volume percent of all size classes coarser than -5ϕ

ρ_c = density of material coarser than -5ϕ

ρ_f = density of material finer than -5ϕ .

The mean density of the material coarser than -5ϕ was measured in the laboratory for each lithologic unit (Table 4). The density of the material finer than -5ϕ in the photographs includes the void space in the deposit. It is equivalent to the dry bulk density of the deposit, which was measured for each window (Table 4). After conversion to weight percentages, the data for the coarse clasts were integrated with the data from the sieve and pipette analyses to produce Table 5.

5.5.2 Results

(1) General statement

The results of the grain-size analyses were plotted as histograms and as cumulative normal probability plots and cumulative Rosin-law plots. Various standard statistics were calculated using a computer program, and they were plotted in different ways. In order to make comparisons with statistics used by

Table 4 Distance from source, density, grain-size, and sorting parameters for debris-avalanche and blast deposits. [distr, distance from source (assumed to be the site of the 1980-85 dome) in km; denco, density of coarse clasts measured for some samples and assumed for others to be average of measured samples for each unit, in g/cm³; denfld, field density computed by sand-cone method, in g/cm³; pct, percentage; gr, gravel; sa, sand; si, silt, cl, clay; mu, mud (silt + clay); fw, Folk and Ward (1957); in, Inman (1954); tr, Trask (1930); mom, moment statistics; md, median; mn, mean; so, sorting; sk, skewness; ku, kurtosis; stand dev, standard deviation; Sprrt, at Spirit Lake, Cold, at Coldwater Lake; Cstl, at Castle Lake]

Sample	distr	denco	denfld	pctgr	pctsa	pctsi	pctcl	pctmu	mommn	momso	fwmd	fwmn	fwso
Older dacite unit													
DXS-2	25.30	1.97	2.43	59.06	32.65	7.54	0.75	8.29	-1.57	3.86	-2.24	-1.71	3.92
DXS-4	15.10	2.07	2.43	37.22	51.44	10.32	1.02	11.34	0.19	3.46	0.41	-0.02	3.39
DXS-6	15.60	2.04	2.39	52.65	43.74	3.21	0.40	3.61	-0.99	2.74	-1.17	-0.98	2.65
DXS-20	12.30	2.08	2.39	21.98	60.62	14.78	2.61	17.39	1.32	3.13	1.00	1.24	2.84
DXS-21	18.40	2.15	2.39	40.52	47.53	10.64	1.31	11.95	-0.18	3.86	0.04	-0.27	3.85
DXS-22	17.60	1.93	2.39	48.61	39.05	11.23	1.11	12.34	-0.64	3.95	-0.82	-0.75	3.97
DXS-24	13.30	1.86	2.39	22.81	65.41	10.13	1.65	11.78	1.04	2.72	0.84	0.83	2.55
825-3(Sprt)	9.40	1.75	2.43	23.83	55.01	17.78	3.39	21.16	1.45	3.94	1.81	1.50	3.84
827-3(Sprt)	9.70	1.98	2.43	24.00	60.50	13.64	1.86	15.50	1.11	3.10	0.96	0.92	3.01
MS-10(Cold)	16.90	1.61	2.43	30.40	55.80	12.28	1.52	13.80	0.80	3.10	0.80	0.64	3.06
826-3(Cstl)	16.40	1.45	2.43	37.95	52.24	8.92	0.88	9.81	0.20	3.12	0.25	0.02	3.12
mean	15.45	1.90	2.41	36.28	51.27	10.95	1.50	12.45	0.25	3.36	0.17	0.13	3.29
stan dev	4.45	0.22	0.02	12.99	9.87	3.84	0.87	4.64	1.00	0.47	1.16	1.00	0.53
Andesite and basalt unit													
DXS-11	13.50	2.13	2.27	49.35	46.05	4.37	0.23	4.60	-1.06	2.95	-0.94	-1.11	2.81
DXS-13	2.50	2.13	2.27	41.23	52.49	5.52	0.75	6.28	-0.49	3.21	-0.16	-0.59	3.16
DXS-14	2.70	1.97	2.27	48.05	45.66	5.72	0.57	6.29	-0.61	2.95	-0.82	-0.75	2.85
DXS-16	11.30	2.07	2.27	56.86	34.34	8.00	0.79	8.80	-1.19	3.58	-1.78	-1.14	3.50
DXS-23	13.00	1.66	2.27	50.81	43.52	5.39	0.28	5.67	-0.87	3.03	-1.06	-0.96	3.01
DXS-25	14.60	1.86	2.27	65.15	30.12	4.21	0.52	4.73	-2.14	3.43	-2.58	-2.29	3.39
DXS-27	17.70	2.08	2.27	27.83	59.17	11.05	1.95	13.00	0.71	3.53	1.08	0.63	3.38
DXS-38	29.70	1.77	2.27	47.78	45.47	6.01	0.74	6.75	-0.93	3.39	-0.86	-0.90	3.47
825-5(Sprt)	9.40	1.84	2.27	69.08	29.29	1.48	0.15	1.63	-2.31	2.93	-3.00	-2.27	2.94
827-2(Sprt)	10.60	1.82	2.27	66.62	28.71	4.15	0.51	4.67	-2.46	3.64	-3.41	-2.76	3.68
MS-9(Cold)	16.90	1.53	2.27	47.92	41.08	9.57	1.43	11.00	-0.80	4.04	-0.69	-0.81	4.00
mean	12.90	1.90	2.27	51.88	41.45	5.95	0.72	6.67	-1.10	3.33	-1.29	-1.18	3.29
stan dev	7.46	0.20	0.00	12.09	9.92	2.69	0.54	3.20	0.92	0.36	1.31	0.95	0.37
Modern dacite unit													
DXS-3	15.70	1.85	2.22	61.01	31.59	6.37	1.04	7.40	-2.04	4.13	-2.71	-2.20	4.15
DXS-12	13.50	1.85	2.22	92.34	6.56	1.01	0.09	1.09	-5.58	2.66	-6.51	-5.87	2.33
DXS-19	11.70	2.13	2.22	53.63	38.12	7.51	0.74	8.25	-0.74	3.42	-1.49	-0.88	3.25
MS-1(Cold)	17.20	2.12	2.22	48.03	41.14	9.20	1.62	10.83	-0.48	3.72	-0.76	-0.56	3.58
mean	14.53	1.99	2.22	63.75	29.35	6.02	0.87	6.89	-2.21	3.48	-2.87	-2.38	3.33
stan dev	2.42	0.16	0.00	19.79	15.71	3.54	0.64	4.13	2.35	0.62	2.56	2.43	0.76

Table 4 Distance from source, density, grain-size, and sorting parameters for debris-avalanche and blast deposits--*Continued.*

Sample	fwsk	fwku	inmd	inmn	inso	insk1	insk2	inku	trmd	trmn	trso	trsk	trku
Older dacite unit													
DXS-2	0.19	0.89	-2.24	-1.45	4.12	0.19	0.29	0.49	4.71	10.71	7.15	0.39	0.12
DXS-4	-0.07	0.82	0.41	-0.24	3.57	-0.18	0.06	0.48	0.75	3.54	6.30	2.12	0.16
DXS-6	0.04	1.17	-1.17	-0.89	2.43	0.11	-0.06	0.95	2.25	3.39	3.16	0.75	0.23
DXS-20	0.11	0.98	1.00	1.36	2.86	0.12	0.14	0.63	0.50	0.91	3.87	0.78	0.17
DXS-21	-0.09	0.90	0.04	-0.43	3.86	-0.12	-0.10	0.64	0.97	4.81	7.40	1.72	0.12
DXS-22	0.05	0.86	-0.82	-0.72	4.18	0.02	0.11	0.48	1.76	6.24	7.83	0.79	0.11
DXS-24	0.07	1.05	0.84	0.83	2.56	0.00	0.24	0.63	0.56	0.95	3.11	0.97	0.18
825-3(Sprt)	-0.18	1.22	1.81	1.34	3.70	-0.13	-0.41	0.77	0.29	0.91	4.57	1.79	0.07
827-3(Sprt)	0.01	1.01	0.96	0.90	3.04	-0.02	0.07	0.62	0.51	1.00	3.97	0.84	0.11
MS-10(Cold)	-0.01	0.93	0.80	0.55	3.14	-0.08	0.09	0.57	0.57	1.55	4.47	1.33	0.15
826-3(Cstl)	-0.03	0.85	0.25	-0.09	3.26	-0.10	0.07	0.51	0.84	2.74	5.21	1.45	0.17
mean	0.01	0.97	0.17	0.11	3.34	-0.02	0.05	0.62	1.25	3.34	5.19	1.18	0.14
stan dev	0.10	0.13	1.16	0.95	0.60	0.12	0.19	0.14	1.29	3.02	1.72	0.54	0.04
Andesite and basalt unit													
DXS-11	0.03	0.77	-0.94	-1.19	3.06	-0.08	0.19	0.39	1.92	6.34	4.82	1.72	0.24
DXS-13	-0.14	0.89	-0.16	-0.81	3.25	-0.20	-0.13	0.56	1.11	4.21	5.06	2.07	0.15
DXS-14	0.11	0.85	-0.82	-0.71	2.97	0.04	0.27	0.51	1.77	4.09	4.51	0.95	0.20
DXS-16	0.24	0.83	-1.78	-0.82	3.64	0.26	0.32	0.52	3.43	8.28	6.68	0.50	0.23
DXS-23	0.08	0.87	-1.06	-0.91	3.18	0.05	0.17	0.47	2.08	4.52	4.64	0.80	0.13
DXS-25	0.15	0.98	-2.58	-2.14	3.40	0.13	0.27	0.63	5.99	11.69	4.98	0.57	0.12
DXS-27	-0.19	1.10	1.08	0.40	3.24	-0.21	-0.31	0.79	0.47	1.39	4.47	1.57	0.07
DXS-38	-0.06	1.06	-0.86	-0.92	3.31	-0.02	-0.19	0.82	1.82	5.52	5.01	1.36	0.16
825-5(Sprt)	0.30	0.95	-3.00	-1.90	2.98	0.37	0.36	0.61	7.99	10.57	4.22	0.35	0.24
827-2(Sprt)	0.27	1.06	-3.41	-2.44	3.96	0.25	0.42	0.42	10.62	9.02	4.53	0.13	0.07
MS-9(Cold)	-0.03	0.90	-0.69	-0.86	4.04	-0.04	-0.04	0.62	1.62	7.61	7.85	1.39	0.08
mean	0.07	0.93	-1.29	-1.12	3.37	0.05	0.12	0.58	3.53	6.66	5.16	1.04	0.15
stan dev	0.16	0.11	1.31	0.79	0.37	0.19	0.25	0.14	3.25	3.10	1.10	0.63	0.07
Modern dacite unit													
DXS-3	0.16	0.89	-2.71	-1.94	4.19	0.18	0.21	0.62	6.55	17.74	8.67	0.38	0.12
DXS-12	0.55	1.53	-6.51	-5.54	2.17	0.45	1.23	0.89	91.28	108.24	2.14	0.83	0.31
DXS-19	0.28	0.71	-1.49	-0.58	3.48	0.26	0.42	0.44	2.80	6.43	7.32	0.38	0.29
MS-1(Cold)	0.11	0.86	-0.76	-0.47	3.64	0.08	0.21	0.60	1.69	5.63	6.78	0.92	0.20
mean	0.28	1.00	-2.87	-2.13	3.37	0.24	0.52	0.64	25.58	34.51	6.23	0.63	0.23
stan dev	0.20	0.36	2.56	2.37	0.86	0.16	0.49	0.19	43.85	49.46	2.84	0.29	0.09

Table 4 Distance from source, density, grain-size, and sorting parameters for debris-avalanche and blast deposits.--Continued.

Sample	distr	denco	denfld	pctgr	pctsa	pctsi	pctcl	pctmu	mommn	momso	fwmd	fwmn	fwso
Modern undifferentiated unit													
DXS-17	12.40	1.96	2.25	55.49	31.22	12.49	0.80	13.29	-0.71	3.68	-1.71	-0.74	3.60
826-2(Cstl)	16.20	1.51	2.25	43.47	46.75	8.80	0.98	9.78	-0.31	3.40	-0.36	-0.43	3.38
827-6(Cstl)	15.90	1.44	2.25	46.73	43.73	8.59	0.95	9.55	-0.82	4.08	-0.49	-0.65	3.99
827-7(Cstl)	15.90	1.50	2.25	45.91	41.55	11.16	1.38	12.54	-0.27	3.76	-0.38	-0.39	3.74
mean	15.10	1.60	2.25	47.90	40.81	10.26	1.03	11.29	-0.53	3.73	-0.74	-0.55	3.68
stan dev	1.81	0.24	0.00	5.25	6.74	1.89	0.25	1.90	0.28	0.28	0.65	0.17	0.26
Mixed block and matrix facies unit													
DXS-1	29.90	1.99	2.30	42.89	43.52	12.36	1.22	13.58	-0.12	3.88	-0.05	-0.21	3.88
DXS-8	25.80	1.76	2.30	41.53	51.23	6.52	0.72	7.24	-0.18	3.15	-0.12	-0.32	3.07
DXS-29	21.40	1.81	2.30	47.93	42.83	7.67	1.57	9.24	-0.75	3.81	-0.71	-0.78	3.75
DXS-30	22.20	1.96	2.26	41.26	48.11	9.26	1.38	10.64	-0.20	3.52	-0.03	-0.22	3.51
DXS-31	23.10	2.10	2.30	35.72	54.97	8.10	1.21	9.31	0.20	3.21	0.43	0.06	3.12
DXS-33	24.50	2.18	2.30	46.33	45.30	7.62	0.75	8.38	-0.70	3.64	-0.60	-0.76	3.63
DXS-34	26.80	1.77	2.39	36.96	51.07	10.41	1.56	11.97	0.15	3.47	0.26	-0.04	3.39
DXS-35	28.10	1.80	2.30	51.04	41.57	6.64	0.74	7.38	-0.96	3.64	-1.15	-0.94	3.53
DXS-36	31.20	1.68	2.30	39.07	53.76	6.53	0.65	7.17	-0.20	3.31	0.08	-0.31	3.32
DXS-37	30.70	1.90	2.30	35.32	51.88	10.62	2.17	12.79	0.29	3.57	0.34	0.06	3.46
mean	26.37	1.89	2.31	41.81	48.42	8.57	1.20	9.77	-0.25	3.52	-0.16	-0.35	3.47
stan dev	3.56	0.16	0.03	5.32	4.83	2.01	0.49	2.37	0.43	0.24	0.51	0.36	0.26
Marginal mixed block and matrix facies unit													
DXS-9	21.70	1.77	2.30	46.10	44.35	8.60	0.96	9.55	-0.72	3.89	-0.45	-0.71	3.86
DXS-26	17.70	1.57	2.30	40.70	48.40	10.02	0.87	10.90	-0.15	3.47	0.06	-0.27	3.44
DXS-28	21.00	1.45	2.30	47.70	41.10	10.19	1.01	11.19	-0.44	3.59	-0.63	-0.48	3.47
DXS-32	23.60	1.66	2.30	34.24	51.55	12.51	1.70	14.21	0.29	3.90	0.83	0.31	3.85
mean	21.00	1.61	2.30	42.19	46.35	10.33	1.13	11.46	-0.26	3.71	-0.05	-0.29	3.65
stan dev	2.46	0.14	0.00	6.08	4.58	1.62	0.38	1.97	0.43	0.22	0.65	0.44	0.23
All of debris avalanche deposit													
mean	17.68	1.85	2.31	45.53	44.78	8.59	1.10	9.70	-0.54	3.47	-0.65	-0.63	3.40
stan dev	6.96	0.22	0.07	13.37	10.62	3.41	0.65	3.98	1.18	0.39	1.45	1.20	0.43
Blast deposit													
DXS-5	13.40	1.82	2.18	32.73	54.70	11.19	1.38	12.58	0.68	3.27	0.82	0.53	3.12
DXS-18	11.50	2.21	2.18	42.09	48.94	7.89	1.08	8.97	-0.23	3.49	0.00	-0.37	3.38
826-4(Cstl)	16.60	2.02	2.18	30.68	52.74	14.09	2.49	16.58	0.94	3.64	1.23	0.78	3.39
mean	13.83	2.02	2.18	35.17	52.13	11.06	1.65	12.71	0.46	3.47	0.68	0.31	3.30
stan dev	2.58	0.20	0.00	6.08	2.93	3.10	0.74	3.81	0.61	0.19	0.63	0.60	0.15

Table 4 Distance from source, density, grain-size, and sorting parameters for debris-avalanche and blast deposits.--Continued.

Sample	distr	denco	denfld	pctgr	pctsa	pctsi	pctcl	pctmu	mommn	momso	fwmd	fwmn	fwso
Old mountain clastics													
DXS-15	0.00	2.41	2.39	83.95	14.02	1.89	0.14	2.03	-3.65	2.88	-4.14	-3.85	2.82
CSX-1	0.00	2.38	2.39	37.30	54.70	7.60	0.40	8.00	0.18	2.71	-0.08	0.05	2.68
CXS-2	0.00	2.53	2.39	41.50	47.70	10.04	0.76	10.80	0.10	2.92	-0.41	-0.07	2.87
CXS-3	0.00	2.44	2.39	0.00	0.00	0.00	0.00	0.00	0.00	0.00	0.00	0.00	0.00
mean	0.00	2.44	2.39	40.69	29.11	4.88	0.32	5.21	-0.84	2.13	-1.16	-0.97	2.09
stan dev	0.00	0.06	0.00	34.35	26.30	4.72	0.33	5.04	1.87	1.42	2.00	1.92	1.40
Sample	fwsk	fwku	inmd	inmn	inso	insk1	insk2	inku	trmd	trmn	trso	trsk	trku
Old mountain clastics- Continued													
DXS-15	0.23	1.23	-4.14	-3.71	2.72	0.16	0.54	0.77	17.65	26.72	3.03	0.81	0.17
CSX-1	0.14	0.82	-0.08	0.12	2.79	0.07	0.31	0.52	1.06	2.28	4.37	0.88	0.26
CXS-2	0.24	0.88	-0.41	0.10	2.92	0.17	0.49	0.59	1.32	2.47	4.46	0.63	0.27
CXS-3	0.00	0.00	0.00	0.00	0.00	0.00	0.00	0.00	0.00	0.00	0.00	0.00	0.00
mean	0.15	0.73	-1.16	-0.87	2.11	0.10	0.34	0.47	5.01	7.87	2.96	0.58	0.17
stan dev	0.11	0.52	2.00	1.89	1.41	0.08	0.24	0.33	8.45	12.62	2.08	0.40	0.13

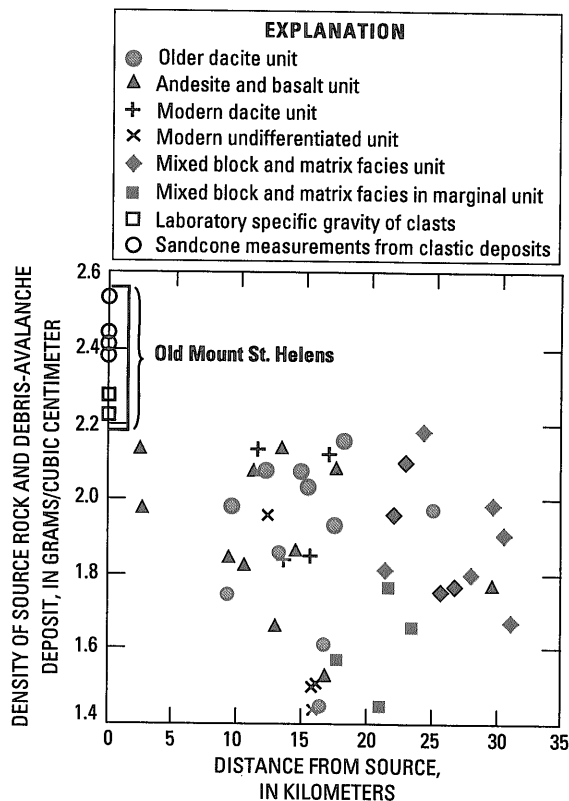


Fig. 22 Density of source rocks and debris-avalanche deposit versus distance from source (0-km values are old mountain densities).

various geologists and engineers, graphically determined values computed by the methods of Folk and Ward (1957), Inman (1952), Trask (1930) are included in Table 4. The Folk and Ward and Inman values for mean, median, and sorting are intended to approximate values determined by the method of moments (Folk, 1974), in which every size interval affects the results. For the irregular distributions of sizes that are typical of the debris-avalanche samples, moment statistics are much better measures (Folk, 1974) than graphically derived statistics, which are calculated from only a few percentage lines and the grain-sizes are assumed to be approximately normally distributed.

(2) Distribution plots

The grain-size distribution of individual samples was plotted on histograms, on cumulative plots, and on Rosin-law plots. Each type of plot illustrates several features characteristic of the avalanche deposit. Grain-size distributions are of three general types. Most are bimodal; the fine-grained peak in the histogram is between -1ϕ and 3ϕ (peaks in a larger than -5ϕ categories are ignored because of the inherent inaccuracies of the measurement of the coarse clasts) and the maxima of this peak generally lies between 0ϕ and 2ϕ . Most of the rest are type 1 unimodal samples with the same peak and a few are type 2 unimodal with a coarser peak (maximum value in a class coarser than -2ϕ).

Table 5 Grain-size data in phi (ϕ) units for debris-avalanche and blast deposits. [Samples located on Pl. 2. Results in percent. Material coarser than -5ϕ analyzed by computation of areas of clasts on 1-m² windows (see text); material finer than -5ϕ analyzed by standard sieve and pipette techniques. "without coarse fraction" indicates that data include only sieved and pipetted fraction (material finer than -5ϕ). Sprt, at Spirit Lake; Cold, at Coldwater Lake; Cstl, at Castle Lake; stan dev, standard deviation]

Sample	-8	-7	-6	-5	-4	-3	-2	-1	0	1	2	3	4	5	6	7	8	9	14
Older dacite unit																			
DXS-2	0.00	6.14	7.32	6.01	10.24	13.03	9.22	7.11	7.19	6.77	6.85	6.09	5.75	2.98	2.24	1.82	0.50	0.00	0.75
DXS-4	0.00	0.00	2.01	1.80	10.23	9.32	7.29	6.58	9.42	8.40	13.27	11.95	8.40	3.86	2.72	2.27	1.47	0.11	0.91
DXS-6	0.00	1.53	3.86	2.14	1.39	10.45	16.83	16.46	13.78	11.93	9.43	5.83	2.77	1.66	0.97	0.51	0.07	0.04	0.36
DXS-20	0.00	0.00	0.00	1.74	0.69	3.44	5.80	10.32	14.35	13.66	12.87	10.71	9.04	5.74	4.70	3.65	0.70	0.35	2.26
DXS-21	0.00	3.83	3.62	3.38	8.74	7.04	6.60	7.31	9.10	9.81	10.34	9.54	8.74	4.06	2.99	2.39	1.19	0.12	1.19
DXS-22	0.00	3.05	5.59	6.84	5.66	12.00	8.88	6.59	7.95	7.61	8.37	7.61	7.52	4.69	3.09	2.22	1.23	0.12	0.99
DXS-24	0.00	0.00	0.00	0.14	0.20	3.00	10.28	9.19	11.08	19.87	15.08	11.48	7.89	4.48	3.30	1.88	0.47	0.12	1.53
825-3(Sprt)	0.00	2.84	2.86	3.07	0.00	3.28	6.84	4.93	6.66	9.40	12.77	12.86	13.32	4.87	6.56	5.08	1.27	0.21	3.17
827-3(Sprt)	0.00	0.00	0.00	0.00	3.60	6.90	6.40	7.10	13.10	13.40	12.30	11.10	10.60	5.27	4.96	3.26	0.16	0.16	1.71
MS-10(Cold)	0.00	0.00	0.00	0.00	4.00	8.50	8.50	9.40	10.60	11.30	13.20	12.10	8.60	5.11	3.73	3.04	0.41	0.28	1.24
826-3(Cstl)	0.00	0.00	0.00	0.00	9.28	10.34	8.96	9.38	9.49	10.98	12.37	10.98	8.42	3.63	2.84	2.06	0.39	0.10	0.79
mean	0.00	1.58	2.30	2.28	4.91	7.94	8.96	8.58	10.25	11.19	11.53	10.02	8.28	4.21	3.46	2.56	0.71	0.15	1.35
stan dev	0.00	2.11	2.59	2.39	4.12	3.53	3.04	3.07	2.61	3.64	2.47	2.45	2.63	1.16	1.50	1.18	0.49	0.10	0.79
Andesite and basalt unit																			
DXS-11	0.00	1.89	1.08	1.09	15.90	11.62	8.77	8.99	13.27	13.16	9.32	6.14	4.17	2.49	1.29	0.51	0.09	0.09	0.14
DXS-13	0.00	0.00	3.65	4.21	9.03	8.27	9.79	6.28	10.94	13.03	14.17	9.03	5.33	2.39	1.69	1.38	0.06	0.13	0.63
DXS-14	0.00	0.00	0.64	2.16	9.48	12.27	12.27	11.23	11.13	11.23	11.03	7.73	4.53	2.52	1.82	1.32	0.06	0.06	0.50
DXS-16	0.00	1.63	4.48	4.58	15.70	12.56	9.00	8.90	7.96	7.01	6.81	6.49	6.07	4.05	2.37	1.23	0.35	0.18	0.62
DXS-23	0.00	0.00	1.65	8.33	6.60	9.67	10.97	13.58	11.81	9.11	9.86	7.63	5.12	3.06	1.48	0.68	0.17	0.00	0.28
DXS-25	0.00	6.49	6.94	5.76	14.62	11.38	11.03	8.93	8.58	8.14	6.57	3.85	2.98	1.80	1.23	1.09	0.10	0.00	0.52
DXS-27	0.00	1.53	2.34	4.37	2.39	4.49	6.12	6.59	9.84	11.28	13.86	13.29	10.90	5.07	3.25	2.47	0.26	0.13	1.82
DXS-38	0.00	5.73	1.18	3.32	9.29	9.00	7.33	11.93	14.96	10.07	8.31	6.85	5.28	2.97	1.89	1.01	0.14	0.07	0.68
825-5(Sprt)	0.00	4.37	2.33	7.66	19.19	16.44	10.96	8.14	7.11	7.19	7.02	5.14	2.83	1.04	0.33	0.08	0.03	0.02	0.13
827-2(Sprt)	0.00	8.33	12.71	1.29	20.34	11.18	6.78	5.99	6.61	7.05	6.69	4.76	3.61	1.87	1.35	0.84	0.09	0.00	0.51
MS-9(Cold)	0.00	7.24	5.03	3.20	8.45	10.54	7.09	6.36	7.18	8.91	10.63	8.00	6.36	3.96	2.86	2.53	0.22	0.22	1.21
mean	0.00	3.38	3.82	4.18	11.91	10.67	9.10	8.81	9.94	9.65	9.48	7.17	5.20	2.84	1.78	1.19	0.14	0.08	0.64
stan dev	0.00	3.14	3.53	2.36	5.60	2.98	2.07	2.53	2.73	2.28	2.75	2.54	2.22	1.16	0.81	0.75	0.10	0.08	0.49
Modern dacite unit																			
DXS-3	7.64	2.96	6.92	8.74	11.03	10.16	7.88	5.67	5.91	7.17	8.35	5.75	4.41	2.52	2.07	1.48	0.30	0.07	0.96
DXS-12	0.00	38.73	21.42	16.91	3.82	4.98	3.84	2.65	2.19	1.58	1.21	0.91	0.67	0.42	0.31	0.22	0.07	0.01	0.08
DXS-19	0.00	0.00	1.03	4.01	14.30	15.46	10.81	8.02	6.28	5.58	8.48	11.04	6.74	3.30	2.06	1.73	0.41	0.08	0.66
MS-1(Cold)	0.00	1.79	2.51	3.95	9.57	13.10	8.89	8.20	8.20	8.89	9.35	7.98	6.72	3.46	2.82	2.38	0.54	0.11	1.52
mean	1.91	10.87	7.97	8.40	9.68	10.93	7.86	6.14	5.64	5.81	6.85	6.42	4.63	2.42	1.81	1.45	0.33	0.07	0.81
stan dev	3.82	18.61	9.31	6.10	4.38	4.52	2.94	2.59	2.51	3.12	3.78	4.27	2.86	1.40	1.06	0.91	0.20	0.04	0.60
Modern undifferentiated unit																			
DXS-17	0.00	0.00	2.82	4.24	13.60	15.76	10.82	8.24	5.77	4.74	6.18	7.11	7.42	6.25	3.59	2.39	0.27	0.13	0.66
826-2(Cstl)	0.00	0.00	3.55	2.06	11.03	8.90	9.03	8.90	10.28	10.15	10.03	8.77	7.52	4.11	3.03	1.27	0.39	0.20	0.78
827-6(Cstl)	9.43	0.00	2.31	0.81	8.62	10.88	8.31	6.36	6.67	8.83	10.47	9.75	8.01	3.91	3.15	1.15	0.38	0.10	0.86
827-7(Cstl)	0.00	0.00	5.18	1.13	12.84	11.56	8.62	6.57	6.66	8.13	9.70	9.21	7.84	3.39	4.39	3.01	0.38	0.25	1.13
mean	2.36	0.00	3.46	2.06	11.52	11.78	9.19	7.52	7.34	7.96	9.10	8.71	7.70	4.41	3.54	1.96	0.35	0.17	0.86
stan dev	4.72	0.00	1.25	1.55	2.22	2.89	1.12	1.25	2.00	2.31	1.97	1.14	0.27	1.26	0.62	0.90	0.06	0.07	0.20

Table 5 Grain-size data in phi (ϕ) units for debris-avalanche and blast deposits--*Continued.*

Sample	-8	-7	-6	-5	-4	-3	-2	-1	0	1	2	3	4	5	6	7	8	9	14
Mixed block and matrix facies unit																			
DXS-1	0.00	4.22	2.05	1.33	10.53	9.98	7.48	7.30	7.48	7.58	9.98	9.98	8.50	3.94	4.35	3.12	0.95	0.14	1.09
DXS-8	0.00	0.00	1.22	2.37	9.73	9.40	9.51	9.30	9.62	10.16	11.67	12.43	7.35	2.97	1.88	1.52	0.14	0.07	0.65
DXS-29	0.00	4.55	3.79	1.85	13.57	9.72	7.99	6.45	7.60	10.01	10.97	7.99	6.26	3.14	2.40	2.03	0.09	0.18	1.39
DXS-30	0.00	1.42	3.87	0.57	7.44	12.24	8.94	6.78	9.04	12.71	11.20	8.66	6.50	3.83	2.87	2.45	0.11	0.21	1.17
DXS-31	0.00	0.00	1.19	2.87	7.10	7.39	8.06	9.11	9.69	11.23	14.58	11.90	7.58	3.72	2.33	1.86	0.19	0.09	1.12
DXS-33	0.00	4.68	3.93	4.20	6.53	9.84	8.38	8.77	9.25	9.94	10.62	9.64	5.84	3.10	2.26	1.59	0.67	0.00	0.75
DXS-34	0.00	0.00	1.60	2.19	10.10	7.91	8.79	6.37	9.88	12.63	12.08	9.66	6.81	4.31	2.87	2.39	0.84	0.00	1.56
DXS-35	0.00	4.49	2.28	3.94	13.40	11.47	8.29	7.16	7.38	8.06	10.00	10.00	6.13	2.95	1.70	1.40	0.59	0.00	0.74
DXS-36	0.00	0.00	4.31	3.92	7.73	7.92	6.80	8.39	10.16	10.34	12.02	12.67	8.57	3.30	1.79	1.22	0.22	0.07	0.57
DXS-37	0.00	0.00	3.04	1.62	8.73	7.21	7.01	7.72	10.76	11.88	12.29	9.54	7.41	4.09	3.20	3.07	0.26	0.26	1.92
mean	0.00	1.94	2.73	2.49	9.49	9.31	8.13	7.74	9.09	10.45	11.54	10.25	7.09	3.54	2.57	2.07	0.41	0.10	1.10
stan dev	0.00	2.24	1.20	1.23	2.49	1.70	0.85	1.09	1.20	1.73	1.35	1.58	0.95	0.50	0.80	0.67	0.32	0.09	0.44
Marginal mixed block and matrix facies unit																			
DXS-9	0.00	6.56	4.36	3.40	9.36	8.58	6.92	6.92	7.21	8.38	12.57	9.36	6.82	3.63	2.48	2.20	0.29	0.10	0.86
DXS-26	0.00	0.00	1.34	4.71	11.68	8.93	7.76	6.28	8.64	11.29	11.98	9.33	7.17	4.14	2.94	2.07	0.87	0.11	0.76
DXS-28	0.00	0.00	2.34	3.60	13.07	11.85	11.76	5.08	6.87	8.28	10.82	8.37	6.77	4.03	3.25	2.35	0.56	0.00	1.01
DXS-32	0.00	5.97	3.04	1.92	3.34	6.32	6.50	7.15	8.17	9.29	12.63	12.45	9.01	5.54	3.98	2.56	0.43	0.14	1.56
mean	0.00	3.13	2.77	3.41	9.36	8.92	8.24	6.36	7.72	9.31	12.00	9.88	7.44	4.34	3.16	2.30	0.54	0.09	1.05
stan dev	0.00	3.63	1.27	1.15	4.30	2.27	2.41	0.93	0.82	1.40	0.84	1.78	1.06	0.83	0.63	0.21	0.25	0.06	0.36
All debris avalanche samples																			
mean	0.39	2.95	3.44	3.44	9.14	9.64	8.59	7.92	9.00	9.69	10.42	8.90	6.78	3.58	2.67	1.93	0.42	0.11	0.99
stan dev	1.81	6.07	3.67	2.99	4.76	3.10	2.15	2.33	2.54	2.92	2.70	2.68	2.32	1.21	1.21	0.97	0.36	0.09	0.59
All debris avalanche samples without coarse fraction																			
mean	0.00	0.00	0.00	0.00	10.46	11.04	9.72	8.87	9.97	10.66	11.44	9.75	7.44	3.94	2.93	2.11	0.46	0.12	1.09
stan dev	0.00	0.00	0.00	0.00	5.61	3.92	2.48	2.34	2.26	2.51	2.37	2.49	2.28	1.18	1.23	1.00	0.39	0.09	0.62
Blast deposit above debris avalanche																			
DXS-5	0.00	0.00	1.09	1.42	4.49	7.12	9.07	9.56	9.46	9.56	10.92	15.11	9.65	4.40	3.27	3.02	0.50	0.00	1.38
DXS-18	0.00	0.00	2.34	4.86	10.96	9.47	7.97	6.48	7.87	9.07	11.36	13.36	7.28	3.59	1.97	1.88	0.45	0.09	0.99
826-4(Cstl)	0.00	0.00	3.22	0.83	3.11	9.22	8.29	6.01	7.88	8.81	12.44	12.85	10.78	4.64	4.64	3.98	0.83	0.17	2.32
mean	0.00	0.00	2.22	2.37	6.19	8.60	8.44	7.35	8.40	9.15	11.57	13.77	9.24	4.21	3.29	2.96	0.59	0.09	1.56
stan dev	0.00	0.00	1.07	2.18	4.19	1.29	0.57	1.93	0.92	0.38	0.78	1.19	1.79	0.55	1.34	1.05	0.21	0.09	0.68
Old mountain clastics (older dacite)																			
DXS-15	0.00	10.07	10.42	11.78	21.13	15.31	9.41	5.82	4.61	3.39	2.71	2.03	1.29	0.98	0.53	0.28	0.10	0.02	0.12
CXS-1	0.00	0.00	0.00	0.00	2.40	8.60	16.10	10.20	13.90	10.80	11.10	11.80	7.10	2.96	2.72	1.68	0.24	0.16	0.24
CXS-2	0.00	0.00	0.00	0.00	2.80	10.60	15.40	12.70	13.80	9.90	8.80	9.80	5.40	3.56	3.24	3.02	0.22	0.32	0.43
mean	0.00	3.36	3.47	3.93	8.78	11.50	13.64	9.57	10.77	8.03	7.54	7.88	4.60	2.50	2.16	1.66	0.19	0.17	0.26
stan dev	0.00	5.81	6.02	6.80	10.70	3.45	3.68	3.48	5.33	4.04	4.34	5.16	2.99	1.35	1.44	1.37	0.08	0.15	0.16

(3) Cumulative plots

Cumulative probability plots of samples of the debris-avalanche deposit graphically illustrate the conformity of the grain-size distributions to a normal distribution, and cumulative Rosin-law plots of the grain-size distributions of samples test the conformity of the distributions to Rosin's law of crushing. Sediments from one source material that have been sorted by a single sorting mechanism generally plot as the normal distribution (Folk, 1966). Rosin's law is a mathematical function that describes the grain-size distribution of a number of different artificial products such as broken coal and cement, and Kittleman (1964) showed that it also applies to the grain-size distributions of granite scree and broken hydrothermal quartz. A straight line on a cumulative probability plot indicates a normal distribution, but a straight line on a Rosin-law plot indicates that a sample follows the Rosin-law distribution.

Murai (1961) suggested that detailed studies of "dry mudflow" (large volcanic debris avalanche) deposit would show that their grain-size distributions closely conform to the Rosin-law distribution. The data from this detailed study suggest otherwise. In nearly every sample, the distribution curves plot closer to a straight line on the normal probability plot than on the Rosin-law plot. For all the samples the Rosin-law curve shows a concave upward trend.

(4) Statistical parameters

Median grain diameter (Md_ϕ) plotted against Inman sorting coefficient (σ_ϕ) is commonly used to discriminate between different types of volcanoclastic deposits (Walker, 1971; Fisher and Schmincke, 1984). The debris avalanche has Inman sorting values (2.17ϕ - 4.19ϕ) comparable to those of pyroclastic flow deposits analyzed by Walker (1971). Although there is considerable overlap in the values of Md_ϕ between the fields for the debris-avalanche deposit and pyroclastic flow deposits, the data show that the Mount St. Helens' debris-avalanche deposit generally has coarser values of median grain size than do pyroclastic flow deposits (although some of Walker's samples probably do not include material too coarse to sieve) but has roughly the same sorting values (Fig. 23). Comparing my debris-avalanche data with tabular data for lahars compiled by Fisher and Schmincke (1984) shows that many samples from the debris avalanche are better sorted than the samples from lahars; this difference in sorting probably indicates that many debris avalanche samples are derived from well-sorted volcanoclastic materials. Samples from the debris avalanche also are generally better sorted and finer grained than samples from the lahars on the southwest flank of Mount St. Helens that were studied by Major and Voight (1986); the difference probably indicates that the debris avalanche samples were shattered during transport and that many

samples were derived from well-sorted volcanoclastic materials.

A ternary diagram (Fig. 24) of gravel, sand, and mud (silt + clay) graphically shows the range of grain-size distributions in the debris-avalanche deposit. Gravel ranges from 22.0 to 92.3 weight percent and has a mean of 45.5 percent; the extreme value represents an intact platy-jointed dome breccia (DXS-12; Fig. 21). Sand ranges from 6.6 to 65.4 percent and has a mean of 44.8 percent. Mud ranges from 1.1 to 21.2 percent and has a mean of 9.7 percent. Fields of the various map units show considerable overlap. The mixed block and matrix facies unit, not surprisingly, lacks the extreme values of the other units.

Fisher and Schmincke (1984) plot the preliminary data for the debris-avalanche deposit from Voight and others (1981) on a triangular plot of sand, silt, and

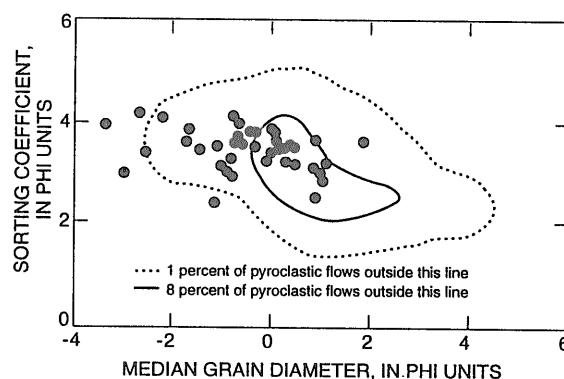


Fig. 23 Median diameter versus sorting coefficient. Field for pyroclastic flow from Walker (1971). Field from Walker does not include material too coarse to sieve.

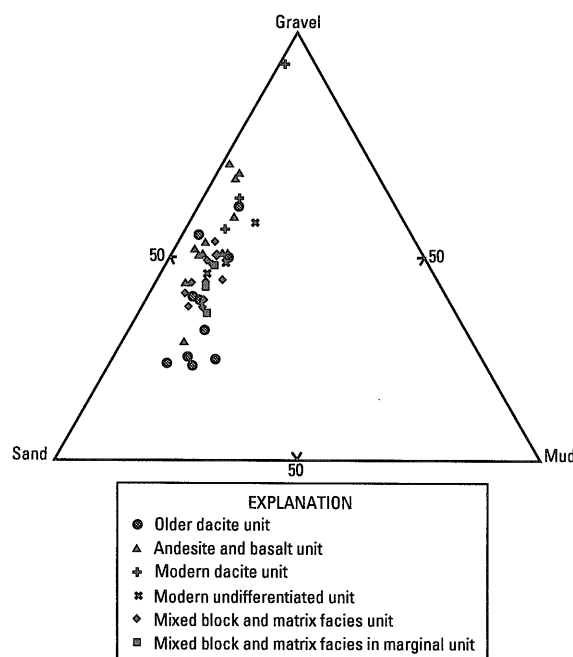


Fig. 24 Triangular plot of percentages of gravel, sand, and mud for samples in debris-avalanche deposit.

clay. Plotting only the size fractions smaller than gravel eliminates the uncertainties involved with material too coarse to sieve. The data from this report (Fig. 24) show significantly less clay than the preliminary data; the difference is probably because the preliminary data were generated by the hydrometer technique, which is less accurate than the pipette analysis used in this report (Folk, 1974; Wayne Steuben, U.S. Geological Survey, oral commun., 1984). These data should not be compared to the field of the Mount St. Helens' blast deposit plotted on Fisher and Schmincke's Fig. 11-5, because the blast deposit data, obtained from Voight and others (1981), were from samples of the uppermost part of the blast deposit (upper A2 of Waitt, 1981), which is atypical of most of the blast deposit.

(5) Lateral variations of statistical parameters

Measurements of median diameter (Md_ϕ) and mean diameter computed by method of moments ($Mn_{m\phi}$) are the average size of the clasts in each sample. As shown in Figs. 25 and 26, these parameters are highly variable near the source, but at more than 20 km from the source, mean diameter and median diameter values cluster around the mean values for the whole deposit for each parameter, -0.65ϕ and -0.54ϕ .

If a significant quantity of clasts were fractured during transport, the deposit should become finer grained in distal areas. This would be expressed by progressive decreases in Md_ϕ , $Mn_{m\phi}$, and percentages of gravel, and by progressive increases in percentages of sand and mud. The absence of these trends indicates that fracturing of clasts did not occur progressively during transport. This is interpreted to mean that fracturing of large clasts of the old mountain occurred mainly at the source, as is also suggested by the density data. Clast-to-clast collisions that resulted in fracturing surely did occur during transport, but not enough of this occurred to significantly affect the grain-size distribution within the debris-avalanche deposit.

Sorting parameters also suggest disaggregation and mixing of debris-avalanche blocks. A plot of sorting coefficient ($\sigma_{m\phi}$) versus distance from source (Fig. 27) shows the deposit does not get systematically better or more poorly sorted as distance from source increases.

6. Conclusions

The geology of the old mountain as mapped by C.A. Hopson (written commun., 1980) and the distribution of map units within the debris avalanche enable interpretations to be made of the resting places of the various parts of the old mountain that were mobilized during the eruption. The morphologic and lithologic maps (Pls. 1 and 2; Fig. 28) help in the construction of

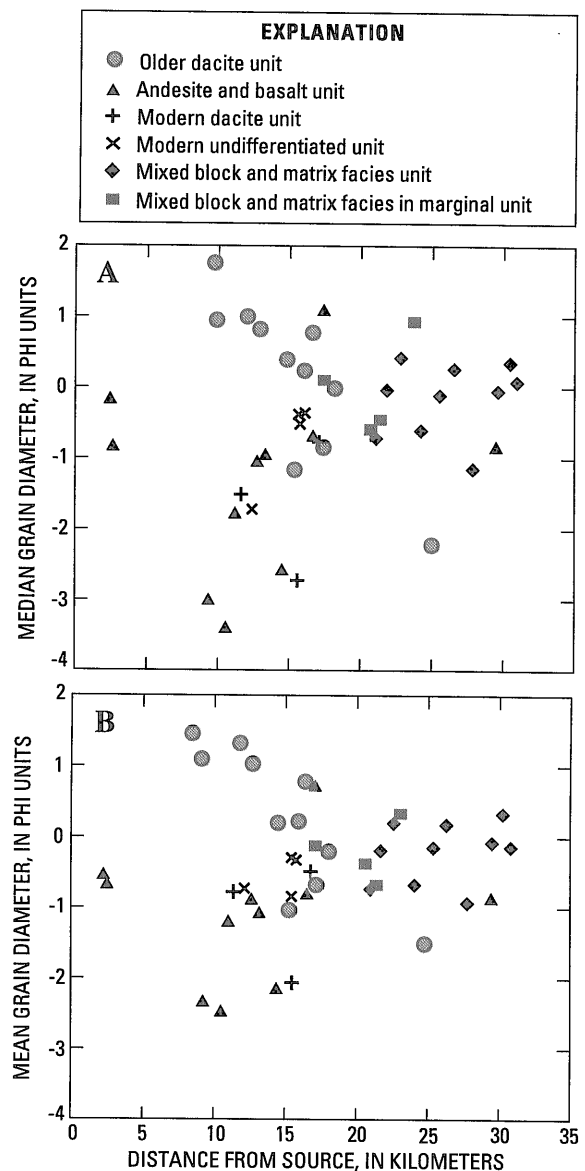


Fig. 25 Computed size parameters versus distance from source. Plots do not include anomalously coarse-grained DXS-12 sample. A, Median grain diameter, measured in phi units, versus distance from source. B, Mean grain diameter computed by method of moments, measured in phi units, versus distance from source.

an interpretation of the initial events of the eruption, an interpretation based primarily on a study of eye-witness photographs. In addition, evidence from the texture and morphology of the deposit enables interpretations of how the volcano broke into the slide blocks of the rockslide, broke into smaller debris-avalanche blocks, moved down the valley as a flowing debris avalanche, and was finally deposited (Fig. 29).

6.1 Slide and blast events

6.1.1 Slide block I

The initial movement of the rockslide-debris ava-

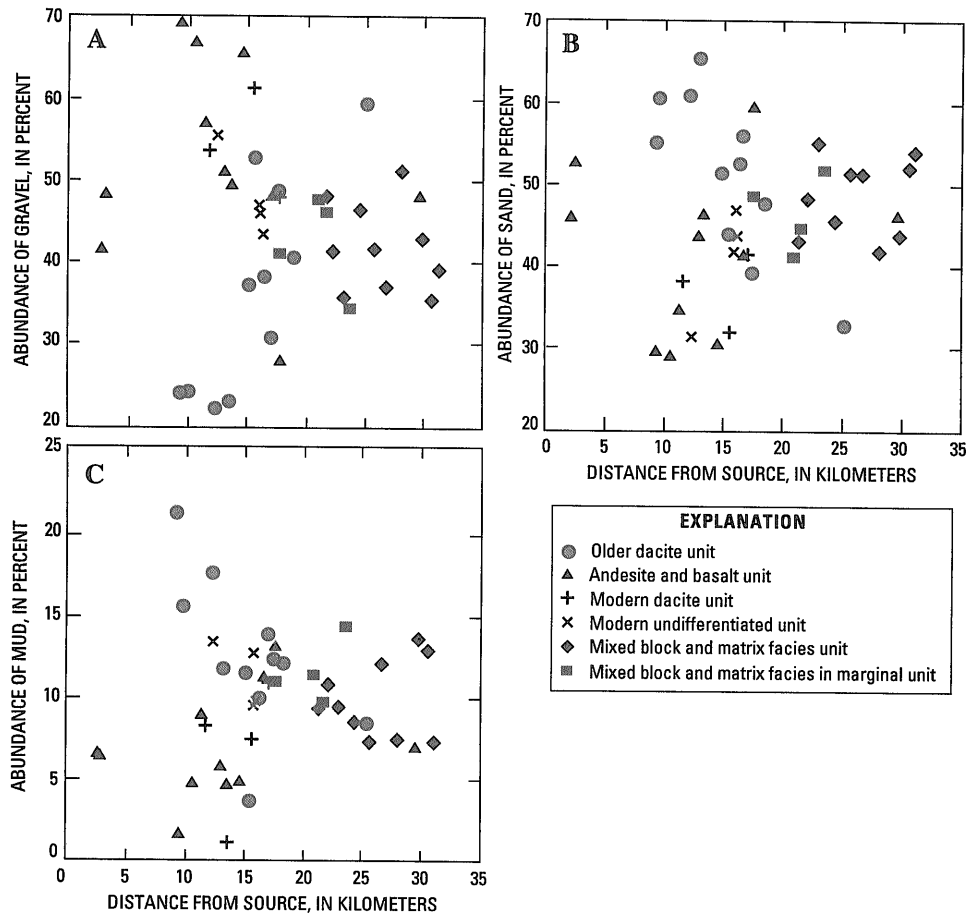


Fig. 26 Percentage of size classifications versus distance from source. A, Percent gravel versus distance from source. Does not include coarse-grained DXS-12 sample. B, Percent sand versus distance from source. C, Percent mud (silt+clay) versus distance from source.

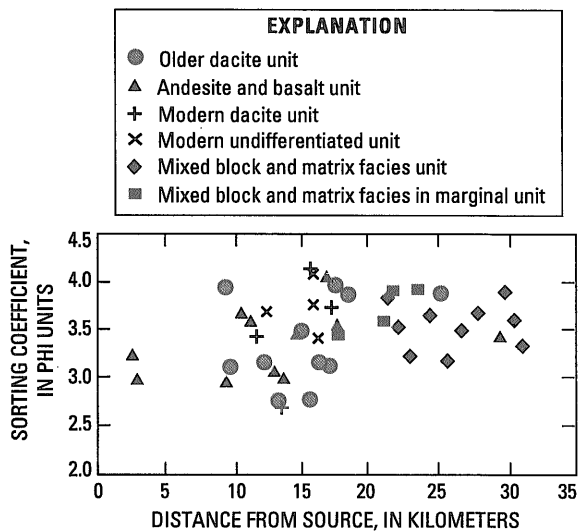


Fig. 27 Sorting coefficient computed by method of moments, measured in phi units, versus distance from source.

lanche is interpreted as a series of retrogressive slope failures (Voight and others, 1983) based on examination of eyewitness photographs (Voight, 1981). The first failure of the series, called slide block I, began to slide northward from the summit of the mountain about 10 s after the 8:32.2 a.m. earthquake on May 18 (Voight and others, 1983). On the basis of an analysis of photographs (Voight, 1981), the slide block reached a maximum velocity of about 80 m/s.

A velocity of 50 to 70 m/s was calculated for the velocity of the moving material at the bottom of Johnston Ridge (Glicken and others, 1981; Voight and others, 1983); the value is based on the height the debris traveled up the ridge. These velocities were calculated from the relation $v=(2gh)^{1/2}$, where h is runup height. The range of velocities results from uncertainty regarding the runup height, and the velocities represent minimum values because the method does not consider frictional dissipation of the slide block's kinetic energy.

Some of slide block I was deposited in Spirit Lake; 0.43 km³ of material (Meyer and Carpenter, 1982) moved into Spirit Lake and caused a seiche that resulted in lake runup of 260 m. Because the water

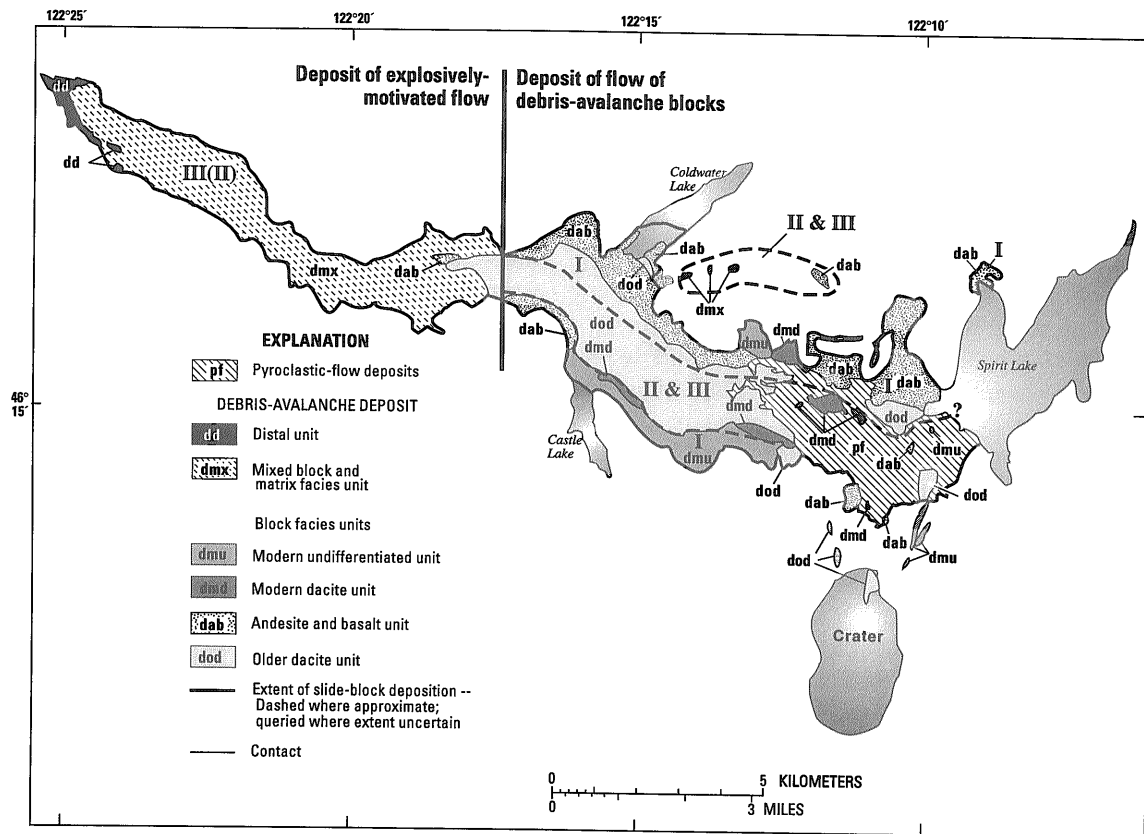


Fig. 28 Generalized lithologic map of debris-avalanche deposit, showing interpretations of areas of deposition of slide blocks; generalized from Pl. 2. (II) indicates primarily slide block III but includes subordinate volume of slide block II.

SCHMATIC REPRESENTATION	PROCESS	EVIDENCE
	At mountain	
	Rockslide-slide block I.	} Eyewitnesses, seismic record.
	Slide blocks II and III-blast.	
Dilation, clasts shatter.	Density measurements.	
TRANSITION TO DEBRIS-AVALANCHE FLOW		
During debris-avalanche flow		
Blocks break into smaller blocks.	Mapping, block measurements	
Blocks disaggregate and mix.	Clast size, exposures.	

Fig. 29 Summary of processes involved in transport of rockslide-debris avalanche.

from the lake did not flow down the North Fork Toutle River, the lake must have been dammed immediately by the debris avalanche. This provides further evidence that the Johnston Ridge unit, which dams Spirit Lake, was part of slide block I.

Other parts of slide block I made a 90° left turn and traveled down the North Fork Toutle River valley. This material was broken into smaller blocks and became a flow of debris-avalanche blocks. The distribution of rock types suggests that the top part of slide

block I was pushed from behind and aside by material from the lower part of slide block I, as well as by material from subsequent slide blocks, and deposited on the margins of the valley.

6.1.2 Slide block II and blast surge

The cryptodome and its surrounding hydrothermal system were unroofed by the first slide block, and the resulting rapid depressurization resulted in the initial explosions of the lateral blast (Kieffer, 1981). Meanwhile, retrogressive failure continued; eyewitness photographs show that a slip surface formed just behind the summit crater and propagated downward, forming the base of the mass called slide block II. The initial blast explosions burst through slide block II and produced a pyroclastic surge (the "blast surge" of Fisher and others, 1987) that quickly overran the first slide block, devastated the landscape in front of the moving slide, and deposited the stratified pyroclastic material known as the blast deposit over ridges and valleys across an area of 550 km² (Hoblitt and others, 1981).

The initial velocity of the front of the blast surge was calculated from timed photographs to be 90 m/s (Moore and Rice, 1984), approximately the sonic velocity of the material (Kieffer, 1981). Modeling by Kieffer (1981) suggests that the velocity of the mate-

rial may have reached a maximum of 325 m/s due to lateral expansion. Because the surge was supersonic, it was not deflected much by topography in the "channelized blast zone", within 11 km north of the crater (Kieffer, 1981).

6.1.3 Slide block III

The blast explosions produced a cloud of pyroclastic debris that obscured the north part of the mountain about 1 minute after the initial earthquake (Voight, 1981). No more slope movements are observed in eyewitness photographs after this time. Explosions resulting from the depressurization of parts of the cryptodome were observed to continue, possibly as new parts of the cryptodome were exposed by continuing mass movements.

These continuing mass movements are collectively called slide block III. Slide block III consisted of many discrete failures; it is likely that the blocks of material from these failures were, at least in part, transported by pyroclastic currents that were generated from the continuing blast explosions. Some of the slide block III material may have moved into Spirit Lake to become part of the 0.43 km³ of material filling Spirit Lake, and some may have moved over passes on Johnston Ridge (Fisher and others, 1987), depositing as the 0.06 km³ of mixed block and matrix facies unit ("avalanche II" of Fisher and others, 1987) in South Coldwater Creek, but most of the 1.3-km³ slide block flowed down the valley of the North Fork Toutle River and was deposited as the mixed block and matrix facies unit west of a break-in-slope near Maratta Creek.

The time of deposition and the composition of the mixed block and matrix facies material of the western part of the debris avalanche (Fig. 28) are consistent with an origin from slide block III. Stratigraphic relations indicate that the bulk of the mixed block and matrix facies material of the western part of the debris-avalanche deposit traveled over the top of the flow of debris-avalanche blocks of the eastern part of

the debris avalanche, and it was thus the last avalanche material to be deposited. The juvenile clasts and the mixed character of the material suggest that the matrix facies represents, at least in part, the deposit of pyroclastic currents generated from the blast explosions that likely originated from slide block III (Fig. 30). The matrix facies carried, and is interconvoluted with, debris-avalanche blocks that probably originated from slide block III. The 1.3-km³ volume of the slide block (Table 3) is more than enough to account for the 0.5-km³ volume of the mixed block and matrix facies in the western part of the deposit.

6.1.4 Final events

After nearly all the material from slide block III moved out of the crater and down the flank of the mountain, the magma continued to depressurize. The depressurizing magma produced blast pyroclastic currents. These currents traveled down the North Fork Toutle River valley and were deposited as blast deposits that rest on top of the avalanche in the 10 km of the valley west of the Pumice Pond (Fig. 18). These currents, generated from the final depressurization, were strongly deflected by topography, as they were not able to surmount Spirit Lake Blockage or Johnston Ridge. Thus, they were subsonic (Kieffer, 1981), much slower than the initial blast surge. Deposition of the entire debris avalanche took about 10 minutes; this time period is based on the length of time the seismic record was saturated by an earthquake generated from the transport of the avalanche (Voight and others, 1983).

6.2 Transition to flow and disintegration of material

Eyewitness photographs show that the failure of the north side of Mount St. Helens began as a slide (displacement occurring along one or several surfaces or relatively narrow zones; Varnes, 1978). It is apparent from the deposit, however, that the material soon

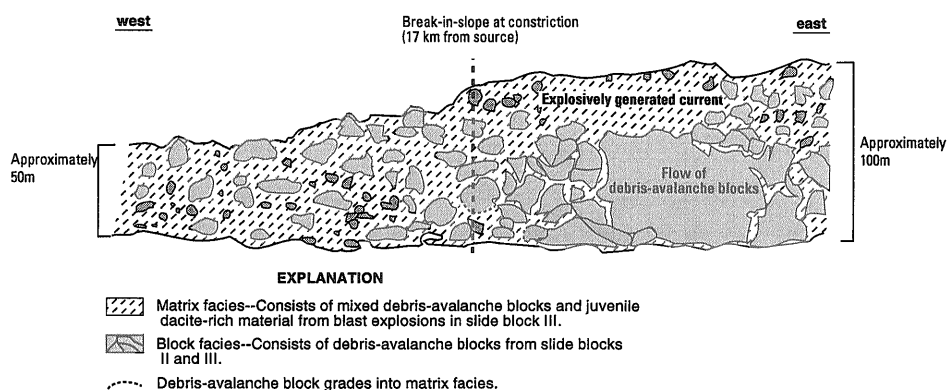


Fig. 30 Schematic cross sectional diagram showing flow of debris-avalanche blocks and the production of matrix facies from disaggregation and mixing of debris-avalanche blocks and from the pyroclastic current generated from blast explosions of slide block III.

disintegrated into particles of various sizes. Part of the material from the crater was accelerated by the blast explosions and became the blast deposits, but the vast bulk of the material was driven by its own weight and took on the character of a flowing debris-avalanche as particles interacted with each other and with interstitial fluids.

The distribution of rock types and the preservation of contacts within the Johnston Ridge unit suggest that a part of slide block I slid relatively intact and without tumbling to form the Johnston Ridge unit (Fig. 28). The material from the balance of slide block I did not surmount the ridge, but rather took a 90° left turn and broke up into smaller pieces (debris-avalanche blocks). The debris-avalanche blocks then flowed together down the valley (Fig. 28).

Photographs show that slide block II began as a simple slide, and then the blast explosions tore through the sliding material to produce the blast surge. A small amount of the remaining material went over the top of Johnston Ridge and was deposited as part of the 0.06 km³ of material in South Coldwater Creek (Fisher and others, 1987), and some went into Spirit Lake; however, most of the rest of the 0.75-km³ slide block probably took a 90° left turn at the base of Johnston Ridge, broke into smaller debris-avalanche blocks, and joined the flow of debris-avalanche blocks travelling downvalley (Fig. 28).

Slide block III consisted of many discrete failures (Voight and others, 1983). Some of the material from these failures may have been carried away by pyroclastic currents generated from the blast explosions, but much of the material from slide block III probably also traveled down the north flank of the mountain, took the 90° left turn, and became part of the flow of debris-avalanche blocks.

The evidence suggests that there were two types of debris-avalanche flow (Fig. 30). The first is the flow of debris-avalanche blocks, made of unconsolidated pieces derived from all three slide blocks, that stopped just west of Maratta Creek, about 17 km from the mountain. The second is a flow of matrix facies that contained suspended debris-avalanche blocks; these suspended blocks were generated from the exploding magma body at the mountain as well as from the disaggregation of debris-avalanche blocks in the flow of debris-avalanche blocks.

The disintegration of material occurred in many different ways (Fig. 29). The material dilated (increased in volume), probably due primarily to fracturing of individual clasts, but possibly also due to changes in packing of the clasts accompanying movement. As previously discussed, debris-avalanche blocks deformed, disaggregated, and mixed with each other.

The lack of a trend of increasing dilation during transport suggests that the material was dilated to its

maximum extent during sliding and was not dilated further during avalanche flow. Dilation, then, was created by sliding and resulted in profound loss of strength (Voight and others, 1983), facilitating continued sliding and the transition to avalanche flow; continued expansion of the material was not required for the avalanche to flow. Theoretical mechanics indicates that this is a general case for mass movements that begin as a slide and transform into a flow (Savage, 1984).

6.3 Fluidization and fluids in the flow

Fluidization in volcanoclastic flows is defined by Wilson (1980) and Sparks (1976) as the condition that occurs when gas is streaming up through the flow at a velocity great enough to support the weight of individual particles. This definition is drawn from the chemical engineering literature. Fluidization is defined by McSaveney (1978) as any process that turns a solid mass of loose debris into a mobile fluid; he defined mechanical fluidization as the process in which internal friction is lowered through separation of clasts in rebounds from countless collisions, and he refers to the process defined by Wilson (1980) and Sparks (1976) as gas-fluidization.

The debris-avalanche deposit is nearly everywhere poorly sorted, with $\sigma_\phi > 1$ (Table 4). Thus, the flowing material had a negligible amount of gas-fluidization, and the parts of it that were an explosively generated pyroclastic current may be considered type 1 pyroclastic flows of Wilson (1980). Wilson notes that features of the deposits of these events can best be explained by considering the flowing material to be a high-concentration dispersion, that is, a high-concentration flow of particles.

However, gases of various kinds were present in the interstices of the avalanche deposit. It is clear from the photographs that the sudden release of the pressure on the volcano's hydrothermal and magmatic system resulted in the transformation of ground water to steam that became incorporated in the rockslide. The fumaroles on the surface of the avalanche after emplacement reflect release of this water vapor, or additional vapor generated from the interaction of hot parts of the avalanche deposit with flowing ground water. Water vapor may have been generated by boiling of the water in the moving avalanche by heat generated from interparticle friction (Goguel, 1978). The juvenile material in the avalanche must have contained juvenile gases that were released as the fragile juvenile clasts (which were probably much hotter than 100°C; Banks and Hoblitt, 1981) broke apart during transport. But the measured temperatures of the debris avalanche just after deposition, which probably approximate emplacement temperatures, (<100°C, average 60°C), suggest that water vapor and juvenile gases, which have temperatures

100°C or greater, were not so volumetrically important as air. Air was probably incorporated during the initial rockslide movement when the material was dilated by about 20 percent.

The flow of debris-avalanche blocks can be considered a grain flow (Bagnold, 1954; Lowe, 1976; Savage, 1984), where particles – either the debris-avalanche blocks or the clasts within the debris-avalanche blocks – collide and create dispersive stresses normal to the movement of the flowing material. The dispersive stress preserves the dilation of the material, and it is the dilation that enables it to flow. This certainly fits the description of mechanical fluidization in the sense of McSaveney (1978). However, although the particles vibrate and collide, in the block facies they commonly keep at or near their original positions relative to one another, resulting in parts of the deposit retaining original volcanic structures or stratigraphy. This implies that particles only infrequently lose contact with one another, similar to particle interaction in flows of material in a quasi-static, rate-independent plastic regime (Savage, 1984). Original structures in deposits are cited by Melosh (1983) in support of a hypothesis of “acoustic fluidization,” where sound waves drive particles apart.

As particles are frequently in contact with one another, the material could not have lost all its strength when it was dilated. The high degree of interparticle friction implies a strength of material that resulted in levees, flow fronts, and longitudinal ridges. These features are also seen in poorly fluidized pyroclastic flows (Wilson, 1980).

The density data from the Mount St. Helens avalanche deposit indicate that dilation of material occurred primarily during the rockslide, and that dilation was partly responsible for the development of avalanche flow. Davies (1982), McSaveney (1978), Melosh (1983), and Savage (1984) suggest that high rates of shear at the base of debris avalanches may cause locally high dilation and reduction of internal friction; alternatively, some experimental work (Hung and Morgenstern, 1984) suggests that this effect may not be important. During the flow of the Mount St. Helens debris avalanche, basal shear or the intense seismic activity (which was probably created by basal shear; Voight and others, 1983) likely created dispersive pressure that preserved the dilation and was responsible for the continued flow of the avalanche.

Internal friction was also reduced by pore fluids. The most important of these was water in liquid or vapor form. Water in the liquid phase is nearly incompressible relative to air, so it probably reduces the number and (or) intensity of interparticle collisions and decreases the momentum transfer of each collision and thereby lowers internal frictional resistance to flow (Richard Iverson, oral commun., 1986). When

water explosively transforms into the vapor phase, it increases substantially in volume, and this expansion has the effect of driving particles apart. This increases dilation and likewise lowers internal friction.

6.4 Turbulence

Flows of material of high concentration and high strength are generally thought to behave in a nonturbulent (or laminar) fashion (Fisher, 1971; Johnson, 1970). Turbulent flows have nonparallel lines of flow, mix together materials in different parts of the moving flow, and are erosive. It has been shown (for example, Bagnold, 1955) that increasing a concentration of particulate matter in a flow of water inhibits turbulence. Johnson (1970) pointed out that debris flows often flow with well-defined “plugs” in which particles move in parallel paths.

Turbulence is a concept generally applied to flows of viscous fluids. When disturbances in the lines of flow of a fluid develop, and the viscous forces cannot dampen these disturbances, the disturbances propagate through the fluid and the fluid is said to be turbulent (Rouse, 1946). A flow of sediment-laden water may approximate a viscous fluid, but a grain flow like the debris avalanche is not a viscous fluid; nevertheless, the concept of turbulence has been applied to grain flows (for example, Enos, 1977).

There is good evidence that parts of the flowing debris avalanche had many of the characteristics of turbulent flows during transport. Although many debris-avalanche blocks retained their coherency, suggesting parallel paths and therefore laminar flow, many blocks disaggregated and mixed together. This mixing is one of the processes that created the matrix facies. In order to mix together, the particles must have followed nonparallel paths. In addition, some exposures (for example, 827-7; Figs. 21 and 31) show disaggregation and rolling of material, and this may imply the first stages of turbulence, where swirls and vortices develop from instabilities in the fluid (Roshko, 1976; Cantwell, 1981).

6.5 The base of the debris avalanche

There may locally have been some slip along an easily sheared layer at the base of the moving debris avalanche. The gas-rich blast surge deposit may have been this easily sheared basal layer; its hot (>100°C; Banks and Hoblitt, 1981), gas-rich nature suggests that gas was present between particles after deposition, preserving a high degree of dilation. However, the irregular topography of the bottom of the valley of the North Fork Toutle River before the eruption indicates that the basal layer could not have been a continuous sheet. In any case, an easily sheared basal layer is certainly not required to explain any features of the debris-avalanche flow or of the debris-



Fig. 31 Disaggregation and rolling of material that may indicate first stages of turbulence. Window 827-7 near Castle Lake.

avalanche deposit.

A mechanism of lubrication of large debris avalanches by an easily sheared basal layer of entrapped air has been called upon to explain features of large-scale mass movements (Shreve, 1968; Fahnestock, 1978). This mechanism has been disputed on theoretical grounds by Hsu (1975, 1978) and Voight and Pariseau (1978).

There is no evidence of air-layer lubrication for the Mount St. Helens debris avalanche. Shreve (1968) noted that for such a layer to form, the source material must be launched into the air and then travel along relatively smooth slopes as a nearly nondeforming sheet of sliding rubble. At Mount St. Helens, the rockslide-debris avalanche scoured the north side of the mountain; the obvious contact with the underlying surface shows it could not have been launched into the air. The area of deposition was not smooth; instead it was the extremely irregular topography of Johnston Ridge and the North Fork Toutle River. Finally, there is abundant evidence that the sliding rubble was dilated, smashed against the ridge just north of the mountain, took a 90° left turn, then traveled down the valley as a flow of debris-avalanche blocks and a poorly fluidized pyroclastic flow; therefore it cannot be considered to be a nondeforming, sliding sheet of rubble.

6.6 Mobility of the debris avalanche

Many authors (for example, Siebert, 1984; Voight and others, 1983, 1985; and Ui, 1983) have noted that large volcanic debris avalanches have greater mobility (lower ratio of fall height H to travel distance L) than nonvolcanic debris avalanches of comparable size. This difference is thought to result from the depressurization of magmatic and (or) hydrothermal systems (blasts) that generally accompany the

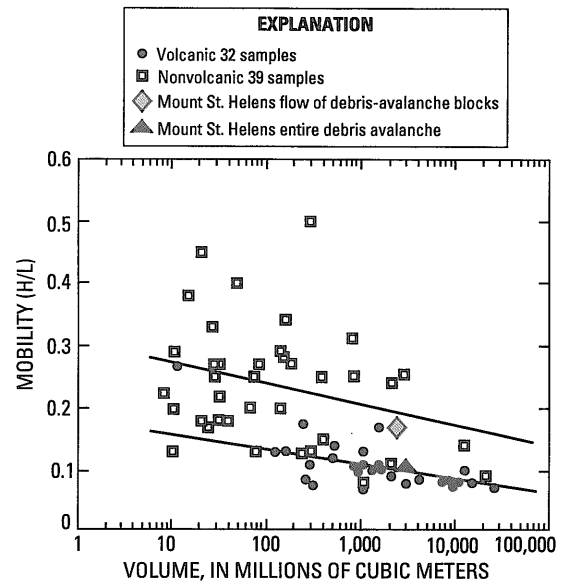


Fig. 32 Mobility (fall height/travel distance; H/L) versus volume for volcanic and nonvolcanic debris avalanches (from Voight and others, 1985). Lower H/L value implies greater mobility for entirety of Mount St. Helens avalanche deposit than for flow of debris-avalanche blocks. Regression lines from Voight and others (1985).

emplacement of the avalanches. The unconsolidated or poorly consolidated material of stratovolcanoes may be finer grained than rocks that make up other mountains; this may also contribute to the mobility of the volcanic events (Ui, 1983), perhaps by promoting grain flow or by producing a high porosity that would allow the source areas of volcanic debris avalanches to have relatively high water contents (Barry Voight, written commun., 1985).

At Mount St. Helens, the flow of matrix facies with

suspended debris-avalanche blocks traveled 29 km from the source, whereas the flow of debris-avalanche blocks without matrix facies traveled only 17 km from the source. Juvenile debris in the matrix facies material is evidence that the greater mobility resulted from the depressurizing magmatic and hydrothermal system (the blast explosions). The greater mobility may have resulted partly from the presence of juvenile and hydrothermal gasses, and their presence probably contributed to the reduction of interparticle friction. Explosive mixing also probably contributed to mobility by promoting dilation and grain flow.

The entire Mount St. Helens avalanche, including the matrix facies, is more mobile than the flow of debris-avalanche blocks (shown on Fig. 32, plot of H/L versus volume from Voight and others, 1985). The entire Mount St. Helens deposit plots within the more mobile field of volcanic debris avalanches, and the flow of debris-avalanche blocks plots within the field of nonvolcanic debris avalanches (see Fig. 32). This evidence supports the idea that the greater mobility of volcanic debris avalanches may result, at least in part, from associated blast explosions.

References

- American Society for Testing of Materials (ASTM) (1977) Standard test method for density of soil in place by the sand-cone method. In American Society for Testing of Materials, Annual Book of ASTM Standards, part 19, 208-211.
- Bagnold, R.A. (1954) Experiments on a gravity-free dispersion of large solid spheres in a Newtonian fluid under shear. Proceedings of the Royal Society of London, series A, 225, 49-63.
- Bagnold, R.A. (1955) Some flume experiments on large grains but little denser than the transporting fluid, and their implications. Proceedings of the Institution of Civil Engineers, part 3, 4, 174-205.
- Banks, N.G. and Hoblitt, R.P. (1981) Summary of temperature studies of 1980 deposits. In Lipman, P.W. and Mullineaux, D.R., eds., The 1980 eruptions of Mount St. Helens, Washington. U.S. Geol. Surv. Prof. Paper 1250, 295-314.
- Bates, R.L. and Jackson, J. A., eds. (1980) Glossary of Geology (2nd ed.). Falls Church, Va., American Geological Institute, 749 p.
- Brugman, M.M. and Meier, M.F. (1981) Response of glaciers to the eruptions of Mount St. Helens. In Lipman, P.W. and Mullineaux, D.R., eds., The 1980 eruptions of Mount St. Helens, Washington. U. S. Geol. Surv. Prof. Paper 1250, 743-756.
- Cantwell, B.J. (1981) Organized motion in turbulent flow. Annual Reviews of Fluid Mechanics, 13, 457-515.
- Christiansen, R.L. and Peterson, D.W. (1981) Chronology of the 1980 eruptive activity. In Lipman, P.W. and Mullineaux, D.R., eds., The 1980 eruptions of Mount St. Helens, Washington. U.S. Geol. Surv. Prof. Paper 1250, 17-30.
- Crandell, D.R. (1971) Postglacial lahars from Mount Rainier volcano, Washington. U. S. Geol. Surv. Prof. Paper 677, 75 p.
- Crandell, D.R., Miller, C.D., Glicken, H.X., Christiansen, R.L. and Newhall, C.G. (1984) Catastrophic debris avalanche from ancestral Mount Shasta volcano, California. Geology, 12, 143-146.
- Criswell, C.W. (1984) Depositional facies of the May 18, 1980, pumiceous pyroclastic-flow deposits at Mount St. Helens. Workshop on Volcanic Blasts, Mount St. Helens, August 13-17, 1984, Program and Abstracts.
- Criswell, C.W. (1987) Chronology and pyroclastic stratigraphy of the May 18, 1980, eruption of Mount St. Helens, Washington. J. Geophys. Res., 92, 10,237-10,266.
- Davies, T.R.H. (1982) Spreading of rock avalanche debris by mechanical fluidization. Rock Mechanics, 15, 9-24.
- Dzurisin, D., Denlinger, R.P. and Rosenbaum, J.G. (1990) Cooling rate and thermal structure determined from progressive magnetization of the dacite dome at Mount St. Helens, Washington. J. Geophys. Res., 95, 2763-2780.
- Enos, P. (1977) Flow regimes in debris flow. Sedimentology, 24, 133-142.
- Evarts, R.C., Ashley, R.P. and Smith, J.G. (1987) Geology of the Mount St. Helens area: record of discontinuous volcanic and plutonic activity in the Cascade arc of southern Washington. J. Geophys. Res., 92, 10,155-10,169.
- Fahnestock, R.K. (1978) Little Tahoma Peak rockfalls and avalanches, Mount Rainier, Washington. In Voight, B., ed., Rockslides and Avalanches 1, Natural Phenomena. Amsterdam, Elsevier, 181-196.
- Fairchild, L.H. (1985) Lahars at Mount St. Helens, Washington. Univ. of Washington, Seattle, Wash., Ph.D. dissertation, 374 p.
- Fairchild, L.H. (1987) The importance of lahar initiation processes. In Costa, J.E. and Wiczorek, G.F., eds., Debris Flows/Avalanches: Process, Recognition, and Mitigation. Geol. Soc. Am. Reviews in Engineering Geol., 7, 51-61.
- Fisher, R.V. (1971) Features of coarse-grained, high-concentration fluids and their deposits. J. Sediment. Petrol., 41, 916-927.

- Fisher, R.V., Glicken, H.X. and Hoblitt, R.P. (1987) May 18, 1980, Mount St. Helens deposits in South Coldwater Creek, Washington. *J. Geophys. Res.*, 92, 10,267-10,283.
- Fisher, R.V. and Heiken, G. (1982) Mount Pelee, Martinique; May 8 and 20, 1902 pyroclastic flows and surges. *J. Volcanol. Geotherm. Res.*, 13, 339-371.
- Fisher, R.V. and Schmincke, H.-U. (1984) *Pyroclastic Rocks*. New York, Springer-Verlag, 472 p.
- Fiske, R.S., Hopson, C.A. and Waters, A.C. (1963) *Geology of Mount Rainier National Park*. Washington U. S. Geol. Surv. Prof. Paper 444, 1-93.
- Folk, R.L. (1966) A review of grainsize parameters. *Sedimentology*, 6, 73-93.
- Folk, R.L. (1974) *Petrography of sedimentary rocks*. Austin, Texas, Hemphill Publishing Co., 182 p.
- Folk, R.L. and Ward, W.C. (1957) Brazos River Bar, a study in the significance of grain-size parameters. *J. of Sedimentary Petrology*, 27, 3-27.
- Galehouse, J.S. (1971) Point counting. In Carver, R.E., ed., *Procedures in Sedimentary Petrology*. New York, Wiley Interscience, 385-408.
- Glicken, H. (1986) *Rockslide-debris avalanche of May 18, 1980, Mount St. Helens Volcano, Washington*. Univ. of California, Santa Barbara, Calif., Ph.D. dissertation, 303 p.
- Glicken, H., Meyer, W. and Sabol, M. (1989) *Geology and ground-water hydrology of Spirit Lake blockage, Mount St. Helens, Washington, with implications for lake retention*. U.S. Geol. Surv. Bull. 1789, 33 p.
- Glicken, H., Voight, B. and Janda, R.J. (1981) *Rock-slide-debris avalanche of May 18, 1980, Mount St. Helens Volcano*. Abstracts, 1981 International Association of Volcanology and Chemistry of the Earth's Interior, Symposium on Arc Volcanism, 109-110.
- Gorshkov, G.S. and Dubik, Y.M. (1970) Gigantic directed blast at Shiveluch Volcano (Kamchatka). *Bull. Volcanol.*, 34, 262-288.
- Goguel, J. (1978) Scale-dependent rockslide mechanisms, with emphasis on the role of pore fluid vaporization, In Voight, B., ed., *Rockslides and Avalanches 1, Natural Phenomena*. Amsterdam, Elsevier, 693-705.
- Hammond, P.E. (1980) *Reconnaissance geologic map and cross sections of southern Washington Cascade Range*. Portland, Oreg., Portland State Univ., Publications of the Dept. of Earth Sci.
- Hoblitt, R.P., Crandell, D.R. and Mullineaux, D.R. (1980) Mount St. Helens eruptive behavior during the past 1,500 years. *Geology*, 8, 555-559.
- Hoblitt, R.P. and Harmon, R.S. (1993) Bimodal density distribution of cryptodome dacite from the 1980 eruption of Mount St. Helens, Washington. *Bull. Volcanol.*, 55, 421-437.
- Hoblitt, R.P., Miller, C.D. and Vallance, J.W. (1981) Origin and stratigraphy of the deposit produced by the May 18 directed blast. In Lipman, P.W. and Mullineaux, D.R., eds., *The 1980 eruptions of Mount St. Helens, Washington*. U. S. Geol. Surv. Prof. Paper 1250, 401-420.
- Hopson, C.A. and Melson, W.G. (1982) Stratigraphy of Mount St. Helens crater walls. *EOS, Transact. Am. Geophys. Union*, 63, 1144.
- Hopson, C.A. and Melson, W.G. (1985) *Kalama eruptive cycle at Mount St. Helens*. Univ. of California, Santa Barbara, Calif., Dept. of Geol. Sci., Annual Res. Review, June 1985.
- Horz, F., Ostertag, R. and Rainey, D.A. (1983) Bunte Breccia of the Ries: Continuous deposits of large impact craters. *Reviews of Geophysics and Space Physics*, 21, 1667-1725.
- Hsu, K.J. (1975) Catastrophic debris streams (sturzstroms) generated by rockfalls. *Geol. Soc. Am. Bull.*, 86, 129-140.
- Hsu, K.J. (1978) Albert Heim: Observations on landslides and relevance to modern interpretations. In Voight, B., ed., *Rockslides and Avalanches 1, Natural Phenomena*. Amsterdam, Elsevier, 71-93.
- Hungr, O. and Morgenstern, N.R. (1984) Experiments on the flow behavior of granular materials at high velocity in an open channel. *Geotechnique*, 34, 405-413.
- Inman, D.L. (1952) Measures describing the size distribution of sediments. *J. Sediment. Petrol.*, 22, 125-145.
- Janda, R.J., Scott, K.M., Nolan, K.M. and Martinson, H.A. (1981) Lahar movement, effects, and deposits. In Lipman, P.W. and Mullineaux, D.R., eds., *The 1980 eruptions of Mount St. Helens, Washington*. U. S. Geol. Surv. Prof. Paper 1250, 461-478.
- Johnson, A.M. (1970) *Physical processes in geology*. San Francisco, Freeman, Cooper and Co., 577 p.
- Johnson, A.M. and Rodine, J.R. (1984) Debris flow. In Brunsten, D. and Prior, D.B., eds., *Slope instability*. New York, John Wiley, 257-361.
- Jordan, R. and Kieffer, H.H. (1981) Topographic changes at Mount St. Helens—large-scale photogrammetry and digital terrain

- models. In Lipman, P.W. and Mullineaux, D.R., eds., *The 1980 eruptions of Mount St. Helens*, Washington. U. S. Geol. Surv. Prof. Paper 1250, 135-142.
- Kelly, J.C. (1971) Mathematical analysis of point count data. In Carver, R.E., ed., *Procedures in sedimentary petrology*. New York, Wiley-Interscience, 409-426.
- Kieffer, S.W. (1981) Fluid dynamics of the May 18 blast at Mount St. Helens. In Lipman, P.W. and Mullineaux, D.R., eds., *The 1980 eruptions of Mount St. Helens*, Washington. U. S. Geol. Surv. Prof. Paper 1250, 379-400.
- Kittleman, L.R. (1964) Application of Rosin's distribution in size-frequency analysis of clastic rocks. *J. Sediment. Petrol.*, 34, 483-502.
- Lipman, P.W., compiler (1981) Geologic map of proximal deposits and features of 1980 eruptions of Mount St. Helens, Washington. In Lipman, P.W. and Mullineaux, D.R., eds., *The 1980 eruptions of Mount St. Helens*, Washington. U. S. Geol. Surv. Prof. Paper 1250, plate 1.
- Lipman, P.W., Moore, J.G. and Swanson, D.A. (1981) Bulging of the north flank before the May 18 eruption -- Geodetic data. In Lipman, P.W. and Mullineaux, D.R., eds., *The 1980 eruptions of Mount St. Helens*, Washington. U. S. Geol. Surv. Prof. Paper 1250, 143-156.
- Lowe, D.R. (1976) Grain flow and grain-flow deposits. *J. Sediment. Petrol.*, 46, 188-199.
- Major, J.J. and Voight, B. (1986) Sedimentology and clast orientations of the 18 May 1980 southwest-flank lahars, Mount St. Helens, Washington. *J. Sediment. Petrol.*, 56, 691-705.
- McSaveney, M.J. (1978) Sherman glacier rock avalanche, Alaska. In Voight, B., ed., *Rockslides and Avalanches 1, Natural Phenomena*. Amsterdam, Elsevier, 197-258.
- Melosh, H.J. (1983) Acoustic fluidization. *Am. Scientist*, 71, 158-165.
- Meyer, W. and Carpenter, P.J. (1982) Filling of Spirit Lake, Washington, May 18, 1980, to July 31, 1982. U.S. Geol. Surv. Open-File Report 82-771, 19 p.
- Mimura, K. and Kawachi, S. (1981) Nirasaki debris avalanche, a catastrophic event at the Yatsugatake volcanic chain, central Japan. In *Abstracts, 1981 International Association of Volcanology and Chemistry of the Earth's Interior, Symposium on Arc Volcanism*, 237.
- Mimura, K., Kawachi, S., Fujimoto, U., Taneichi, M., Hyuga, T., Ichikawa, S. and Koizumi, M. (1982) Debris avalanche hills and their natural remnant magnetization -- Nirasaki debris avalanche, central Japan. *J. Volcanol. Soc. Jpn.*, 88, 653-663.
- Moore, J.G., and Albee, W.C. (1981) Topographic and structural changes, March-July 1980. In Lipman, P.W. and Mullineaux, D.R., eds., *The 1980 eruptions of Mount St. Helens*, Washington. U. S. Geol. Surv. Prof. Paper 1250, 123-134.
- Moore, J.G. and Rice, C.J. (1984) Chronology and character of the May 18, 1980, explosive eruption of Mount St. Helens. In *Explosive Volcanism: Inception, Evolution, Hazards*. Washington, D.C., National Academy Press, 133-142.
- Moore, J.G. and Sisson, T.W. (1981) Deposits and effects of the May 18, 1980, pyroclastic surge. In Lipman, P.W. and Mullineaux, D.R., eds., *The 1980 eruptions of Mount St. Helens*, Washington. U. S. Geol. Surv. Prof. Paper 1250, 421-433.
- Mullineaux, D.R. and Crandell, D.R. (1981) The eruptive history of Mount St. Helens. In Lipman, P.W. and Mullineaux, D.R., eds., *The 1980 eruptions of Mount St. Helens*, Washington. U. S. Geol. Surv. Prof. Paper 1250, 3-16.
- Murai, I. (1961) A study of the textural characteristics of pyroclastic flow deposits in Japan. *Tokyo Univ. Earthq. Res. Inst. Bull.*, 39, 133-248.
- Pevear, D.R., Dethier, D.P. and Frank, D. (1982) Clay minerals in the 1980 deposits from Mount St. Helens. *Clays and Clay Minerals*, 30, 241-252.
- Pierson, T.C. and Scott, K.M. (1985) Downstream dilution of a lahar: transition from debris flow to hyperconcentrated streamflow. *Water Resources Res.*, 21, 1511-1524.
- Roshko, A. (1976) Structure of turbulent shear flows: a new look. *Am. Inst. Aeronaut. Astronaut. J.*, 14, 1349-1357.
- Rouse, H. (1946) *Elementary Mechanics of Fluids*. New York, Dover Publications, 376 p.
- Rowley, P.D., Kuntz, M.A. and Macleod, N.S. (1981) Pumiceous pyroclastic flow deposits. In Lipman, P.W. and Mullineaux, D.R., eds., *The 1980 eruptions of Mount St. Helens*, Washington. U. S. Geol. Surv. Prof. Paper 1250, 489-512.
- Savage, S.B. (1984) The mechanics of rapid granular flows. *Advances in Applied Mechanics*, 24, 289-366.
- Scott, K.M. (1988) Origins, behavior, and sedimentology of lahars and lahar-runout flows in the Toutle-Cowlitz River system. U. S. Geol. Surv. Prof. Paper 1447-A, 76 p.
- Scott, K.M. (1989) Origin, behavior, and sedimentology of prehistoric catastrophic lahars at Mount St. Helens, Washington. In Clifton, H.E., ed., *Sedimentologic Conse-*

- quences of Convulsive Geologic Events. Geol. Soc. Am. Spec. Paper 229, 23-36.
- Shreve, R.L. (1968) The Blackhawk Landslide. Geol. Soc. Am. Spec. Paper 108, 1-47.
- Siebert, L. (1984) Large volcanic debris avalanches: Characteristics of source areas, deposits, and associated eruptions. *J. Volcanol. Geotherm. Res.*, 22, 163-197.
- Sisson, T.W. (1995) Blast ashfall deposit of May 18, 1980 at Mount St. Helens, Washington. *J. Volcanol. Geotherm. Res.*, 66, 203-216.
- Smith, D.R. (1984) The petrology and geochemistry of High Cascade Volcanics in Southern Washington. Mount St. Helens Volcano and the Indian Heaven basalt field. Rice Univ., Houston, Texas, Ph.D. dissertation, 409 p.
- Smith, D.R. and Leeman, W.P. (1987) Petrogenesis of Mount St. Helens dacitic magmas. *J. Geophys. Res.*, 92, 10,313-10,334.
- Sparks, R.S.J. (1976) Grain-size variations and implications for the transport of pyroclastic flows. *Sedimentology*, 23, 147-188.
- Trask, P.D. (1930) Mechanical analysis of sediments by centrifuge. *Econ. Geol.*, 25, 581-599.
- Ui, T. (1983) Volcanic debris avalanche deposits -- identification and comparison with non-volcanic debris stream deposits. *J. Volcanol. Geotherm. Res.*, 18, 135-150.
- Ui, T. (1985) Debris avalanche deposits associated with volcanic activity. Proceedings, IVth International Conference and Field Workshop on Landslides, Tokyo, Japan, 405-410.
- Ui, T. and Glicken, H. (1986) Internal structural characteristics of a debris avalanche from Mount Shasta, California, U.S.A.. *Bull. Volcanol.*, 48, 189-194.
- Varnes, D.J. (1978) Slope movement types and processes. In Shuster, R.L. and Krizek, R.J., eds., *Landslides, Analysis and Control*. Transportation Research Board, Spec. Rep. 176, 11-33.
- Verhoogen, J. (1937) Mount St. Helens, a recent Cascade Volcano. *Bull. Dept. of Geol. Sci., Univ. of California*, 14, 263-309.
- Voight, B. (1981) Time scale for the first moments of the May 18 eruption. In Lipman, P.W. and Mullineaux, D.R., eds., *The 1980 eruptions of Mount St. Helens, Washington*. U. S. Geol. Surv. Prof. Paper 1250, 69-86.
- Voight, B., Glicken, H., Janda, R.J. and Douglass, P.M. (1981) Catastrophic rockslide-avalanche of May 18. In Lipman, P.W. and Mullineaux, D.R., eds., *The 1980 eruptions of Mount St. Helens, Washington*. U. S. Geol. Surv. Prof. Paper 1250, 347-378.
- Voight, B., Janda, R.J., Glicken, H. and Douglass, P.M. (1983) Nature and mechanics of the Mount St. Helens rockslide-avalanche of 18 May 1980. *Geotechnique*, 33, 243-273.
- Voight, B., Janda, R.J., Glicken, H. and Douglass, P.M. (1985) Reply to discussion on Nature and mechanics of the Mount St. Helens rockslide-avalanche of 18 May 1980. *Geotechnique*, 35, 357-368.
- Voight, B. and Pariseau, W.G. (1978) Rockslides and avalanches: an introduction. In Voight, B., ed., *Rockslides and Avalanches 1, Natural Phenomena*. Amsterdam, Elsevier, 1-67.
- Waite, R.B., Jr. (1981) Devastating pyroclastic density flow and attendant air fall of May 18 - stratigraphy and sedimentology of deposits. In Lipman, P.W. and Mullineaux, D.R., eds., *The 1980 eruptions of Mount St. Helens, Washington*. U. S. Geol. Surv. Prof. Paper 1250, 439-460.
- Walker, G.P.L. (1971) Grain-size characteristics of pyroclastic deposits. *J. Geol.*, 79, 696-714.
- Wilson, C.J.N. (1980) The role of fluidization in the emplacement of pyroclastic flows: an experimental approach. *J. Volcanol. Geotherm. Res.*, 8, 231-249.
- Yamaguchi, D.K. and Hoblitt, R.P. (1995) Tree-ring dating of pre-1980 volcanic flowage deposits at Mount St. Helens, Washington. *Geol. Soc. Am. Bull.*, 107, 1077-1093.
- Yamaguchi, D.K. and Lawrence, D.B. (1993) Tree-ring evidence for 1842-1843 eruptive activity at the Goat Rocks dome, Mount St. Helens, Washington. *Bull. Volcanol.*, 55, 264-272.

Received December 1, 1997

Accepted December 15, 1997

米国ワシントン州，セント・ヘレンズ火山において
1980年5月18日に発生した岩石すべり-岩屑なだれ

Harry GLICKEN

要 旨

セントヘレンズ火山の岩石すべり-岩屑なだれは、三つのすべりブロックに分かれ発生した。すべりブロックIは、1980年5月18日8時32分(太平洋夏時間)のM5.1の地震に伴って発生した。続いて、爆発を続けていたクリプトドームがすべりブロックIIを突き破って飛び散り、“プラストサージ”が発生した。すべりブロックIIIは、多くの斜面崩壊によって発生し、クリプトドームから発生し続けていた火砕サージによって運ばれた。流れ山地形を持つ、体積が2.5km³の岩屑なだれ堆積物は、ブロック相(あまりほぐれずに元の形を比較的良く保ったまま運ばれた噴火前の山体の断片)とマトリックス相(古い山体の岩片とクリプトドーム起源のデイサイト片の混合物)とからなる。ブロック相は、5つの岩相に区分される。マトリックス相は、爆発によって生じたすべりブロックIIIの流れに由来する物質と、岩屑なだれブロックがほぐれて混合してできた物質からなる。

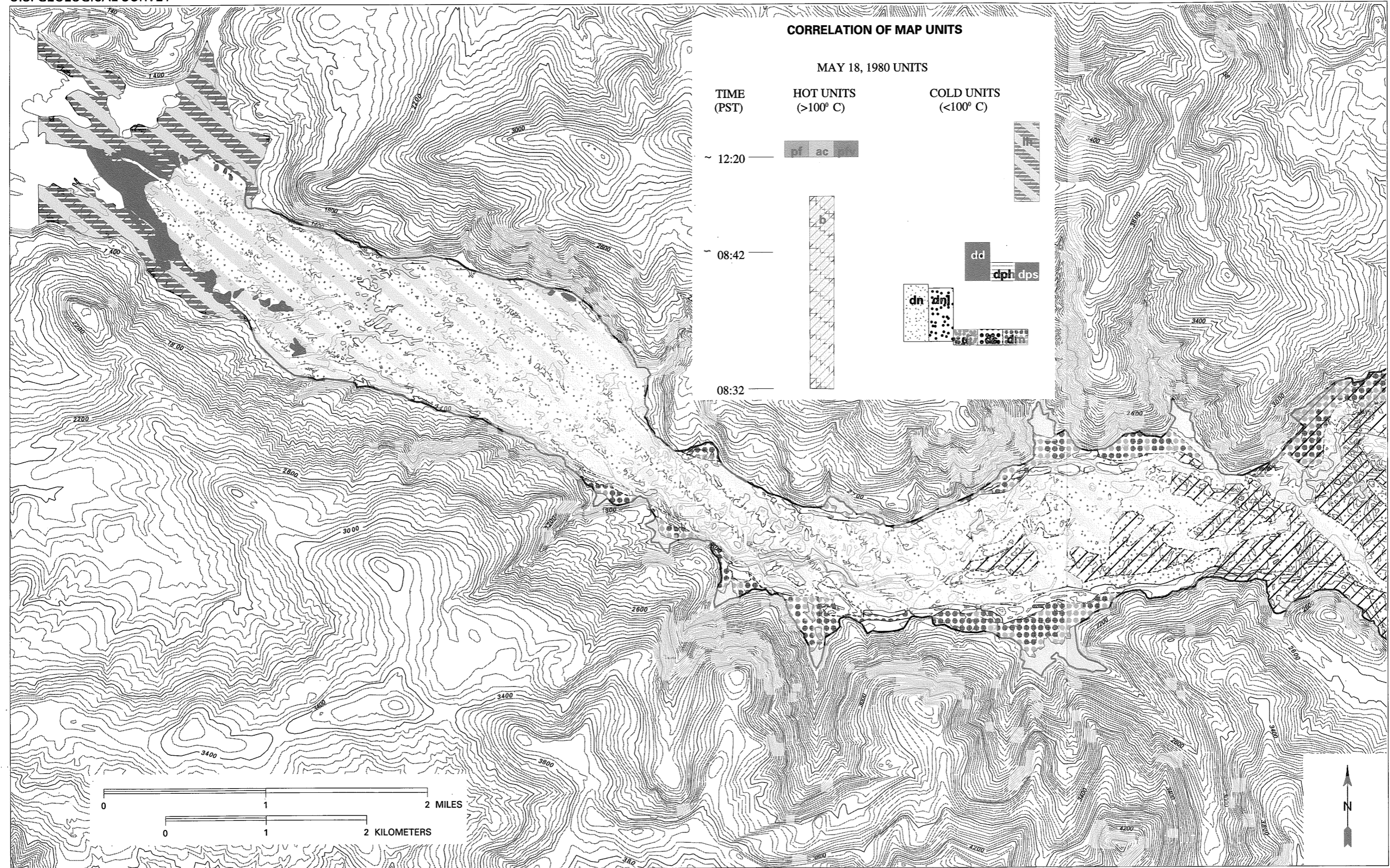
岩屑なだれは、流走中ではなく、山体からブロックがすべり落ちる際にすでに膨らんでいた。岩屑なだれは、粒子流として流れたと考えられる。すなわち、岩屑なだれブロックやブロック内部の岩片が、互いに衝突することによって運動方向と直交方向に分散圧力が生じ、この分散圧力によって、岩屑なだれは膨んだまま流れ続けることができた。

(訳：宝田晋治・鹿野和彦)

Appendix: Reference of figure and plate numbers to the original text.

This text	Original text	This text	Original text	This text	Original text	This text	Original text
Fig. 1	Fig. 1	Fig. 9	Fig. 13	Fig. 17	Fig. 40	Fig. 25	Fig. 57
Fig. 2	Fig. 2	Fig. 10	Fig. 16	Fig. 18	Fig. 41	Fig. 26	Fig. 58
Fig. 3	Fig. 3	Fig. 11	Fig. 17	Fig. 19	Fig. 48	Fig. 27	Fig. 59
Fig. 4	Fig. 6	Fig. 12	Fig. 30	Fig. 20	Fig. 49	Fig. 28	Fig. 60
Fig. 5	Fig. 8	Fig. 13	Fig. 31	Fig. 21	Fig. 50	Fig. 29	Fig. 61
Fig. 6	Fig. 10	Fig. 14	Fig. 33	Fig. 22	Fig. 51	Fig. 30	Fig. 63
Fig. 7	Fig. 11	Fig. 15	Fig. 35	Fig. 23	Fig. 55	Fig. 31	Fig. 64
Fig. 8	Fig. 12	Fig. 16	Fig. 38	Fig. 24	Fig. 56	Fig. 32	Fig. 65
Plate 1	Plate 3	Plate 2	Plate 4				

Note: Original text was released as Open File Report 96-677 on the web page of the Cascades Volcano Observatory, U.S. Geological Survey. It can be accessed at <http://vulcan.wr.usgs.gov/Projects/Glicken/framework.html>.



**MORPHOLOGIC MAP OF DEBRIS-AVALANCHE DEPOSIT
MAY 18, 1980, MOUNT ST. HELENS, WASHINGTON**

U.S. DEPARTMENT OF THE INTERIOR
U.S. GEOLOGICAL SURVEY

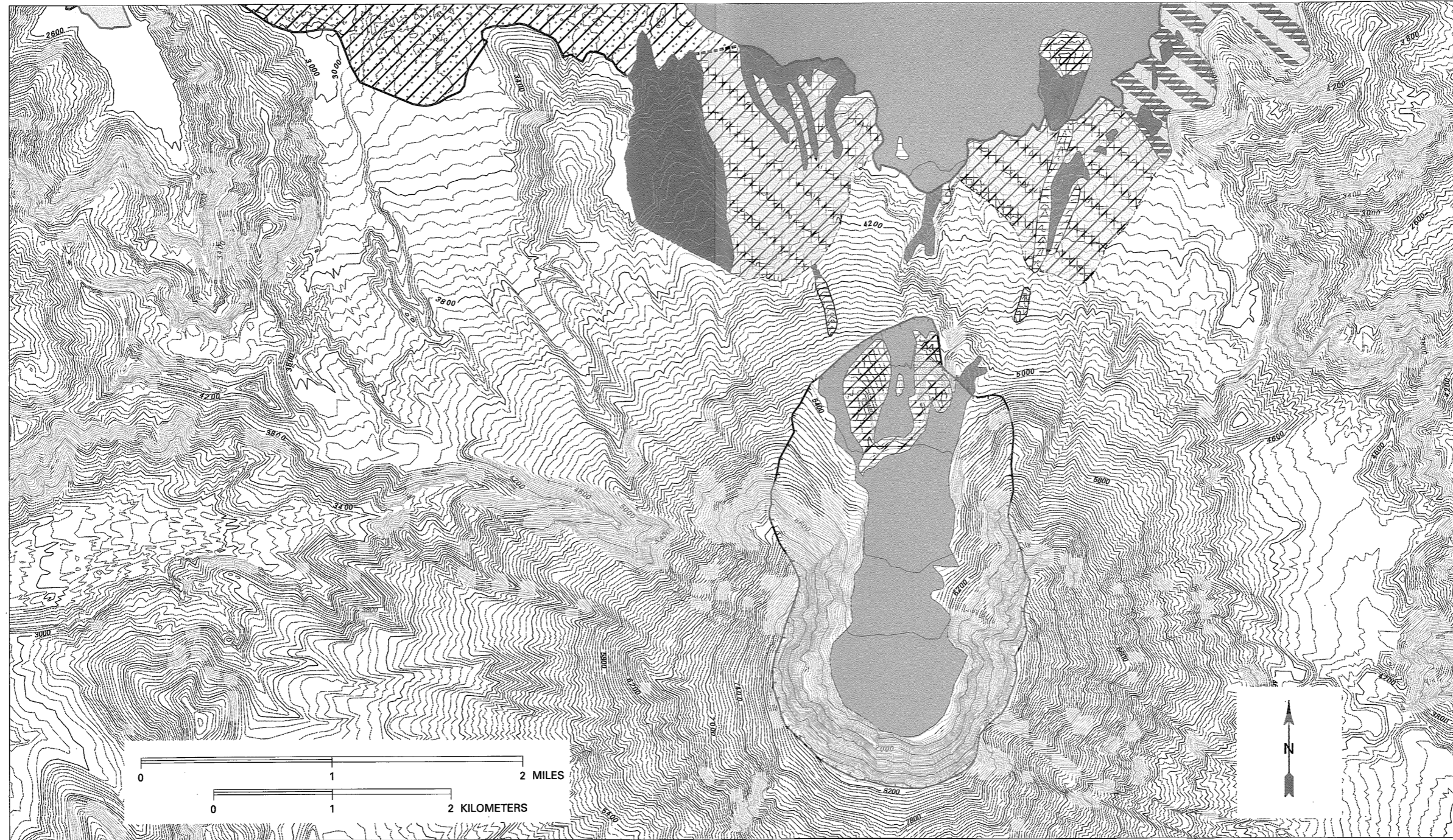
OPEN-FILE REPORT 96-677
PLATE 1 (2 OF 4)



**MORPHOLOGIC MAP OF DEBRIS-AVALANCHE DEPOSIT
MAY 18, 1980, MOUNT ST. HELENS, WASHINGTON**


U.S. DEPARTMENT OF THE INTERIOR
U.S. GEOLOGICAL SURVEY

OPEN-FILE REPORT 96-677
PLATE 1 (3 OF 4)





**MORPHOLOGIC MAP OF DEBRIS-AVALANCHE DEPOSIT
MAY 18, 1980, MOUNT ST. HELENS, WASHINGTON**


DESCRIPTION OF MAP UNITS

 Areas covered by or reworked by water. Data from June 1980 aerial photographs.


PYROCLASTIC-FLOW DEPOSITS

 Ash- cloud deposits -- Deposits from ash clouds of the pyroclastic flows of May 18, 1980. Unconsolidated ash and lapilli, predominantly vitric, well- sorted, and <0.5 mm diameter (Rowley and others, 1981; Glicken and others, 1989). Shown only where covering debris- avalanche deposit and thick enough (> approximately 3 m) to conceal hummocks of the debris- avalanche deposit.


 Pyroclastic- flow deposits -- Deposits of the basal parts of the pumiceous pyroclastic flows of May 18, May 25, June 12, July 22, August 7, and October 16- 18, 1980. Generally poorly- sorted unconsolidated ash and lapilli with rare larger clasts (Rowley and others, 1981).

 Pyroclastic- flow veneer deposits -- Veneer of pumiceous pyroclastic flows of 1980 on the north flank of Mount St. Helens. Generally less than 2 m thick.

LAHAR DEPOSITS


 Lahar deposits -- Deposits of volcanic mudflow, debris flow, and subordinate flood deposits of May 18, 1980. Unsorted, generally unstratified, unconsolidated lapilli and brown ash with larger clasts. Contains all rock types from the old mountain and, locally, the "blast" dacite. Deposits have flat or ropy surfaces and are ponded between hummocks. The screen pattern with no "lh" indicates where lahar deposit covers debris- avalanche deposit. In patterned areas, isolated hummocks not covered by lahars are not delineated.

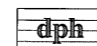
BLAST DEPOSITS


 Blast deposits -- Deposits of pyroclastic currents generated from explosions of 0832 PDT to about 0844 PDT, May 18, 1980. Unconsolidated lapilli and olive- gray ash with rare larger clasts; generally unsorted and unstratified where shown on map. Contains all rock types from the old mountain and the gray, semi- vesiculated, juvenile "blast" dacite. Deposits have wavy, undulating surfaces and are thicker in depressions than on tops of hummocks. Pattern with no "b" indicates where blast deposit, generated from the crater after the rockslide- debris avalanche, rests on top of debris- avalanche deposit; shown where it covered the debris- avalanche deposit before erosion.

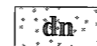
DEBRIS-AVALANCHE DEPOSIT

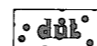
Distal unit


 Distal unit -- Jumbled masses of broken trees, wood debris, and organic- rich soil mixed with volcanic material from Mount St. Helens, in proportions up to 30%. Masses form hummocks up to 9 m high.


 Proximal hummocks unit -- Hummocks of debris avalanche material in crater and on north flank of Mount St. Helens.


 Proximal scattered unit -- Small (generally <5 m across), isolated, scattered hummocks of material resting on pre- 1980 deposits. Hummocks cover less than 1% of mapped area.

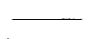
 North Fork unit -- Hummocky, cratered mass of material in North Fork Toutle River between levees that does not show evidence for interaction with Johnston Ridge or Spirit Lake.

 Debris avalanche levees on the margins of the North Fork unit.

 Johnston Ridge unit -- Debris- avalanche deposit that shows evidence for interaction with Johnston Ridge. Material forms terraces, ridges, hummocks, and craters.

 Spirit Lake unit -- The portion of the debris avalanche that moved to the northeast and into Spirit Lake. Forms islands in the lake, conical hummocks, topped by flat- lying broken trees, and hummocks covered by reworked sediment.

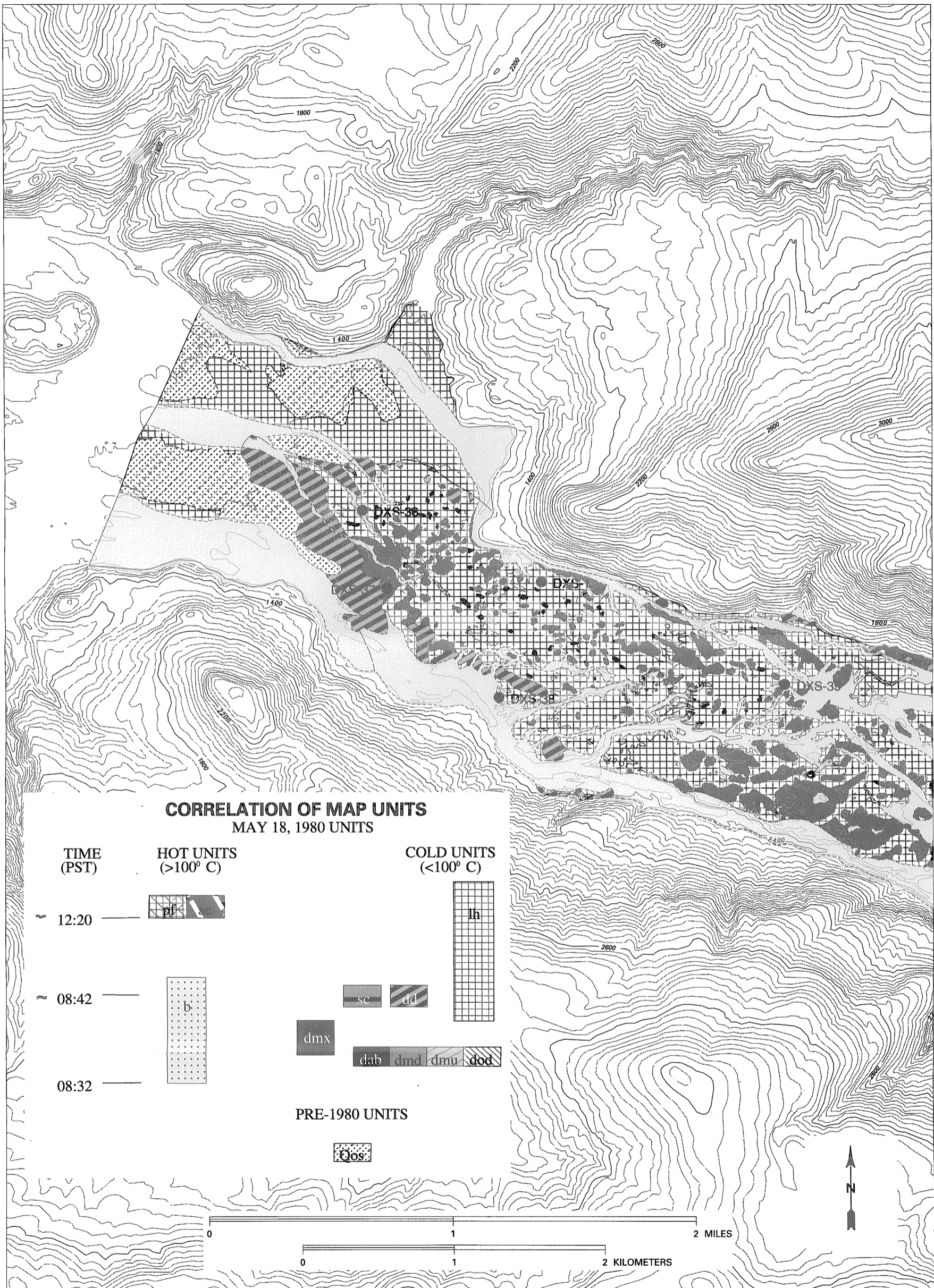
 Marginal unit -- Material on the valley wall side of the levees of the debris- avalanche deposit. Generally forms lobes, but hummocks resembling those of North Fork unit also present.

 CONTACT - Dashed where approximately located

 BOUNDARY OF AREA UNDERLAIN BY DEBRIS-AVALANCHE DEPOSIT - excluding proximal units

 THRUST FAULTS IN DEBRIS-AVALANCHE DEPOSIT

 RIM OF CRATER FORMED MAY 18, 1980 (SOURCE AREA OF DEBRIS-AVALANCHE DEPOSIT)



LITHOLOGIC MAP OF DEBRIS-AVALANCHE DEPOSIT
MAY 18, 1980, MOUNT ST. HELENS VOLCANO, WASHINGTON
WESTERN PART

EXPLANATION (Plates 2A and 2B)
DESCRIPTION OF MAP UNITS

W Areas covered by, eroded by, or reworked by water. Data from summer 1982 aerial photographs.

D Areas disturbed during construction of spillways at Castle Lake and Coldwater Lake.

PYROCLASTIC-FLOW DEPOSITS

af Ash-cloud deposits -- Deposits from ash clouds of the pumiceous pyroclastic flows of May 18, 1980. Unconsolidated ash and lapilli, predominantly vitric, well-sorted, and <0.5 mm diameter (Rowley and others, 1981; Glicken and others, 1989). Shown only where covering debris-avalanche deposit and thick enough (> approximately 1 m) to conceal the lithology of the debris-avalanche deposit in summer 1982.

pf Pyroclastic flow deposits -- Deposits of the basal parts of the pumiceous pyroclastic flows of May 18, May 25, June 12, July 22, August 7, and October 16-18, 1980. Generally poorly-sorted unconsolidated ash and lapilli with rare larger clasts (Rowley and others, 1981).

LAHAR DEPOSITS

lh Lahar deposits -- Deposits of volcanic mudflow, debris flow, and subordinate flood deposits of May 18, 1980. Unsorted, generally unstratified, unconsolidated lapilli and brown ash with rare larger clasts. Locally stratified into two or more flow units. Contains all rock types from the old mountain and, locally, the gray juvenile "blast" dacite. Deposits have flat or ropy surfaces and are ponded between hummocks. Shown where covering debris-avalanche deposit and thick enough (> approximately 1 m) to conceal the lithology of the debris avalanche in summer 1982.

BLAST DEPOSITS

b Blast deposits -- Deposits of pyroclastic currents generated from blast explosions of 0832 PDT to about 0844 PDT, May 18, 1980. Unsorted, generally unstratified, unconsolidated lapilli and olive-gray ash with rare larger clasts. Contains all rock types from the old mountain and the gray, semi-vesiculated juvenile "blast" dacite. Deposits have wavy, undulating surfaces and are thicker in depressions than on tops of hummocks. Locally stratified into two or more flow units. Shown only where covering debris-avalanche deposit and thick enough (> approximately 1 m) to conceal the lithology of the debris avalanche in summer 1982.

SCOUR-PRODUCT DEPOSIT

sc Scour-product deposits -- Deposits of material produced by scouring of ridges adjacent to the North Fork Toutle River Valley by the moving debris avalanche. Consists of woody debris, organic-rich soil, and clasts of Tertiary bedrock.

DEBRIS-AVALANCHE DEPOSIT

Distal unit

ad Distal unit -- Jumbled masses of broken trees, wood debris, and organic-rich soil mixed with volcanic material from Mount St. Helens, in proportions up to 30%. Masses form hummocks up to 9 m high.

Block facies unit

dab Andesite- and- basalt unit -- Rubble consisting primarily of dark gray, black, very dark green, and red augite- hypersthene andesite and olivine basalt. Derived from andesite and basalt lava flows and volcanoclastic rocks of the modern (less than 2500 years old) Mount St. Helens.

dabc Avalanche blocks -- Hummocks in coherent avalanche blocks that consist of more than a single rock type. Blocks preserve structures such as igneous dikes and stratigraphic layering that closely resemble structures observed in the Mount St. Helens crater.

dmd Modern dacite unit -- Rubble composed primarily of gray, red, and pink nearly aphyric augite- hornblende- hypersthene dacite. Derived from Goat Rocks and Summit domes of modern (less than 2500 years old) Mount St. Helens. Surface of unit studded with clasts >10 cm across.

dmu Modern undifferentiated unit -- Rubble consisting of rocks from both the modern dacite and the andesite- and- basalt units.

dod Older dacite unit -- Rubble consisting of gray, red, pink, yellowish- brown, and green hornblende- hypersthene dacite. Derived from the pre- Castle Creek (older than 2500 years) Mount St. Helens. Distinguished from modern dacite by abundant large (>2 mm long) phenocrysts of plagioclase and hornblende.

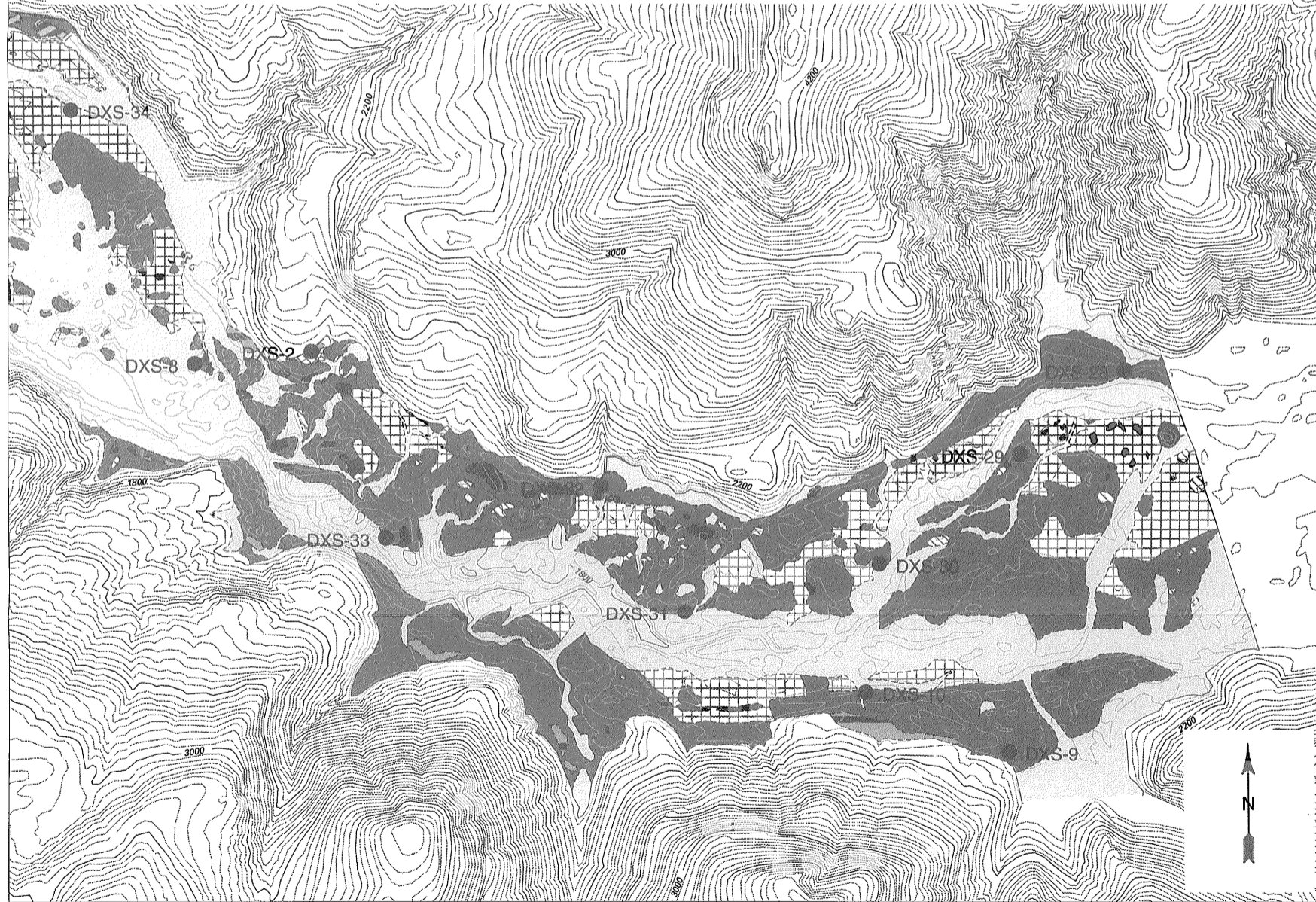
Mixed block and matrix facies unit

dmx Mixed block facies and matrix facies unit -- Rubble consisting of matrix facies as well as debris avalanche blocks of all rock types from the pre- 1980 Mount St. Helens. The debris avalanche blocks are too small to delineate on map (< 15 m across).

OLD MOUNT ST. HELENS

Old Old Mount St. Helens -- Basaltic and andesitic lava flows, dacite domes and volcanoclastic deposits derived from the pre- 1980 Mount St. Helens. Range in age from about 100 to 40,000 years old.

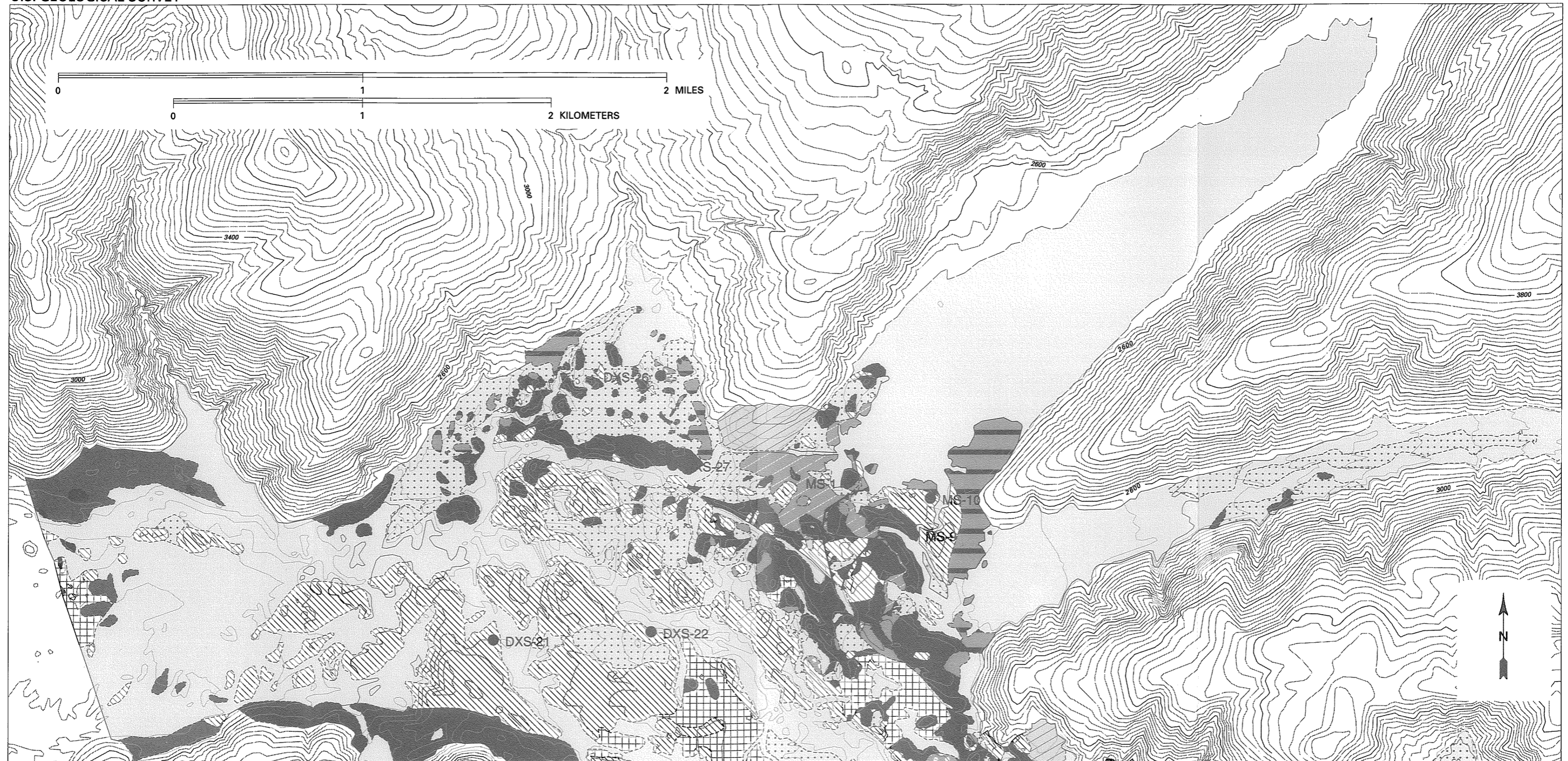
CONTACT - Dashed where approximately located, dotted where inferred
THRUST FAULTS IN IMBRICATE AREA - Approximately located
DXS-27 **SAMPLE LOCALITIES** (location of "windows"; see text)



**LITHOLOGIC MAP OF DEBRIS-AVALANCHE DEPOSIT
MAY 18, 1980, MOUNT ST. HELENS VOLCANO, WASHINGTON
WESTERN PART**

U.S. DEPARTMENT OF THE INTERIOR
U.S. GEOLOGICAL SURVEY

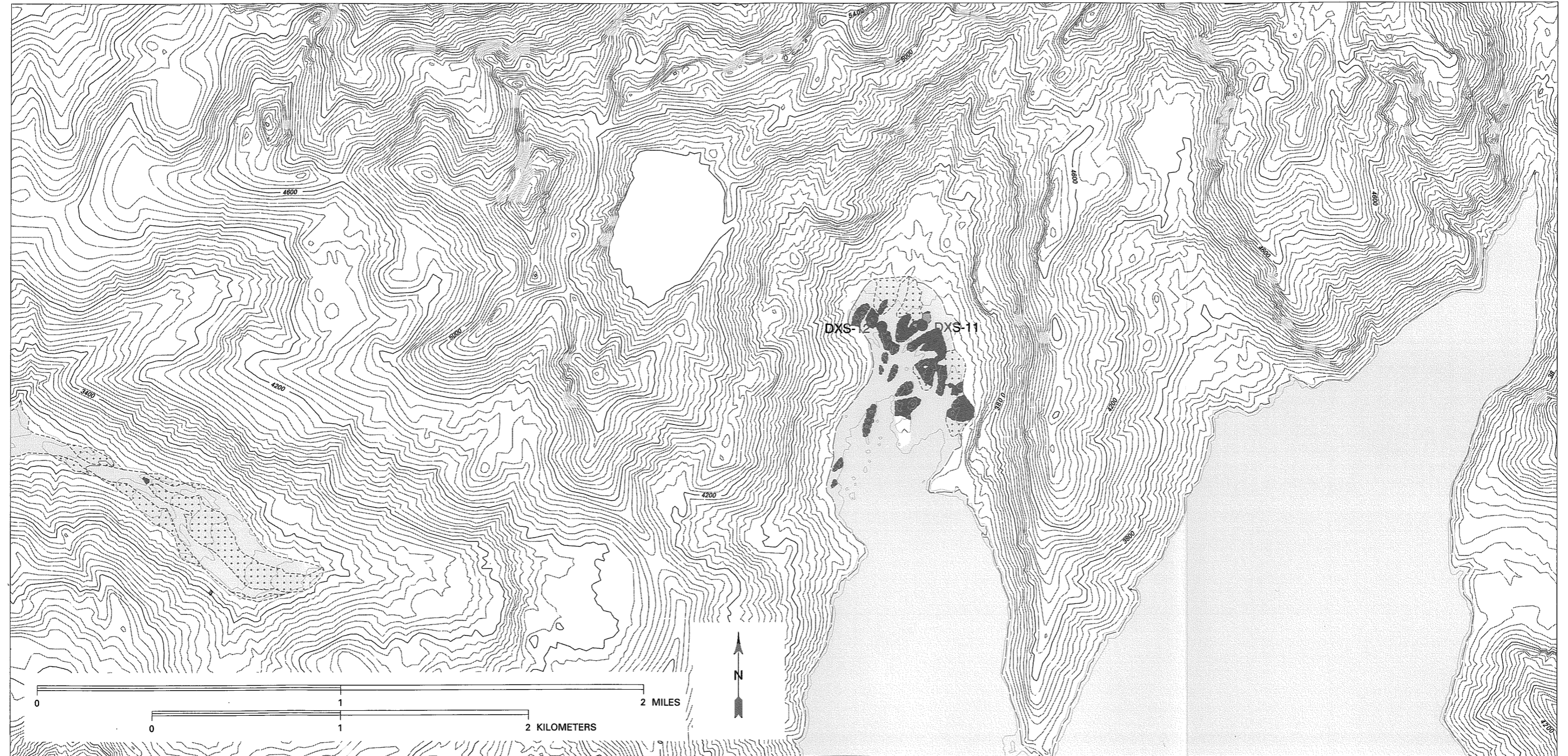
OPEN-FILE REPORT 96-677
PLATE 2B (1 OF 4)



**LITHOLOGIC MAP OF DEBRIS-AVALANCHE DEPOSIT
MAY 18, 1980, MOUNT ST. HELENS VOLCANO, WASHINGTON
EASTERN PART**

U.S. DEPARTMENT OF THE INTERIOR
U.S. GEOLOGICAL SURVEY

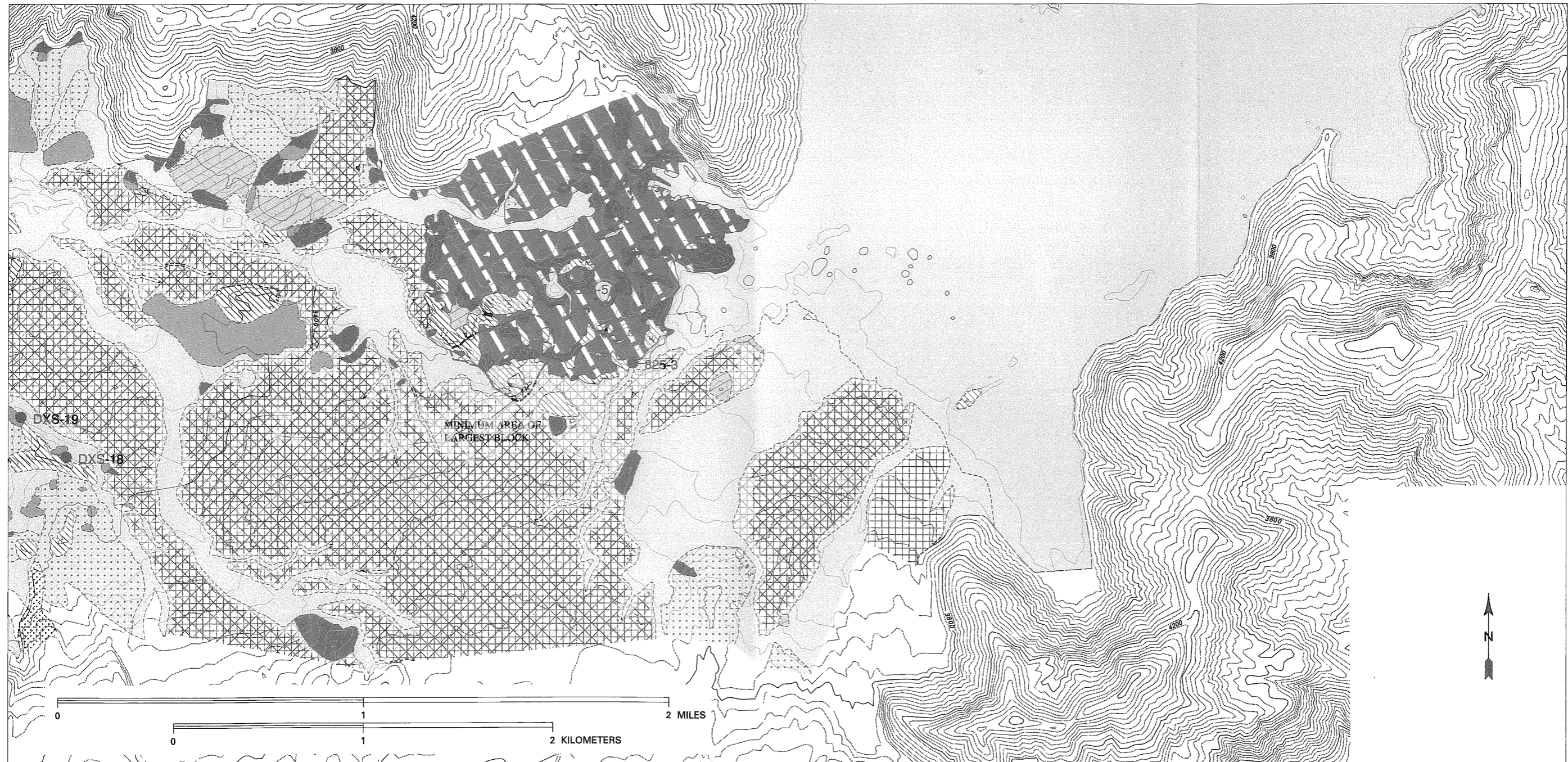
OPEN-FILE REPORT 96-677
PLATE 2B (2 OF 4)



**LITHOLOGIC MAP OF DEBRIS-AVALANCHE DEPOSIT
MAY 18, 1980, MOUNT ST. HELENS VOLCANO, WASHINGTON
EASTERN PART**

U.S. DEPARTMENT OF THE INTERIOR
U.S. GEOLOGICAL SURVEY

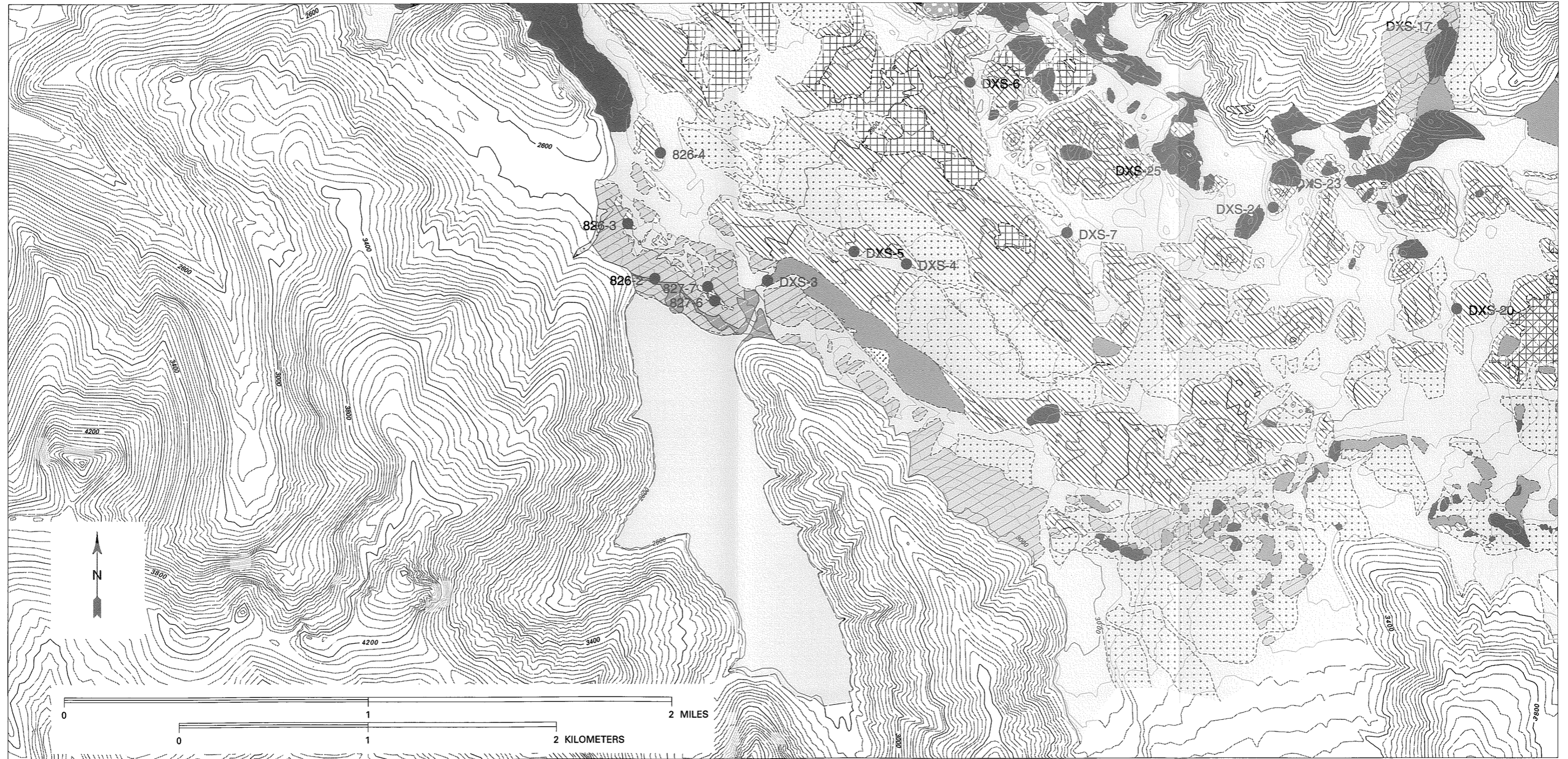
OPEN-FILE REPORT 96-677
PLATE 2B (3 OF 4)



**LITHOLOGIC MAP OF DEBRIS-AVALANCHE DEPOSIT
MAY 18, 1980, MOUNT ST. HELENS VOLCANO, WASHINGTON
EASTERN PART**

U.S. DEPARTMENT OF THE INTERIOR
U.S. GEOLOGICAL SURVEY

OPEN-FILE REPORT 96-677
PLATE 2B (4 OF 4)



**LITHOLOGIC MAP OF DEBRIS-AVALANCHE DEPOSIT
MAY 18, 1980, MOUNT ST. HELENS VOLCANO, WASHINGTON
EASTERN PART**